The Role of Iron Storage Proteins in *Pseudomonas aeruginosa* Bacterial Iron Homeostasis

By

Kate Eshelman

Submitted to the graduate degree program in Chemistry and the Graduate Faculty of the University of Kansas in partial fulfillment of the requirements for the degree of Doctor of Philosophy.

_____

Chair: Mario Rivera, PhD.

_____

Heather Desaire, PhD.

_____

Krzysztof Kuczera, PhD.

_____

David Benson, PhD.

_____

Scott Hefty, PhD

_____

Josephine Chandler, PhD

Date Defended: April 28th, 2016

The Dissertation Committee for Kate Eshelman

certifies that this is the approved version of the following dissertation:

The Role of Iron Storage Proteins in *Pseudomonas aeruginosa* Bacterial Iron Homeostasis

_____

Chair: Mario Rivera, PhD.

Date approved: April 28th, 2016

Abstract

Pseudomonas aeruginosa is a gram-negative bacterium that causes infections in immune compromised patients. There have been an increasing number of multi-drug resistant *P. aeruginosa* infections which is leading to the need to develop new targets for antibiotics. A potential new target is to disrupt iron homeostasis by disrupting the function of the iron storage protein, bacterioferritin B (BfrB). The structure and function of BfrB has been passionately studied in our lab, which has led to new understanding of iron uptake and iron release from BfrB. Iron mobilization from BfrB requires binding from the bacterioferritin-associated ferredoxin (Bfd), a process that our lab has demonstrated in vitro using X-ray crystallography, and binding studies. These studies also allowed the lab to determine the key residues in both proteins that stabilize the BfrB:Bfd complex.

In my work, we have taken the insights from the *in vitro* studies and applied them to investigate the consequences of blocking the BfrB:Bfd interaction in *P. aeruginosa* cells. We first show that iron is essential to bacterial growth by testing the effects of an iron sequestering polymer developed in collaboration with Prof. Cory Berkland's lab at the University of Kansas. The iron-sequestering polymer is capable of delaying bacterial growth and increasing the sensitivity of wild type (wt) *P. aeruginosa* to the antibiotics ciprofloxacin and gentamicin.

I then studied cell growth and iron handling in response to mutating the *bfrB* gene (Δ*bfrB*), the *bfd* gene (Δ*bfd*), or introducing a double mutation (E81A/L68A) in the *bfrB* gene in the chromosome of *P. aeruginosa*. From our previous *in vitro* studies, we predicted that E81/L68A BfrB mutant (herein denoted bfrB*) would not bind BfrB in *P. aeruginosa* cells. We demonstrate

through these studies that BfrB and the BfrB:Bfd interaction are essential for iron homeostasis in *P. aeruginosa*.

The structural dynamics of BfrB have also been analyzed. We show that by mutating residues in the B-pores of the protein, we affect the function of the relatively distant ferroxidase center, which in turn inhibits iron oxidation and uptake. We show that concerted motions linking the pores and the catalytic center are essential for the function of BfrB.

Lastly, our lab is engaged in developing compounds for blocking the BfrB:Bfd interaction. I have developed assays to show the effect of these compounds on cell growth and survival, and demonstrated that the compounds being developed in the lab boost the killing activity of existing antibiotics against *P. aeruginosa* cells.

Acknowledgements

I would first like to thank my advisor Dr. Mario Rivera. You taught me the importance of details whether it was during experiments or presenting data. I never stopped learning and was always being challenged as a student in your lab. I hope in my future career I will have your enthusiasm for research and the desire to always want to know what's new.

Thank you to my chemistry undergraduate professors at Wagner College. Without your help and guidance I would have never chosen to major in chemistry or continued my education at a higher level.

Thank you to all the past and present Rivera lab members. I appreciate all your help and enjoyed working beside you.

I am very grateful for the support of my family. Mom, Dad, and Sarah you were always willing to listen to the good and the bad. I'm thankful for your diligent prayers and thoughts. You helped me push through to the very end when I had to jump over the highest hurdle. Sarah and Lee, thank you for giving me adorable nieces. They always bring joy and a smile to my face.

Thank you to all the friends I made in the graduate program. Going through graduate school is not possible unless you have fellow students to vent and dance your problems away.

Thank you to the Betty and Zontal family. I will cherish the times I was able to escape from the lab and throw a Frisbee with some of the most extraordinary people I have ever met in my life. You gave me laughter, friendships, and a tradition that will last for many years to come.

Table of Contents

Table of Figures

Chapter 1 : Introduction

Iron is Essential for Growth

Iron is essential for most species including mammals and bacterial pathogens. Fe can be used as a cofactor and a prosthetic group in essential enzymes that are involved in many cellular functions and metabolic pathways [1]. Iron exists in two redox states, Fe^{2+} or Fe^{3+}, each of which can have high or low spin states [2]. These properties of iron allow it to be incorporated into proteins as a biocatalyst or electron carrier [2]. For iron to be biologically active, it has to be incorporated into proteins as a mono- or binuclear species or in Fe-S clusters or in heme groups [2]. The incorporation of iron into proteins also allows for the redox potential of iron (range from -300 to +700 mV) to be controlled [2]. For optimal growth, most bacterial organisms require 0.3-1.8 μM extracellular iron concentrations [3]. Iron is needed for metabolic processes such as replication, electron transport, TCA cycle, oxygen transport, nitrogen fixation, glycolysis, and DNA synthesis [1, 2]. Although iron is necessary, it has poor bioavailability and can induce oxidative stress to the cell.

Iron has poor bioavailability because Fe^{3+} is almost insoluble under aerobic and neutral pH conditions, with solubility around 10^{-18} M [1]. Fe^{2+} is water soluble at neutral pH, but it can react with hydrogen peroxide (produced by cell metabolism) to form hydroxyl radicals and Fe^{3+} through the Fenton reaction [4]. Fe^{3+} can be reduced back to Fe^{2+} by superoxide or other reducing agents in the cell, as illustrated in Figure 1-1 (Haber-Weiss cycle). This oxidative stress can be toxic to the cell because there is no internal defense system for hydroxyl radicals [4]. The

production of hydroxyl radicals causes protein denaturation and damage to DNA [1, 4]. To ensure sufficient iron concentrations for cellular processes, but prevent iron-induced toxicity, the free intracellular iron concentration is regulated around 10 μM [5].

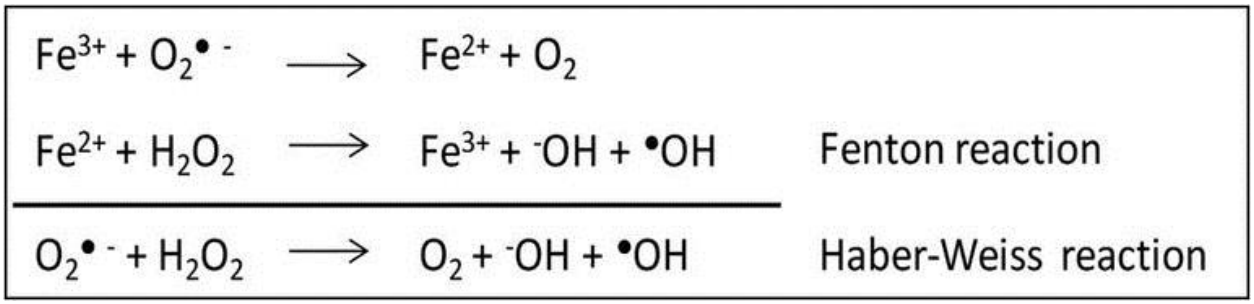

Figure 1-1: Haber-Weiss reactions cycle, in which iron catalyzes the formation of the highly toxic hydroxyl radical.

Pseudomonas aeruginosa as a model bacterial organism

Pseudomonas aeruginosa is an opportunistic pathogen that causes infections in immune compromised patients such as cystic fibrosis patients [6]. It has become very difficult to treat due to the increasing resistance of antibiotics. The strains PA01 and PA14 are ideal to study in a laboratory setting and have had an abundance of research completed to study iron homeostasis [7]. We hope to use this information to develop potential therapeutics as well as further understand the complex system of iron regulation in the cell. Background information on iron regulation will be focused on what occurs in *P. aeruginosa* as well as examples in other bacterial strains.

Iron Acquisition

Iron is not only used for essential functions in the cell, but it also affects the virulence of pathogens in the host. Free iron is toxic to the host cells similar to bacteria. The concentration of free intracellular iron in a mammalian host will be around 10^{-9} µM [3]. The host restricts the concentration of free iron by sequestering soluble iron in iron-binding proteins, such as transferrin, lactoferrin, or heme proteins [3]. Lactoferrin, an iron chelating glycoprotein, binds iron with extremely high affinity, and thus functions as a primary defense mechanism to restrict the growth of pathogens in a mammalian host. For example, lactoferrin has been shown to inhibit *Pseudomonas aeruginosa* biofilm formation which provides a potential therapeutic to combat *P. aeruginosa* biofilm formation in cystic fibrosis patients[1, 8]. In response, *P. aeruginosa* and other pathogens have developed multiple strategies to obtain iron in its host [8]. The pathogens obtain iron through pathways such as (*i*) sequestering heme from heme-binding proteins like hemoglobin, (ii) secreting siderophores to capture and internalize Fe^{3+}, reducing Fe^{3+} to Fe^{2+} for its subsequent internalization via specific ferrous iron transporter (Feo), and degrading iron-binding molecules like transferrin using enzymes [3].

Under anaerobic and typically iron-repressed conditions, Feo transcription will be induced. In *P. aeruginosa*, ferrous iron is transported through the FeoABC system [9]. There are three proteins coded by the Feo operon, FeoA, FeoB, and FeoC. FeoA, which is a small 9.3 kDa cytosolic protein, is thought to activate FeoB [9]. FeoB is an 83 kDa protein with a soluble N-terminal domain and membrane integral C-terminal domain, and FeoC is a small 8.7 kDa cytosolic protein that is thought to regulate transcription of FeoB expression [9]. FeoB is most likely a Fe^{2+} permease and has been shown to be related to virulence in pathogens such as

Helicobacter pylori and *Campylobacter jejuni* [9], In *P. aeruginosa*, FeoB is essential for cell survival in the anaerobic environment of biofilms [9].

To obtain ferric iron, bacteria, as well as yeast, fungi, and plants, will produce high affinity extracellular ferric chelators called siderophores [10]. Siderophores are small molecules, less than 1,000 Da, which have binding affinities greater than 10^{30} for Fe^{3+} [2]. There are over 500 siderophores that have been characterized and they can be found in pathogenic and non-pathogenic bacteria [2, 11]. In the case of gram-negative bacteria, secreted siderophores form a complex with Fe^{3+} (ferri-siderophore), which is recognized and internalized by an outer membrane (OM) receptor. The complex is too large to go through porins which allow molecules such as glucose, phosphate, and amino acids to travel into the cell [10]. The ferri-siderophore will be transported to the inner membrane (IM) using the energy transducing TonB-ExbB-ExbD system, which is located in the IM and periplasm [12]. The complex will then interact with an ATP-binding cassette (ABC transporter), which will deliver it into the cytoplasm [2, 12]. The OM siderophore receptors are not present when there is sufficient iron, but are induced under iron starvation conditions. The OM receptors have a high specificity towards the ferri-siderophore complex. In the genome of *P. aeruginosa*, there are 35 TonB-dependent OM receptors which shows the importance of the capability of bringing in large amounts of iron bound siderophores [2].

P. aeruginosa secretes two siderophores, pyoverdine and pyochelin to chelate ferric iron and bring it into the cell [8]. Pyoverdine (Figure 1-2) is considered the main siderophore released by *P. aeruginosa* under iron limiting conditions and has a binding affinity of 10^{32} M^{-1}

for Fe^{3+} [13]. The structure of pyoverdine is made up of a partially cyclized octapeptide attached to the 2,3-diamino-6,7-dihydroxyquinoline-based chromophore [14]. Ferric iron is chelated by the catechol group on the chromophore and the two hydroxyornithine side chains [14]. When pyoverdine is not bound by iron it exhibits green fluorescence and at pH 7.4 has an absorbance at 405 nm, but when bound with Fe^{3+} the fluorescence is quenched [15].

To import the Fe^{3+}-pyoverdine complex into the cell, it will bind to the outer membrane receptor FpvA (Figure 1-3A and 1-3B) and be actively transported into the cell by TonB-ExbB-ExbD system [13, 16]. The FpvA is made up of 22 antiparallel β-strands to form a beta-barrel in the OM that forms a large pore about 35-40 Å in diameter [16]. In the pore there is a globular plug domain that prevents large molecules from crossing the membrane [16]. It undergoes a conformational change with the energy from the TonB system to allow the ferri-siderophore complex to pass through the receptor and enter the cell [16].

Pyoverdine also has other functions besides binding Fe^{3+}. During infections, pyoverdine competes with transferrin for iron [13]. Pyoverdine has been shown to be related to quorum sensing, and in bacteria like *P. aeruginosa*, it helps the colonization in low iron environments such as host tissue by competing with transferrin for iron [17]. It is also thought to be essential in the pathogen's virulence, the development of mature biofilms, and to be competitive with other bacteria in soil [17].

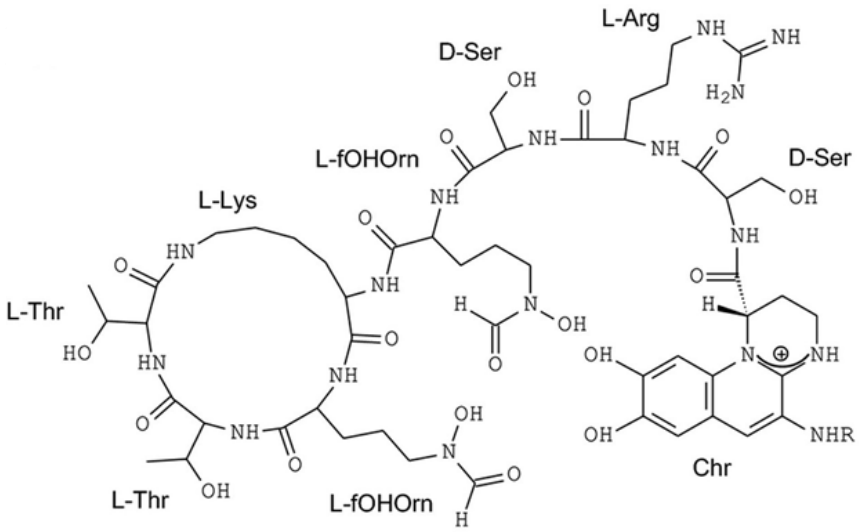

Figure 1-2: Structure of pyoverdine from *P.aeruginosa* without iron [16]. Chr is the chromophore of the structure which fluoresces unless bound to Fe^{3+}.

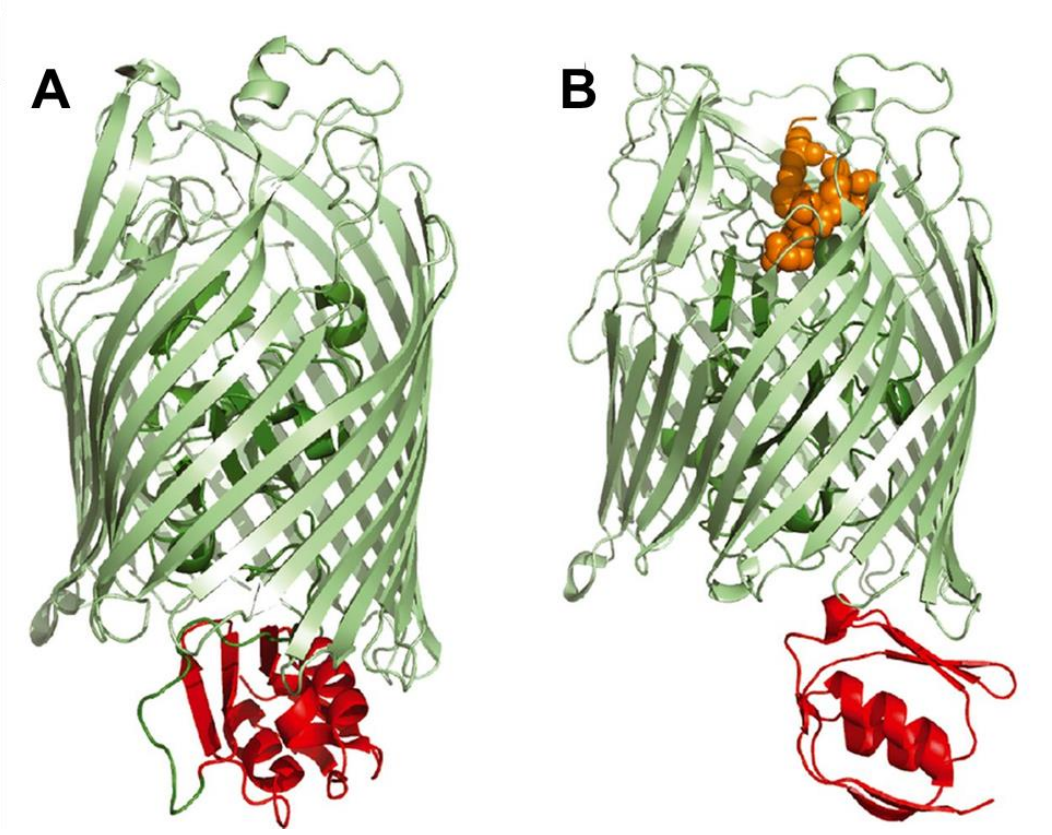

Figure 1-3: (A) The pyoverdine OM receptor, FpvA. In light green is the beta-barrel found in the OM. In dark green is the plug and in red is the signaling domain. (**B**) In orange is the ferri-siderophore complex binding to FpvA [16].

Heme is the most abundant source of iron in mammals [2], so it is intuitive that bacteria would develop ways to acquire heme from the host to utilize the bound iron. Bacteria are capable of using the heme, hemoglobin, or hemopexin-heme complex as sources of iron [2]. Pathogens are able to release heme from the proteins that bind it in the host by secreting hemolysins and proteases. The released heme will either be captured by the bacteria or could possibly be taken back by the host protein [2]. There are two classes of heme acquisition in gram-negative bacteria: (*i*) direct binding of heme to OM receptors or (*ii*) the secretion of

hemophores to capture and deliver the heme to cognate surface receptors [18]. The heme or heme-hemophore complexes will bind to OM receptors and then use the TonB-ExbB-ExbD system to transport the heme groups across the OM [2]. Hemophores that bind hemoglobin and hemopexin will also deliver heme to the OM receptors [2]. An ABC permease will transport the heme across the CM and be degraded by a heme oxygenase [2]. *P. aeruginosa* has 2 interdependent heme uptake systems, the Phu, ***P****seudomonas* **h**eme **u**tilization system and Has, **h**eme **a**ssimilation **s**ystem [18]. The Phu system encodes an OM receptor, PhuR, where heme is sequestered and brought into the cell by PhuT, the periplasmic transport system [18]. PhuT interacts with the PhuUV ABC transporter in the cytoplasm, where the heme is sequestered by PhuS. PhuS transfers heme to heme oxygenase for subsequent break down of the heme into CO, biliverdin, and iron [19]. In *P. aeruginosa,* the hemophore, $HasA_{p,}$ acquires heme from the host and is brought to the OM receptor HasR [18, 19]. In the cytosol the heme is degraded by heme oxygenase into biliverdin, which releases iron and carbon monoxide [8, 18]. A full schematic of the different iron uptake pathways is described in Figure 1-4.

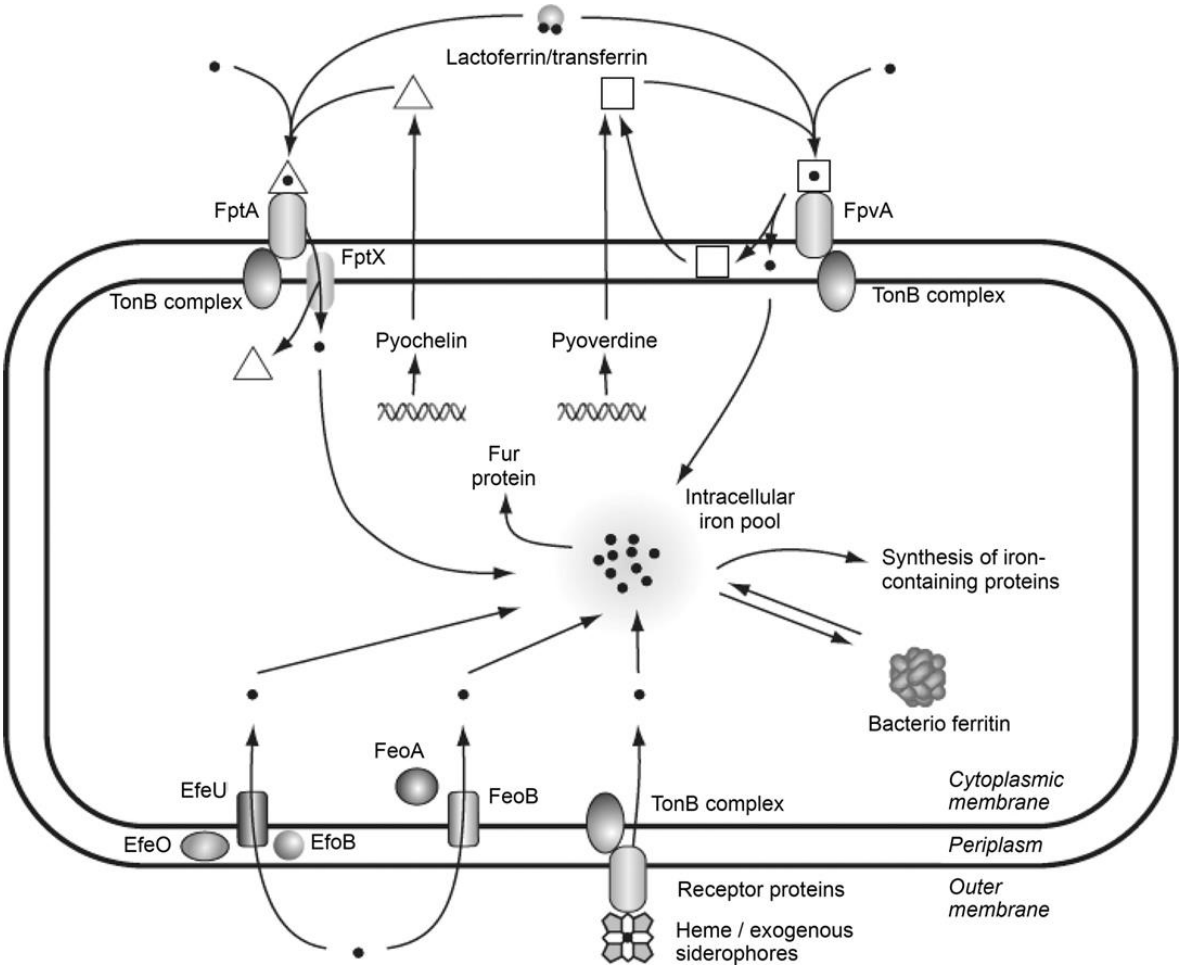

Figure 1-4: A schematic of iron uptake pathways that supply iron to *P.aeruginosa*. The scheme shows the uptake pathways of iron through the release of siderophores pyoverdine and pyochelin, and their membrane receptors FpvA and FptA to bring in the ferri-siderophore complex. At the bottom of the diagram is the intake of ferrous iron through Feo, and the heme receptor proteins to bring heme into the cytoplasm. The iron is shown to go to the intracellular iron pool and is then distributed to iron-utilizing proteins, iron storage proteins like bacterioferritin, and also to FUR, the master ferric uptake regulator [20].

FUR

To prevent oxidative stress and the buildup of free iron in the cell, iron concentration is tightly regulated with the aid of the ferric uptake regulator, FUR [4]. FUR is a transcriptional repressor with Fe^{2+} as its cofactor [4]. Fur can actively repress iron acquisition genes under iron-replete conditions [8]. When there is a high concentration of iron, Fe^{2+} is bound to FUR, which binds to the promoter site of iron acquisition genes, preventing their transcription [4, 21]. FUR is also a positive regulator of genes such as iron storage proteins and iron-containing metabolic enzymes. Under low iron conditions, Fe^{2+} will no longer bind to FUR which allows transcription of the small regulatory RNAs, PrrF1 and PrrF2 in *P. aeruginosa*, which will inhibit the expression of the iron storage proteins [4, 8, 21]. Iron acquisition genes directly regulated by FUR include the small Fe^{3+} chelating molecules, siderophores, like pyochelin and pyoverdine in *P.aeruginosa*, heme acquisition proteins, and the direct import of Fe^{2+}. In low iron conditions there is a decrease in expression of iron storage proteins and iron containing metabolic proteins [22]. This is essential for the bacteria to maintain enough iron in the cytoplasm iron pool for necessary functions [23].

Iron Storage

The necessity to have iron for biological functions, but the potential for cell damage from iron has led organisms to evolve safe strategies to store iron, which utilize the iron storage proteins, ferritins. Ferritins are large spherical proteins that store iron in their internal cavity as a ferric mineral [24]. Ferritins have been described as having the primary function of storing excess available iron to prevent oxidative stress and providing a source of iron that can be used

when there is low iron availability in the environment [24]. The potential of iron toxicity leads to the tight regulation of iron and the storage of excess iron in iron storage proteins [1, 25]. In *P. aeruginosa* and in other pathogens there are three types of ferritin-like molecules- the DNA binding protein (DPS), the classical bacterial ferritin (Ftn) and the bacterioferritin (Bfr) [26].

DPS

DPS are present in bacteria and archaea [26]. DPS has a different structure and function in the cell compared to the bacterial ferritins and the bacterioferritin. DPS is made of 12 subunits (Figure 1-5) and can accumulate up to 500 Fe atoms [27]. Iron is accumulated by oxidizing Fe (II) to Fe (III) at the ferroxidase center which is at the interface of adjacent subunits [26]. DPS in some bacteria such as *E. coli* have been shown to bind DNA and protect it from oxidative degradation [27]. Not all DPS have been shown to bind DNA such as in *Listeria monocytogenes.* In this bacteria, iron is stored in DPS and the primary function is suspected to be in protecting the cell from oxidative stress caused by free iron [1, 12].

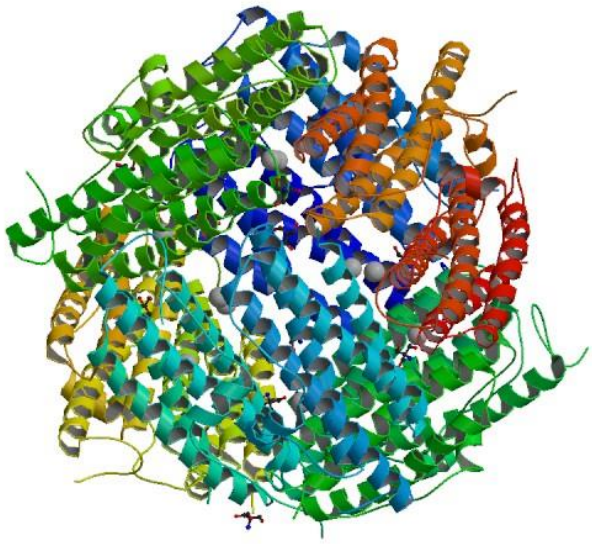

Figure 1-5: Crystal structure of *E.coli* DPS (PDB 1L8I). Each subunit is shown in an alternating color. The 12 subunit structure forms an assembly with a hollow interior that can hold approximately 500 iron atoms.

Mammalian Ferritin

Ferritins (Ftn) are found in eukaryotes as well as in bacteria [28]. The mammalian ferritins differ from the ferritins found in bacteria in that mammalian ferritins are assembled from two types of subunits, whereas bacterial ferritins are assembled from a single type of subunit [29]. The subunits that make mammalian ferritins are termed the heavy (H) and the light (L) chains, which assemble into a 24-mer structure (Figure 1-6). There is only 55% sequence identity between the H and L chains, but the chains are mutually interchangeable to form the 24 subunit structure [30]. The H chains are catalytically active because they contain the ferroxidase centers where Fe^{2+} is oxidized to Fe^{3+} prior to its storage in the interior cavity. The L chains do

not harbor ferroxidase centers, but they have been shown to contain nucleation sites where iron can nucleate to form a mineral [31].

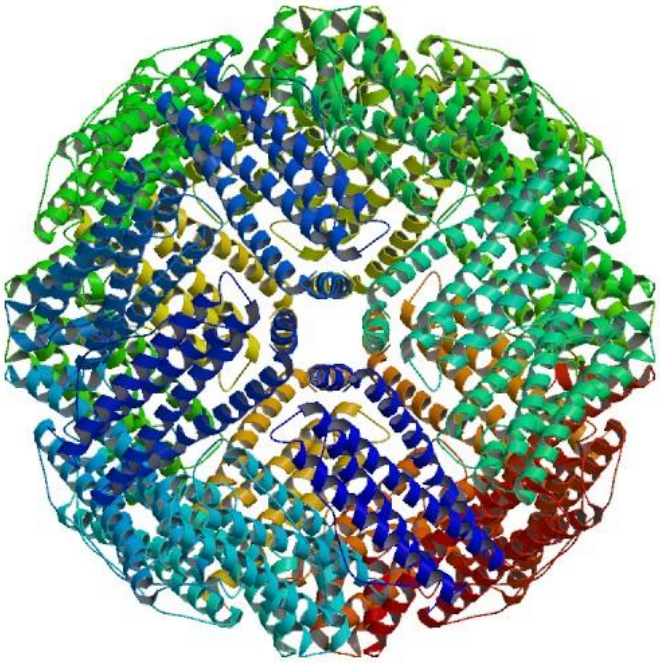

Figure 1-6: X-ray crystal structure of horse spleen apoferritin (PDB 4V1W) [32]. Each subunit is shown in an alternating color.

Bacterial Ferritins and Bacterioferritin

Bacterial ferritins (Ftn) and Bacterioferritin (Bfr) are unique to bacteria. These proteins have similar 24-mer structures to the ferritins found in mammals but have significant subunit differences [33]. The structures of *E.coli* Ftn and *P.aeruginosa* Bfr can be seen in Figure 1-7A and 1-7B. They are both made from 24 identical subunits that assemble into a spherical, hollow cage that can hold approximately 4,500 iron atoms [31]. The structure and sizes of both types of protein are similar, having a total mass of approximately 450 kDa, with an external diameter of

120 Å, and a cavity with 80 Å diameter. The storage of the ferric mineral is possible by oxidizing ferrous ions at the ferroxidase centers. Both Ftn and Bfr contain ferroxidase centers in every subunit, where the binding of ferrous iron to form a di-iron center takes place immediately prior to oxidation to the ferric iron and translocation into the cavity of the proteins [34]. The ferroxidase centers are located in the middle of each subunit, which is composed of a four-helix bundle [34]. Bfr are unique among ferritin-like molecules in that these proteins bind heme between 2 subunits [31]. Depending on the bacterial strain, the two proteins have been shown to either be a primary iron storage protein or be related to controlling oxidative stress. For example, it was shown in *E.coli* that without the Ftn there was a 50% less total iron in the cell, and the growth rate of the mutant bacteria was reduced under low iron conditions. In comparison, in *C. jejuni* and *H. pylori* the Bfr mutants are more sensitive to redox stress [2]. The role of Bfr in *Salmonella Typhimurium* is essential for iron storage and full virulence, but Ftn does not contribute to storing large amounts of iron [28]. The function of iron stored in *Salmonella* Bfr contributed to lowering oxidative stress produced by hydroxyl radicals and reactive oxygen species, and it was also shown to be required for the iron-sulfur cluster aconitase enzyme to undergo repair following oxidative damage [28].

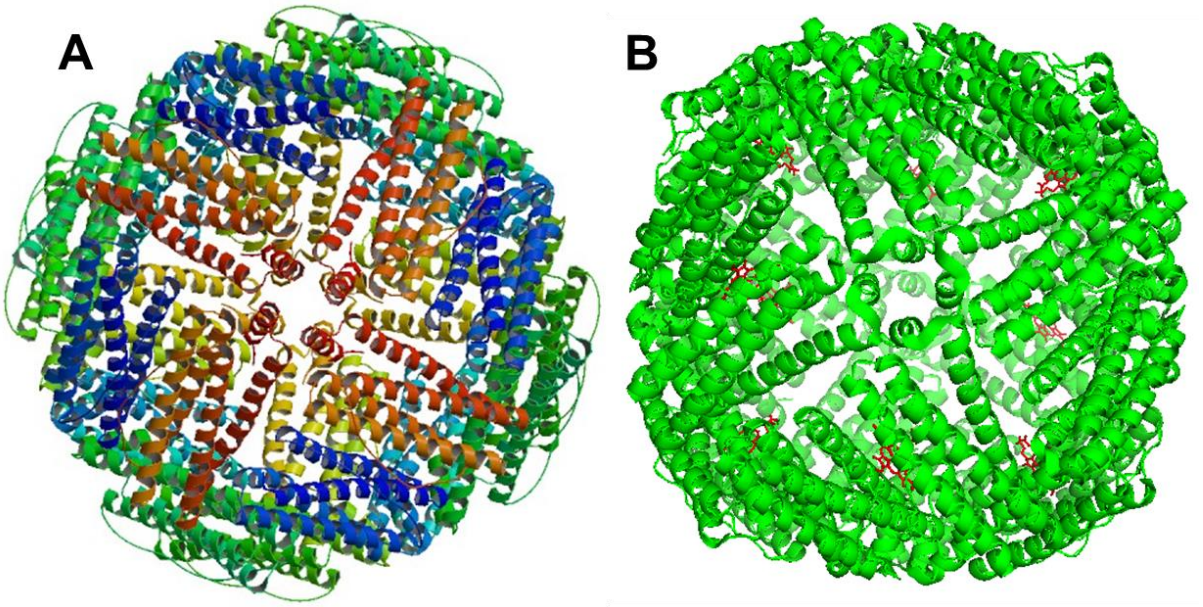

Figure 1-7: (A) X-ray crystal structure of *E.coli* ferritin (PDB 1EUM) 24-mer structure viewed along the 4-fold axis of symmetry [35]. Each individual subunit has been given a different color. (**B**) The X-ray crystal structure of *P. aeruginosa* bacterioferritin (PDB 3IS8) 24-mer structure viewed along the 4-fold axis of symmetry; the heme molecules (red) are located in between 2 subunits [36].

In *Pseudomonas aeruginosa* both types of iron storage proteins, the bacterial ferritin (FtnA) and the bacterioferritin (BfrB) are present [37]. The functions of these two iron storage proteins remain enigmatic, although, as will be shown in this work, we now know that BfrB is the main iron storage protein in *P. aeruginosa* cells. Although FtnA and BfrB have a similar structure, they have less than 18% amino acid sequence homology [38]. Like a typical bacterial ferritin, FtnA does not contain heme. BfrB has a methionine at position 52 which allows for the

protein to coordinate a heme molecule in between two subunits; M52 is not present in FtnA [37]. This leads to a different process of iron mobilization from BfrB compared to FtnA [37]. Adjacent to the *bfrB* gene is the bacterioferritin- associated ferredoxin (*bfd*) gene, which is also been conserved in other pathogens [39]. Bfd has been shown to be necessary for iron release from BfrB [39]. The crystal structure of the BfrB-Bfd (Figure 1-8) complex shows Bfd binding above the heme in BfrB. This allows for the passing of electrons from Bfd into the core of BfrB to reduce the ferric mineral and be released as ferrous iron [39]. The scheme of how electrons are passed into the core of BfrB is seen in Figure 1-9. The electrons are passed from NADPH to the ferredoxin reductase (FPR) to Bfd which then pass the electrons into the core of BfrB through the heme to reduce Fe^{3+} to Fe^{2+} which can then be released to the cytosol.

Further investigations in our laboratory determined the essential interactions between the Bfd and BfrB residues [40]. The essential residues in BfrB that promote binding of Bfd have been shown to be residues leucine 68, glutamate 81, and glutamate 85 (Figure 1-10) [40]. This was elucidated by making site directed mutations of these residues to alanine and performing binding studies using SPR and *in vitro* iron mobilization assays. The dissociation constant (K_d) of the BfrB:Bfd complex was determined to be 3.3 µM at pH 7.4 [40]. The mutations resulted in significantly higher $K_{d;}$ 258 µM with E81A, 298.5 µM with L68A, and 590 µM with E85A [40]. Importantly, introducing the double mutation E81A/L68A in BfrB resulted in complete abrogation of binding. In the *in vitro* assays of iron mobilization from BfrB, this double mutant BfrB acted the same as the control with no Bfd present in the assay. The E81A/L68A double mutant eliminated the Bfd interaction with BfrB, which inhibited the transfer of electrons from Bfd, and the release of iron from the core of BfrB. These results support that Bfd interacts with

BfrB and this interaction is required for the release of iron from BfrB which led to the work that will be discussed in this Dissertation.

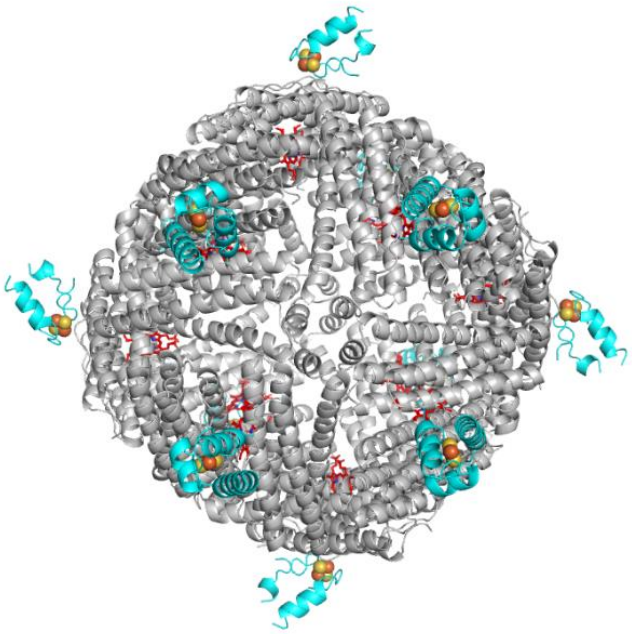

Figure 1-8: X-ray **c**rystal structure of the BfrB-Bfd complex from *P. aeruginosa* (PDB 4E6K) [39]. The BfrB protein is gray with the heme molecules being shown in red. Located above each of the heme molecules is Bfd, shown in cyan, with its [2Fe-2S] cluster in orange and yellow.

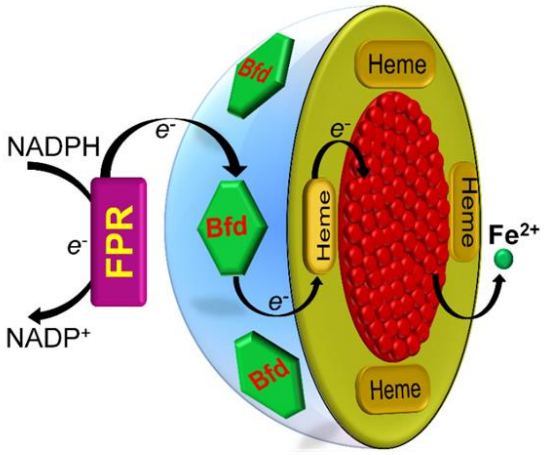

Figure 1-9: Schematic of electron transfer from NADPH to the ferredoxin reductase (FPR) to Bfd [40]. The electron from Bfd passes through the heme in BfrB into the core, which reduces the stored Fe^{3+} to Fe^{2+}.

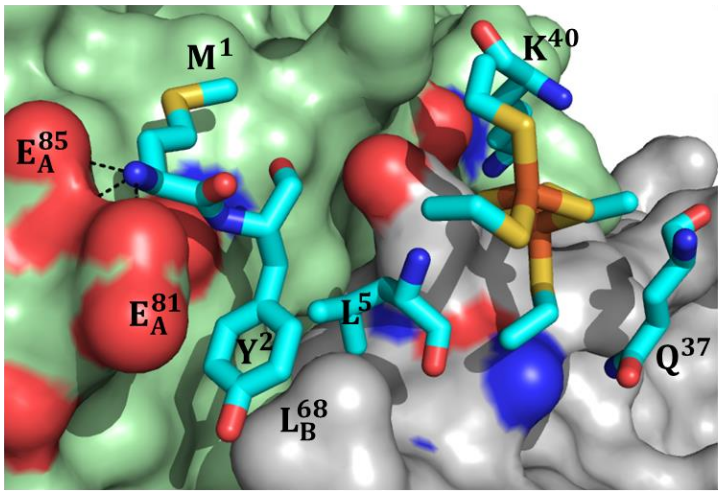

Figure 1-10: Key residues of the BfrB-Bfd interaction. BfrB is shown in grey and green and Bfd is in cyan. The essential BfrB residues for Bfd binding are the glutamate 85, glutamate 81 and leucine 68. Glutamate 81 and leucine 68 provide a cleft where tyrosine 2 from Bfd can be inserted [40].

Targeting Iron for Antimicrobials

There is a need for new antibiotic targets due to an increase in antibiotic resistance. To address this issue, one focus of research has been to explore the inhibition of iron uptake by the bacterial cell [41]. Iron is not only needed for important biological functions, but it is necessary for virulence [1]. In the mammalian host, the amount of free Fe is approximately 10^{-18} M to prevent acute and chronic infections [42]. Preventing iron uptake or disrupting iron homeostasis is probably valid target for new antibiotics because bacteria need iron to survive, but if not properly regulated, it could lead to oxidative stress. For example, small molecules have been developed to inhibit the production of siderophores secreted by *Mycobacterium tuberculosis* and *Yersinia pestis* [43]. By disrupting bacterial strategies to scavenge iron, it is thought that the growth will be inhibited. Also, mutant strains lacking the iron scavenging systems in *Y. pestis* were avirulent in mice and unable to grow in iron limiting media [43]. Researchers have attempted to inhibit iron scavenging systems, but most pathogens have multiple iron uptake pathways that cannot be targeted all at once [44]. Iron chelation therapy has also been tested, but some pathogens are capable of using the chelated iron complex to form secondary infections [44].

Tricking the bacteria to uptake other metals in place of iron has been suggested as an alternative method. The transition metal gallium has been used in a 'Trojan horse" strategy because Ga^{3+} has similar chemical properties as Fe^{3+}, so the cell will uptake Ga and not release siderophores. Importantly, Ga^{3+} cannot be reduced to Ga^{2+}, so it is unable to perform the biological functions carried out by iron. Thus, gallium was shown to reduce biofilm formation

and to reduce iron uptake through the *pvdS* (siderophore) pathway. This eventually led to Ga replacing iron and affecting cellular function.

Research Problem and Rationale

Targeting bacterial iron homeostasis is a potentially valid target for developing novel antibiotics due to the potential toxicity caused to the bacterial cell by iron homeostasis dysregulation. To target bacterial iron homeostasis it is necessary to understand how bacteria control iron storage and subsequent mobilization of stored iron into the cytosol of bacterial cells, so one may specifically target the protein's function. In *P. aeruginosa* there are three ferritin-like proteins, but only two (FtnA and BfrB) are considered to function as iron storage proteins. To disrupt iron homeostasis, it was necessary to determine where the iron was being stored, FtnA or BfrB. In this dissertation, we describe results that show that BfrB is the primary iron storage protein in *P. aeruginosa*, as well as how we capitalized from the insights gained from our laboratory *in vitro* studies to design experiments aimed at probing the consequences of blocking the BfrB:Bfd interaction in *P. aeruginosa* cells. Results from these studies will be described and discussed in detail in Chapter 3.

To understand how we might perturb the function of BfrB in *P. aeruginosa* cells, we investigated the protein's dynamic properties that endow BfrB with the function of oxidizing Fe^{2+} to Fe^{3+}, and how perturbation of dynamics in sites remote to the ferroxidase sites inhibits ferroxidase activity. We also studied the phenotypes of cells with deletions in the *bfrB* and *bfd* genes, as well as mutant cells where the *bfrB* gene carries the E81A/L68A double mutation in the chromosome of *P.aeruginosa.* These investigations have provided insight into the bacteria's

response when the function of iron storage or release is disrupted, and strongly suggest that targeting bacterial iron homeostasis is a viable approach to develop anti-infectives. We also demonstrated, in collaboration with the Berkland laboratory, that chelating iron available in the environment by irreversibly sequestering it in polymers severely weakens bacterial cells. The development of novel therapeutics by disrupting the BfrB:Bfd interaction has also been tested. The bacteria's ability to uptake iron is probably a poor target due to the bacteria's multiple mechanisms of obtaining iron. On the other hand, targeting bacterioferritin function may offer several advantages. First, bacterioferritins are unique to bacteria, so small molecules developed to bind bacterioferritin would be specific to bacterioferritin and would not bind to the eukaryotic ferritin. The BfrB-Bfd genes have been found in multiple pathogens, which provide the possibility of developing molecules with broad spectrum of action, which indicate that our approach, and what we learn from our investigations with *P. aeruginosa*, will likely be of widespread impact. In addition, small molecules that affect iron homeostasis in *P. aeruginosa* could also be used as probes to investigate iron homeostasis in other pathogens.

References

1. Schaible, U.E.K., S.H.E, *Iron and Microbial Infection.* Nature 2004. **2**: p. 946-953.
2. Andrews, S.C., Robinson, A.K., Rodriguez-Quinones, F., *Bacterial iron homeostasis* FEMS Microbiol. Reviews, 2003. **27**: p. 215-237.
3. Vasil, M.L.O., Urs A., *The response of Pseudomonas aeruginosa to iron: genetics, biochemistry and virulence.* Mol. Microbiol., 1999. **34**: p. 399-413.
4. Touti, D., *Iron and oxidative stress in bacteria.* Arch. Biochem. Biophys., 2000. **373**: p. 1-6.
5. Keyer, K., Imlay, J.A., *Superoxide accelerates DNA damage by elevating free-iron levels.* PNAS USA, 1996. **93**: p. 13635-13640.
6. Yang, Z.S., Ma, L.Q., Zhu, K., Yan, J.Y., Bian, L., Zhang, K.Q., Zou, C.G., *Pseudomonas toxin pyocyanin triggers autophagy: Implications for pathoadaptive mutations.* Autophagy, 2016. **9**: p. 1-14.
7. Visca, P., Leoni, L., Wilson, M.J., Lamont, L.L., *Iron transport and regulation, cell signalling and genomics: lessons from Escherichia coli and Pseudomonas.* Mol. Microbiol., 2002. **45**: p. 1177-1190.
8. Reinhart, A., Powell, D., Nguyen, A., O'Neill, M., Djapgne, L., Wilks, A., Ernst, R., Oglesby-Sherrouse, A., *The prrF-Encoded Small Regulatory RNAs Are Required for Iron Homeostasis and Virulence of Pseudomonas aeruginosa.* Infect. and Immun., 2015. **83**: p. 863-75.
9. Seyedmohammada, S., Fuentealbab, N.A., Marriottc,R.A.J., Goetzead, T.A., Edwardsona,J.M., Barrerab,N.P., Venterc, H. , *Structural model of FeoB, the iron transporter from Pseudomonas aeruginosa, predicts a cysteine lined, GTPgated pore.* Bioscience Rep., 2016. **DOI: 10.1042/BSR20160046**.
10. Chu, B.C., Garcia-Herrero,A., Johanson,T.H., Krewulak,K.D., Lau,C.K., Peacock,R.S., Slavinskaya,Z., Vogel, H.J., *Siderophore uptake in bacteria and the battle for iron with the host; a bird's eye view.* BioMetals 2010. **23**: p. 601-611.
11. Nishio, T., Ishida, Y., *Production of dihydroxamate siderophore alcaligin by Alcaligenes xylosoxidans subsp. xylosoxidans.* Agric. Biol. Chem., 1990. **54**: p. 1837-1839.
12. Andrews, S., Norton, I., Salunkhe, A.S., Goodluck, H., Aly, W.S.M., Mourad-Agha, H., Cornelis, P., *Control of Iron Metabolism in Bacteria*, in *Metallomics and the Cell*, L. Banci, Editor 2013, Springer.
13. Schalk, I.J.H., Christophe; Dugave, Christophe; Poole, Keith; Abdallah, Mohamed A.; Pattus, Franc, *Iron-free pyoverdin binds to its outer membrane receptor FpvA in Pseudomonas aeruginosa: a new mechanism for membrane iron transport.* Mol. Microbiol., 2001. **39**: p. 351-360.
14. Tzou DL1, W.E., Abdallah MA, Kieffer B, Atkinson RA., *A low-temperature heteronuclear NMR study of two exchanging conformations of metal-bound pyoverdin PaA from Pseudomonas aeruginosa.* Biopolymers, 2006. **79**: p. 139-149.
15. Xiao, R.a.K., W.S, *Fluorescent Pseudomonad Pyoverdines Bind and Oxidize Ferrous Ion.* Applied and Environmental Microbiology, 1998. **64**: p. 1472–1476.

16. Llamas, M.A., Imperi,F., Visca, P., Lamont, I.L., *Cell-surface signaling in Pseudomonas: stress responses, iron transport, and pathogenicity.* FEMS Microbiol. Reviews, 2014. **38**: p. 569-597.
17. Cornelis, P., *Iron Uptake and metabolism in pseudomonads.* Applied microbiology and biotechnology, 2010. **86**: p. 1637-1645.
18. Benson, D.R., Rivera, M., *Heme Uptake and Metabolism in Bacteria*, in *Metallomics and the Cell*, L. Banci, Editor 2013, Springer.
19. Smith, A., Wilks, A., *Differential Contributions of the Outer Membrane Receptors PhuR and HasR to Heme Acquisition in Pseudomonas aeruginosa.* J.Biol. Chem., 2015. **290**: p. 7756-7766.
20. Reid, D.W., Anderson, G.J., Lamont, I.L., *Role of lung iron in determining the bacterial and host struggle in cystic fibrosis.* Am. J. Physiol.: Lung Cell. Mol. Physiol., 2009. **297**: p. L795-L802.
21. Wilderman, P.J., *Identification of tandem duplicate regulatory small RNAs in Pseudomonas aeruginosa involved in iron homeostasis.* PNAS, 2004. **101**: p. 9792-9797.
22. Kadner, R., *Regulation by Iron: RNA Rules the Rust.* J. Bacteriol., 2005. **187**: p. 6870-6873.
23. Vasil, M.L., *How we learnt about iron acquisition in Pseudomonas aeruginosa: a series of very fortunate events.* Biometals., 2007. **20**: p. 587-601.
24. Crow, A., Lawson, T.L., Lewin, A., Moore, G.R., Le Brun, N.E., *Structural Basis for Iron Mineralization by Bacterioferritin.* JACS, 2009. **131**: p. 6808-6813.
25. Andrews, S.C., *Iron storage in bacteria.* Adv Microb Physiol, 1998. **40**: p. 281-351.
26. Velayudhan, J.C., M; Richardson, A; Main-Hester, K; Fang, F. , *The role of ferritins in the physiology of Salmonella enterica sv. Typhimurium: a unique role for ferritin B in iron-sulphur cluster repair and virulence.* . Mol. Microbiol., 2007. **63**: p. 1495-1507.
27. Karas, V.O., Westerlaken, I., Meyer, A.S., *The DNA-Binding Protein from Starved Cells (Dps) Utilizes Dual Functions To Defend Cells against Multiple Stresses.* J. Bacteriol., 2015. **19**: p. 3206-3215.
28. Velayudhan, J., Castor, M., Richardson, A., Main-Hester, K., Fang, F., *The role of ferritins in the physiology of Salmonella enterica sv. Typhimurium: a unique role for ferritin B in iron-sulphur cluster repair and virulence.* Mol. Microbiol., 2007. **63**: p. 1495-1507.
29. Yao, H., Rui, H., Kumar, R., Eshelman, K., Lovell, S., Battaile, K.P., Im, W., Rivera, M., *Concerted Motions Networking Pores and Distant Ferroxidase Centers Enable Bacterioferritin Function and Iron Traffic.* Biochem., 2015. **54**: p. 1611-1627.
30. Harrison, P.M., *The Structure and Function of Ferritin.* Biochem. Education, 1986. **14**: p. 154-162.
31. Carrondo, M.A., *Ferritins, iron uptake and storage from the bacterioferritin viewpoint.* EMBO J., 2003. **9**: p. 1959-1968.
32. Russo, C.J., Passmore, L.A., *Electron Microscopy. Ultrastable Gold Substrates for Electron Cyromicroscopy.* Science, 2014. **346**: p. 1377.
33. Velayudhan, J., Castor, M., Richardson, A., Main-Hester, K., Fang, F., *The role of ferritins in the physiology of Salmonella enterica sv. Typhimurium: a unique role for*

ferritin B in iron-sulphur cluster repair and virulence. Mol. Microbiol., 2007. **63**: p. 1495-1507.
34. Chrichton, R.R., Declercq, J.P., *X-ray structures of ferritins and related proteins.* Biochimica et biophysica acta, 2010. **1800**: p. 706-718.
35. Stillman, T.J., Hempstead, P.D., Artymiuk, P.J., Andrews, S.C., Hudson, A.J., Treffry, A., Guest, J.R., Harrison, P.M., *The high-resolution X-ray crystallographic structure of the ferritin (EcFtnA) of Escherichia coli; comparison with human H ferritin (HuHF) and the structures of the Fe(3+) and Zn(2+) derivatives.* J. Mol. Biol., 2001. **307**: p. 587-603.
36. Weeratunga, S., Lovell,S., Yao,H., Battaile,K., Fischer,C., Gee,C., Rivera,M, *Structural Studies of Bacterioferritin B from Pseudomonas aeruginosa Suggest a Gating Mechanism for Iron Uptake via the Ferroxidase Center.* Biochemistry, 2010. **49**: p. 1160-1175.
37. Yao, H., Jepkorir, G., Lovell, S., Nama, P.V., Weeratunga, S., Battaile, K.P., Rivera, M., *Two distinct ferritin-like molecules in Pseudomonas aeruginosa: the product of the bfrA gene is a bacterial ferritin (FtnA) and not a bacterioferritin (Bfr).* Biochem., 2011. **50**: p. 5236-5248.
38. Ruvinsky, A.M.V., I.A., and Rivera, M., *Local packing modulates diversity of iron pathways and cooperative behavior in eukaryotic and prokaryotic ferritins.* J.Chem.Phys., 2014. **140**: p. 115104.
39. Yao, H., Wang, Y., Lovell, S., Kumar, R., Ruvinsky, A.M., Battaile, K.P., Vakser, I.A., Rivera, M., *The structure of the BfrB-Bfd complex reveals protein-protein interactions enabling iron release from bacterioferritin.* J. Am. Chem. Soc., 2012. **134**: p. 13470-13481.
40. Wang, Y., Yao, H., Cheng, Y., Lovell, S., Battaile, K.P., Midaugh, C.R., Rivera, M., *Characterization of the Bacterioferritin/Bacterioferritin Associated Ferredoxin Protein-Protein Interaction in Solution and Determination of Binding Energy Hot Spots.* Biochem., 2015. **54**: p. 6162-6175.
41. Moreau-Marquis, O.T., G.A., Stanton, B.A., *Tobramycin and FDA-approved iron chelators eliminate Pseudomonas aeruginosa biofilms on cystic fibrosis cells.* Am J Respir Cell Mol Biol. , 2009. **3**: p. 305-313.
42. Bullen J.J, R.H.J., Spalding P.B, Ward C.G., *Iron and infection: the heart of the matter.* FEMS Immunol Med Microbiol., 2005. **43**: p. 325-330.
43. Stirretta, K.L.F., J.A; Jayaprakashb, V; Sinhab,B.N; Renc,T; Quadria,L.E., *Small molecules with structural similarities to siderophores as novel antimicrobials against Mycobacterium tuberculosis and Yersinia pestis.* Bioorganic & Medicinal Chemistry Letters, 2008. **18**: p. 2662–2668.
44. Kaneko Y, T.M., Olakanmi O, Britigan BE, Singh PK. , *The transition metal gallium disrupts Pseudomonas aeruginosa iron metabolism and has antimicrobial and antibiofilm activity.* J.of Clinical Investigation, 2007. **4**: p. 877-888.

Chapter 2 : Iron sequestration in polymers has antimicrobial properties

Introduction

Pseudomonas aeruginosa is a gram-negative bacterium that causes infections in immune compromised patients, such as burn victims and cystic fibrosis patients [1]. Multidrug resistance has become a serious problem with *P. aeruginosa* infections because it has an unusual number of efflux pumps [2] and the ability to form biofilms. The efflux pumps are capable of exporting antimicrobial agents and the biofilm creates a barrier that protects the cells from taking in the antibiotics [1, 3].

The formation of biofilms is greatly dependent on the presence of iron. Iron concentration in the environment less than 1 μM or greater than 100 μM slows biofilm growth [1]. Iron is essential not only for biofilm growth, but it is an essential nutrient for cell growth and metabolism because it participates in a variety of cellular functions such as the tricarboxylic acid (TCA) cycle and DNA synthesis [4]. Since iron is essential for many primary functions, removing iron from the environment can weaken bacteria, and increase the susceptibility of bacteria to antibiotics [1, 5].

Some iron chelators have been tested in combination with current antibiotics that show increased killing. In one study, the FDA approved iron chelators, deferasirox and deferoxamine, were used in combination with the antibiotic Tobramycin to treat biofilms grown on cystic fibrosis epithelial cells [6]. The biofilm formation was reduced by 90% and there was

approximately 7 logs of increased killing in presence of the iron chelators [6]. In other studies, specific iron chelators do not enhance the efficacy of antibiotics. For example, the study completed by Liu used the small iron chelators, 2,2-bipyridl (10 μg/mL), acetohydroxamic acid (80 μg/mL) and EDTA (5 μg/mL) in combination with ciprofloxacin which had similar survival to treatment with ciprofloxacin alone [7]. The chelators did have an effect on biofilm formation when they were tested in combination with an efflux pump inhibitor. Except for EDTA which showed a decrease in biofilm formation; EDTA can cause the release of lipopolysaccharides from the cell wall which was thought to have helped promote the formation of biofilms [7].

High affinity iron chelators that have been tested for antimicrobial activity have been inspired by the siderophores, which are high affinity ($K_d < 10^{-25}$ M) Fe^{3+} chelators, such as mycobactins and carboxymycobactins from *Mycobacterium tuberculosis* and yersiniabactin from *Yersinia pestis* [8]. In the study presented in this chapter, a polymer harboring the chelating moiety of the siderophore enterobactin was synthesized. Developing polymers with iron chelating groups provides advantages relative to small molecular weight chelators. These polymers, in addition to having high binding affinity for Fe^{3+}, also have large binding capacity and can sequester iron inside the polymeric structure, where it is not available to bacteria. The polymer is a non-absorbable chelator which could be used as a topical treatment of bacterial infections such as *P. aeruginosa* infections on burns [9]. Cross-linked polymeric materials cannot be absorbed through skin which would reduce concerns about toxicity. There may be a synergistic effect with iron sequestering materials and antibiotics which could reduce the minimum inhibitory concentrations (MIC) of the antibiotics.

The polymer was synthesized by cross-linking primary amine groups in polyallylamine (PAI) with N,N'-methylenebis(acrylamide) (MBA) and conjugating with 2,3-dihydroxybenzoic acid (DHBA) (Figure 2-1) [9]. The iron sequestering polymer (PAI-DHBA) was synthesized with different molar ratios of the cross-linker to the number of total amines. The ratio of DHBA/amines was prepared to be 0, 5, 10, 15, 20, 25, 30, 35, and 40, which was designated as G0, G5, G10, etc. The iron stability constant, iron sequestration capacity, and iron selectivity was tested with the PAI-DHBA with these different ratios and the PAI-DHBA, G25, was chosen to be used in the studies described in this chapter because it showed the highest selectivity with optimal iron-sequestering capacity and stability constant [9]. The growth of bacteria in the presence of G25 was found to be significantly slowed. In addition, some antibiotics were found to be more effective at killing *P. aeruginosa* when used in the presence of G25.

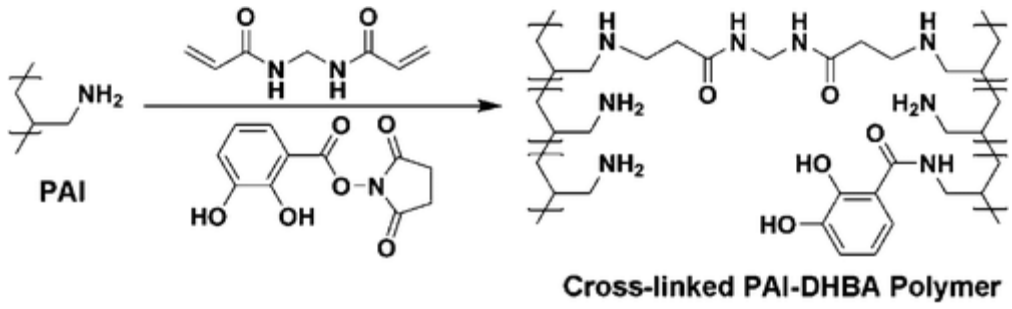

Figure 2-1: Synthesis of the cross-linked PAI-DHBA iron sequestering polymer [9].

Experimental

Materials:

Ciprofloxacin hydrochloride was purchased from MP Biomedicals, Inc. Gentamicin sulfate, sodium ethylene diamine tetraacetate (EDTA), agar, iron sulfate hepta-hydrate, glucose, potassium hydroxide, and casamino acids (BD Falcon) and potassium chloride (KCl) were purchased from Fisher Scientific. Potassium phosphate monobasic, potassium phosphate dibasic, magnesium sulfate, tryptophan, and citric acid were purchased from Sigma. Luria broth media (LB, pH 7.1) was purchased from Teknova. N, N-bis (2-hydroxybenzyl) ethylenediamine-N, N-diacetic acid (HBED) was purchased from Strem Chemicals, Inc. Sodium chloride (NaCl) was purchased from Acros Organics. Potassium dihydrogen phosphate (KH_2Po_4) and disodium hydrogen phosphate (Na_2HPO_4) were purchased from Santa Cruz Biotechnology, Inc.

Bacterial Strains and Growth Conditions

P. aeruginosa strain PA01 purchased from the University of Washington Genome Sciences was used in all studies. *P. aeruginosa* was grown in M63 minimal media, as modified by O'Toole and Kolter [10]. M63 media was prepared by dissolving 2 g/L KH_2PO_4, 13.6 g $(NH_4)_2SO_4$, 3 µM $FeSO_4$-$7H_2O$ and 1 mM $MgSO_4$ per 1L water and autoclaving. Then 2 g glucose, 5 g casamino acids, 0.25 g tryptophan, 4 g citric acid are added. The pH was adjusted to 7.0 with the addition of KOH and then filter sterilized. All glassware was acid washed by soaking in 1% Trace Select concentrated nitric acid (Sigma) and rinsing with nanopure water five times.

Bacterial Growth Using PAI-DHBA-Treated Media

The iron-sequestering polymer PAI-DHBA (G25) was utilized in the following studies with *P.aeruginosa*. The polymer cPAI (G0), without the DHBA iron chelating moiety, or PAI-DHBA (G25) powder was washed twice with phosphate buffer saline (PBS at pH 7.4) and once with deionized water, and then lyophilized. A 50 mL aliquot of M63 media containing 1, 10, or 20 mg/mL insoluble G25 was incubated for 20 min with shaking (230 rpm, 37 °C). In addition, 50 mL of M63 media was also incubated with G0 (13.9 mg/mL) for 20 min to control for the absence of DHBA moieties in the polymer; 13.9 mg/mL G0 was used because this mass is equivalent to 20 mg of G25, which is composed of 13.9 mg of cPAI and 6.1 mg of DHBA. After incubation the polymer was removed from the media by centrifuging the 50 mL at 4000 rpm at 4 °C for 15 min. The supernatant was transferred to an acid washed 250 mL Erlenmeyer flask. 10 mL of the supernatant was removed to measure the iron content using inductively coupled plasma optical emission spectrometry (ICP-OES). Bacterial growth was also examined using M63 media without the addition of iron.

Bacteria were grown from a single colony in 5 mL of LB overnight with shaking at 230 rpm and 37 °C. The overnight inoculum was centrifuged for 12 min at 4000 rpm and 4 °C, and then resuspended in M63. The resuspended cells were added to the 40 mL of polymer-treated or untreated media to give a starting OD_{600} = 0.01. The cells were cultured with shaking at 230 rpm and 37 °C. 1-2 mL was sampled every hour to measure the OD_{600}. At 2, 4, 6, 8, 10 h of growth, 100 µl was sampled and serially diluted in PBS. Ten, 10 µL drops of the dilutions were plated on LB agar and incubated at 37 °C for 18 h. The colony forming units/mL was determined by counting single colonies multiplying by the dilution factor and dividing by the volume plated.

Bacterial Growth in the Presence of PAI-DHBA

An overnight culture in LB was diluted in fresh LB to OD_{600} = 0.3. 10 µL of the diluted culture was added to 1 mL of M63 in a 24 well flat-bottomed plate to give a starting OD_{600} = 0.003. 1, 5, 10, or 20 mg/mL of G25 was added to each well to compare the bacterial growth at different amounts of polymer. The plate was wrapped with parafilm and incubated with shaking at 40 rpm, 37 °C for 12h. The entire culture was removed and serially diluted in PBS and plated on LB agar. The agar plates were incubated for 16-18 h at 37 °C. Single colonies were enumerated to determine the CFU/ mL.

Bacterial Growth in the Presence of PAI-DHBA Compared to Traditional Iron Chelating Agents

The experiment was setup in 24 well plates as previously described. 20 mg of PAI-DHBA or 208 mg of EDTA (500 µM) was added to the media immediately after inoculating with *P. aeruginosa*. The CFU/mL was determined after 5, 6, and 12 h of incubation.

PAI-DHBA as an Adjuvant to Conventional Antibiotics

Ciprofloxacin (1 µg/mL) or gentamicin (24 µg/mL) was added to 24-well plate cultures after 5 h of growth. G25 was added to M63 immediately after inoculation with *P. aeruginosa* or together with the antibiotics after 5 h of growth. At different time of incubation (5, 6, 7, and 9 h), the entire content of each well was serially diluted and plated on LB agar to determine CFU/mL. cPAI (G0) was also tested with ciprofloxacin by adding polymer immediately after inoculating with overnight culture.

Ciprofloxacin was also added to 1 mL cultures after 12 h of incubation in the 24 well plate. G25 (20 mg/mL) was added to media either immediately after inoculation or simultaneously with ciprofloxacin. CFU/mL was determined at 12, 13, 14, 16, and 24 h of growth.

Results

PAI-DHBA is Specific to Iron in the Media

To determine which DHBA/ amine ratio (G0 through G40) would be used for the susceptibility testing, the PAI-DHBA polymers were tested for their iron stability constant, iron sequestration capacity and the iron selectivity (Figures 2-2A, 2-2B, and 2-2C). The iron affinity constant was determined by a ligand competition assay with EDTA which has a log stability constant of 25.1. Figure 2-2A shows that all polymers have at least 10^3 times stronger iron affinity than EDTA[9]. In Figure 2-2B the iron sequestration capacity of the polymers shows the maximum iron adsorption by the polymers (mg Fe/g PAI-DHBA). Theoretically, the iron sequestration was expected to continue to increase, but at G20, the experimental capacity begins to plateau. This was explained by the possible increase of the polymer's hydrophobicity due to DHBA moieties which limited the ability of iron to access the interior of the gel-particle [9]. It was essential to measure the specificity of iron compared to other metals in the media that could affect bacterial growth. To measure the specificity, multiple metals including Fe, Ca, Cu, Mn, Ni, K, and Zn were put into solution at 0.4 mM, and the metal/polymer ratio was fixed at 0.2 mmol per gram of polymer. The polymer absorbed almost all the iron in each sample and very little of the other metals (Figure 2-2C). The PAI-DHBA polymer G25 had the highest selectivity

with optimal iron-sequestering capacity and stability constant. It was then chosen for the testing of antimicrobial activity. M63 media is prepared with the addition of two metals, magnesium and iron. To ensure the G25 polymer was going to be specific towards iron, the total metals absorbed was analyzed. The polymer was capable of sequestering all of the iron in M63 but only 12% of Mg^{2+}, as shown in Figure 2-3. The swelling of the polymer most likely caused the Mg^{2+} to be physically absorbed with water rather than be specifically chelated.

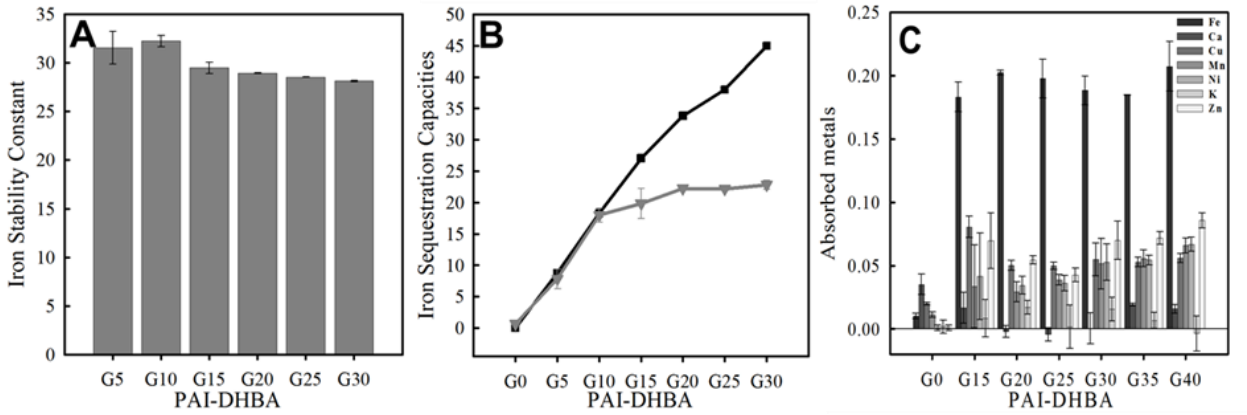

Figure 2-2: (**A**) The iron stability constant (log scale) of the PAI-DHBA polymers was determined using a ligand competition assay. The chelation of iron by PAI-DHBA in water was competed with the water soluble iron chelator, EDTA. (**B**) The iron sequestration capacities (mg Fe/g PAI-DHBA) were determined theoretically in black squares and experimentally in gray triangles. The PAI-DHBA polymers were incubated in the presence of a $FeCl_3$ solution for a week and the remaining Fe was determined. (**C**) The absorbed metals (mmol metal/g PAI-DHBA) were used to determine the selectivity of the PAI-DHBA polymers. These studies were completed by Jian Qian [9].

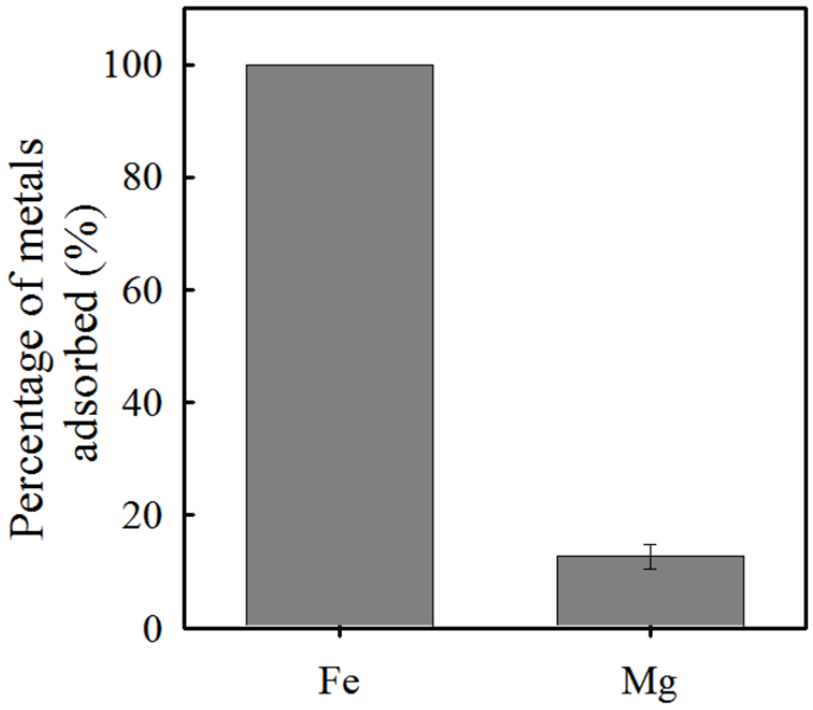

Figure 2-3: Metal selectivity study for PAI-DHBA polymer in M63 media. One mL of media was incubated with 20 mg of G25. This shows the polymer is selective to iron and does not sequester other important metals in the M63 media; therefore the effect on growth is specific to iron sequestration and not magnesium.

PAI-DHBA Treated Media Suppresses Bacterial Growth

P. aeruginosa was grown in the presence of media that was treated with 0, 1, 10, and 20 mg/mL of G25. At 1 and 10 mg/mL G25 there was a delay in bacterial growth, but at 20 mg/mL there was cell death (Figure 2-4A). The polymer at 20 mg/mL is capable of chelating all available iron from the media (Figure 2-3) which leaves nothing for the bacteria to use. Without

iron available to the cells in the culture, cells likely become iron deficient and cannot grow resulting with some cells dying.

The treatment with (G0) which has no iron-chelating DHBA moieties exerted little difference to bacterial growth, similar to that seen with untreated control (Figure 2-4B). When media was not supplemented with iron, there was a longer logarithmic phase and the cell count was about a log lower than the culture in iron-supplemented media after 10 h of incubation. By completely depleting the culture of iron by the addition of 20 mg/mL of G25, the bacteria was unable to grow and led to cell death. This shows that the effect on cell growth is due to the iron sequestration by the chelating moiety of G25 and not the polymer. Polymers have been shown to have antibiotic properties, so it was necessary to verify it was not contributing to the killing of the bacteria [11].

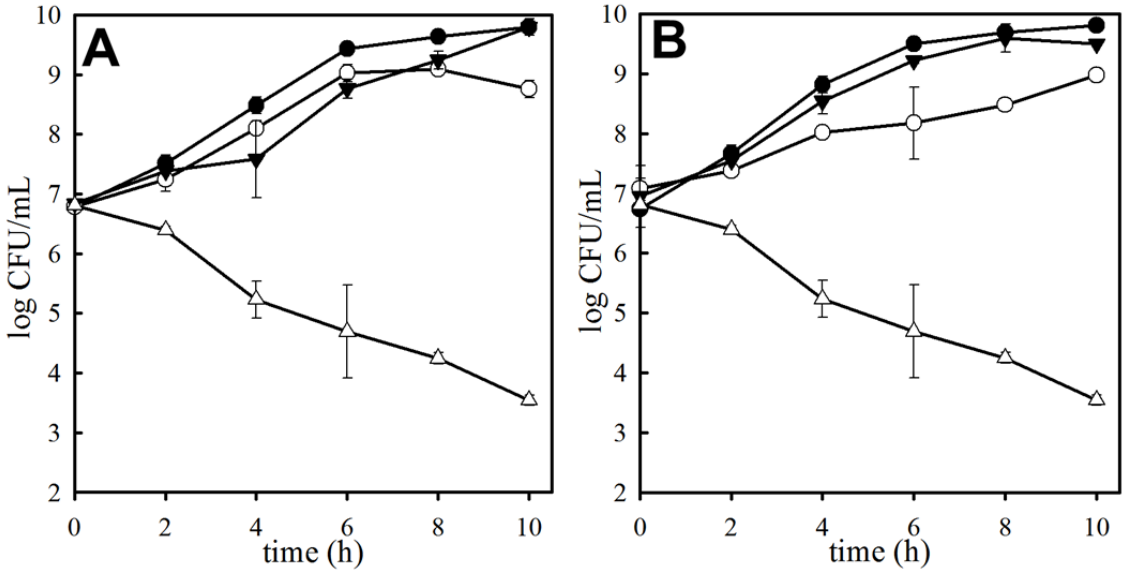

Figure 2-4: Growth curve in the presence of G25. (**A**) M63 was treated with 1 mg/mL (open circle), 10 mg/mL (filled triangle), 20 mg/mL (open triangle), or untreated (filled circle). G25 slows the rate of growth compared to untreated cultures, and results in a lower cell count after 10 h of incubation with 1 mg/mL. At 20 mg/mL of G25, the bacteria are unable to grow and cell death occurs. (**B**) Treating M63 with polymer only, G0 (filled triangle), does cause a delay in bacterial growth. When the media does not have iron added (open circle) there is a slight delay in growth and the final log CFU/mL does not reach the same cell count as the untreated (filled circle). With the addition of 20 mg/mL G25 (open triangle), the cells are unable to survive and cell death occurs.

Treatment of the media with the polymer immediately after inoculation was also investigated. Bacteria were inoculated into 1 mL of media in 24 well-plates, followed by immediate addition of G25 at 0, 1, 5, 10, 15, and 20 mg/mL. After incubating for 12 h each well

was serially diluted and plated on PIA to determine the total cell count. As the polymer concentration increased the cell count decreased, as seen in Figure 2-4. Because of these observations, subsequent experiments were carried out with 20 mg/mL of G25.

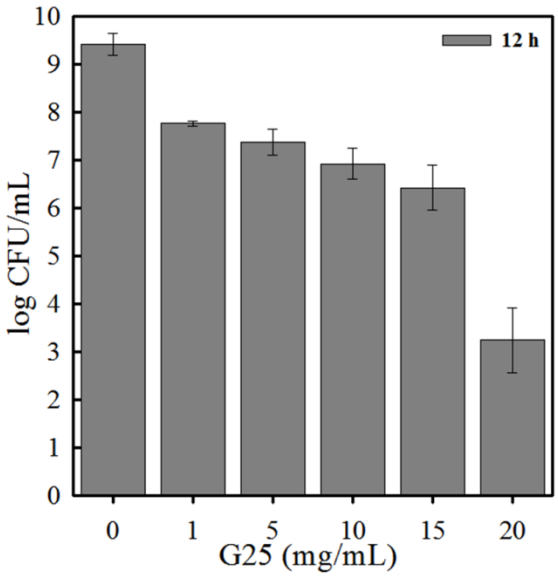

Figure 2-5: The effect of cell growth after 12 h in the presence of different concentrations (0, 1, 5, 10, 15, and 20 mg/mL) of G25. Cultures were grown in 24 well plates and the log CFU/mL was determined after 12 h of incubation. The addition of 20 mg/mL G25 had the greatest effect on bacterial growth.

PAI-DHBA is a More Potent Inhibitor of Bacterial Growth than Traditional Iron Chelators

The PAI-DHBA polymer was compared to other traditional iron chelators to determine if it would have a higher efficacy to prevent or delay bacterial growth. 500 µM of EDTA, a well-known iron (III) chelator, was added to M63 and the effect on cell growth was compared to

untreated culture and culture treated with 20 mg/mL G25. In the presence of EDTA, there was a slight delay in growth after incubating for 5 and 6 h, but after 12 h of growth, the bacterial cell count was similar to that observed in the untreated culture. In comparison, the culture treated with 20 mg/mL of G25 was significantly decreased in cell count at 5, 6, and 12 h, as seen in Figure 2-6. The affinity of EDTA for Fe (III) at pH 7.0 is 10^{25} [12]. Pyoverdine, iron (III) siderophore, released from *P. aeruginosa* also has an affinity constant of 10^{25} [13]. *P. aeruginosa* may have produced pyoverdine when it sensed iron deprivation caused by EDTA. Because of the reversible binding of iron (III) to EDTA, the pyoverdine siderophore can gradually compete with EDTA and allow the cells to acquire iron. In contrast, the polymer sequesters iron nearly irreversibly within its structure, where pyoverdine cannot access, thus preventing the siderophores from capturing the iron from the polymer and leading to the inhibition of iron uptake and cell death.

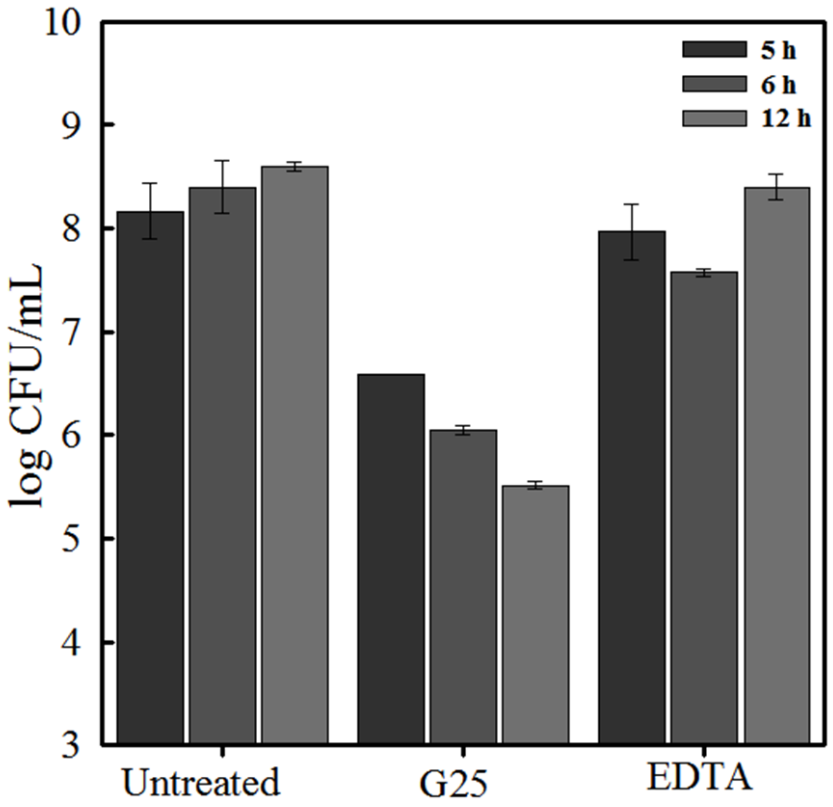

Figure 2-6: The growth of *P. aeruginosa* in the presence of 20 mg/mL G25 compared to 500 µM EDTA. G25 is capable of delaying growth and causes cell death. EDTA causes a slight delay after 6 h of culture, but is unable to prevent the bacteria from recovering and continuing to grow.

Adjuvant Effect of Iron-Sequestering Polymer on the Antimicrobial Activity of Ciprofloxacin and Gentamicin against *P. aeruginosa*

The addition of iron chelators to antibiotics has shown to increase the bactericidal effect of antibiotics [5, 14]. Common antibiotics used to treat *P. aeruginosa* infections belong to the antibiotic classes known as aminoglycosides and fluoroquinolones, such as gentamicin and

ciprofloxacin, respectively [1]. To investigate the adjuvant effect of the polymer to antibiotics, the bacterial survival was tested in two types of conditions. One condition consisted of culturing the bacteria in the presence of G25 (20 mg/mL) for 5 h, then adding the antibiotics (ciprofloxacin at 1 μg/mL or gentamicin at 24 μg/mL) and collecting samples of the cultures at 6, 7, and 9 h. The second condition allowed the bacterial culture to reach mid-log phase (approximately 5 h), then simultaneously add G25 and antibiotics. The cell counts were enumerated at 6, 7, and 9 h of culturing. The concentrations of the antibiotics were used from the reported MICs against *P. aeruginosa* [15].

In Figure 2-7A, the first set of bars show the growth of the bacteria untreated, labelled [G25(-)/Cipro(-)]. When Cipro only [G25(-)/Cipro(+)], was added at 5 h of culturing there was a gradual decrease of survival ending with approximately 4 log CFU/mL of cell survival. When G25 was added at the beginning of growth and Cipro was not added [G25(+)/Cipro(-)], the cell growth was delayed compared to being untreated and cell death occurred to an average around 5 log CFU/mL. The addition of G25 at the beginning of growth and the addition of Cipro at 5 h [G25(+)/Cipro(+)], decreases the viable cells to about 3 log CFU/mL. The addition of G25 immediately after inoculation decreases the viable cells in the culture, so when Cipro is added there is a lower amount of viable cells compared to cultures with Cipro treatment only.

In Figure 2-7B, the G25 was added at the same time as Ciprofloxacin during 5 h of incubation. When G25 was added at 5 h, there is a gradual decrease in cell survival to an average of 6 log CFU/mL at 9 h. The cell survival with G25 and Cipro combined [G25(+)/Cipro(+)] shows faster killing than Cipro alone [G25(-)/Cipro(+)] and the cell survival

is about a log lower. This shows that G25 in combination with Cipro has an adjuvant effect and causes faster killing compared to G25 alone or Cipro alone. In Figure 2-6C, we show that the polymer alone (G0) does not have any antibiotic effect. Although, there is less killing when G0 and Cipro are added together, which may suggest there is some interference with the polymer causing deactivation or sequestering the antibiotic to inhibit it from going into the bacterial cell.

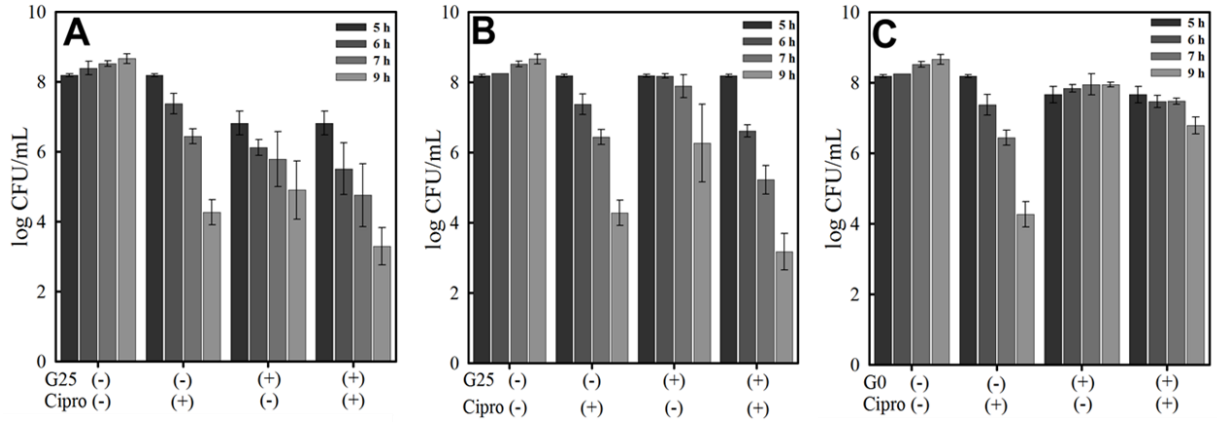

Figure 2-7: (**A**) 20 mg/mL of G25 was added immediately after inoculation and then 1 µg/mL of Cipro was added after incubating culture for 5 h. Samples were collected after 6, 7, and 9 h of incubating to determine cell survival after treatment. (**B**) 20 mg/mL of G25 and Cipro were added together or individually after incubating cultures for 5 h. (**C**) The polymer only (G0) was added immediately to the culture after inoculation and Cipro was added after 5 h of incubating.

Adjuvant Effect of G25 and Gentamicin

The above experiments were repeated using Gentamicin (Gent) instead of Ciprofloxacin to see if there were synergistic effects. Figure 2-8A shows that by adding G25 at the beginning of the culture and Gent at 5 h of incubation [G25(+)/Gent (+)] there are almost 3 logs of killing

from 5 h of growth to 9 h of incubation; whereas, the killing of Gent only [G25(-)/Gent(+)] has only about a log of killing from 5 h to 9 h of treatment. When G25 and Gent are added together [G25(+)/Gent(+)] there is a synergistic effect of about 3 logs of killing after 9 h of incubating .

In Figure 2-8B, G25 is added at 5 h with Gent [G25(+)/Gent(+)] and there is more killing than compared to Gent alone. The log CFU/mL count decreases at each hour and has about a 2 to 3 log decrease in cell survival. This shows there is a synergistic effect if not a greater effect on the susceptibility of *P. aeruginosa* to Gent when G25 is present to reduce the available iron.

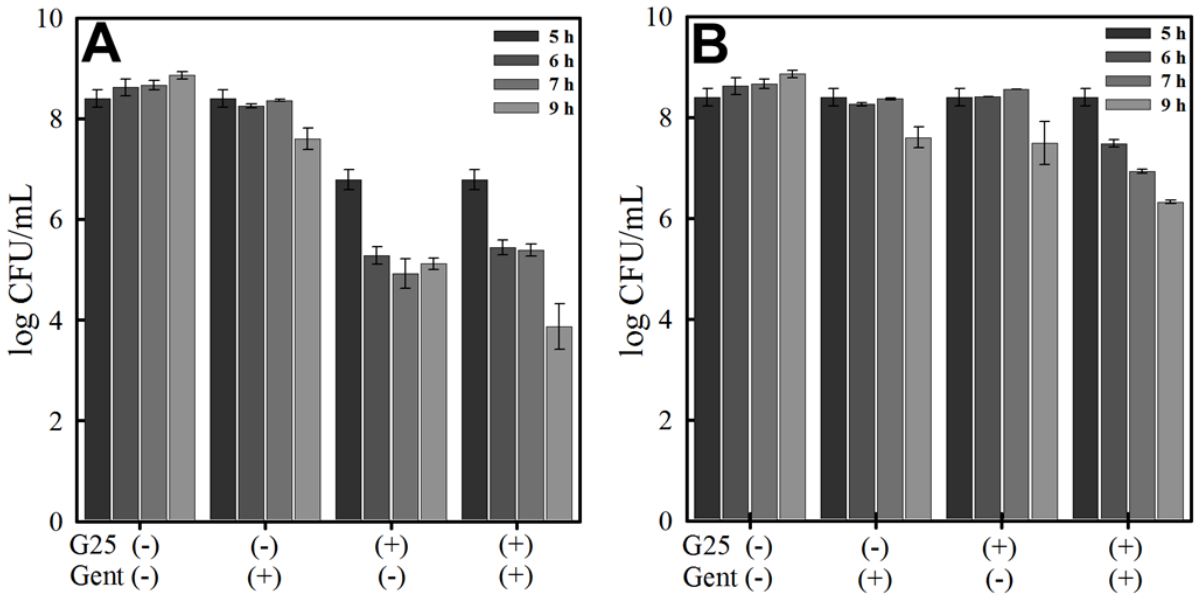

Figure 2-8: Survival of *P. aeruginosa* during log phase when treated with G25 and/or Gent. **(A)** 20 mg/mL of G25 was added immediately after inoculation while 24 µg/mL of gentamycin was added after incubating the culture with or without G25 for 5 h. Samples were collected after 6, 7, and 9 h of incubation to determine cell count by CFU/mL. There were about 2 logs of increased killing with Gent and polymer compared to the polymer only and a difference of 4 logs

of Gent and polymer compared to Gent only. **(B**) Gentamicin (24 µg/mL) and G25 (20 mg/mL) was added after 5 hours and samples were collected after 6, 7, and 9 h to determine cell count. The final log CFU/mL was about 1.5 logs lower with Gent and G25 compared treatment of Gent or G25 only.

Adjuvant Effect of G25 and Ciprofloxacin during Stationary Phase

The effect of the bacteria's susceptibility during the stationary growth phase was also tested in the presence of Cipro and when G25 was added immediately after inoculation or added after 12 h of incubation. In Figure 2-9A, there is about a 4 to 5 log decrease from 12 h to 24 h in cell survival when cultures are treated with Cipro only [G25(-)/Cipro(+)]. In the G25 only treated cultures [G25(+)/Cipro(-)] the cell count varies but stays between 4 and 5 log CFU/mL This shows that there is a limited amount of viable cells that are able to persist in the presence of G25 for 24 hours in the low iron conditions. When Cipro is added to the cultures treated with G25 from the beginning of growth [G25(+)/Cipro(+)] the log CFU/mL decreases from about 5 log CFU/mL to 3 log CFU/mL showing that G25 decreases the number of surviving cells in combination with Cipro.

When G25 was added after 12 h of growth in combination with Cipro, [G25(+)/Cipro(+)], there was about a log increase in killing compared to Cipro only, [G25(-)/Cipro(+)], at 24 h seen in Figure 2-9B. Interestingly, when G25 was added during stationary phase, it did not cause a decrease in cell count. This could be explained by previous iron uptake. The iron that was necessary for cell growth could have already been taken in by the cell and stored in iron storage proteins such as bacterioferritin. Since the iron had already been used or

brought into the cells, G25 would not be capable of removing iron from the media that would be needed for cell growth.

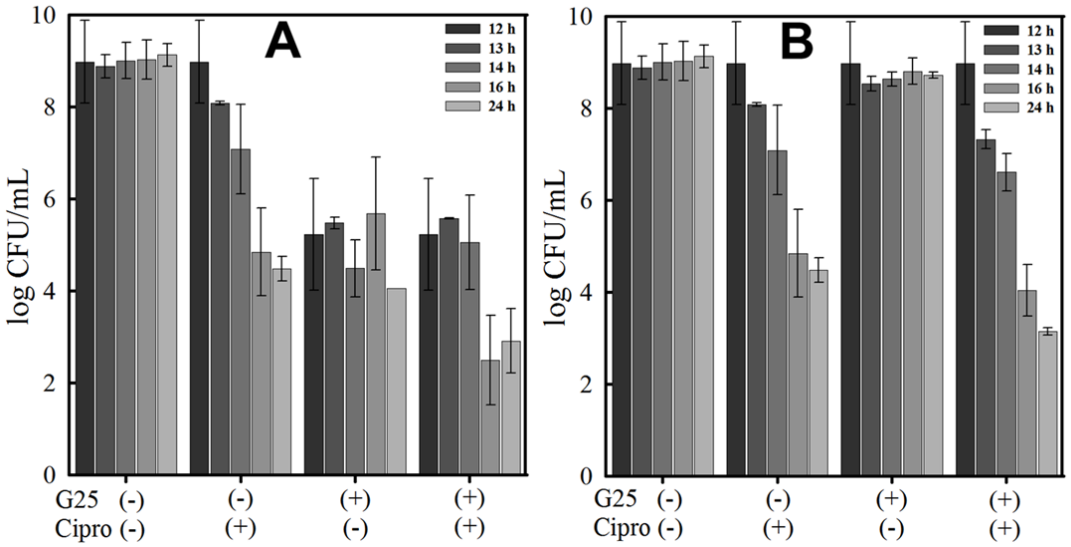

Figure 2-9: Survival of *P. aeruginosa* during stationary phase when treated with G25 and/or Cipro. (**A**) The culture was inoculated and 20 mg/mL of G25 was added immediately. The cultures were grown for 12 h to reach stationary phase and then treated with 1 µg/mL of Cipro. The effect of the polymer in combination with Cipro increased the amount of killing by 1.5-2 logs killing compared to Cipro only or G25 only. (**B**) The addition of the polymer only, Cipro(-) and G25(+), after 12 h did not have a very significant decrease compared to Cipro(+) and G25(+) which saw about 2 logs more killing after 24 h than Cipro(+) and G25(-).

Discussion

The iron sequestering polymer PAI-DHBA, which harbors moieties similar to the chelating ligands of siderophores released by bacteria have high iron affinity and specificity (Figure 2-2). The concentration of 20 mg/mL G25 was determined to be the most effective

concentration to limit cell growth and also to cause cell death. Concentrations below 20 mg/mL caused a slight delay in growth, but there was no killing effect (Figure 2-4). This concentration must have irreversibly removed all iron from the media which prevented the bacteria from obtaining iron to use for the necessary functions of cell metabolism, such as the TCA cycle and DNA synthesis. This also suggests why G25 at 20 mg/mL had a better effect than when EDTA was tested. EDTA is not capable of irreversibly chelating the iron, which allows the bacteria to compete for iron, leading to initial stagnation, followed by growth recovery (Figure 2-6). The recovery is most likely because siderophores secreted by bacterial cells can compete for the iron bound to EDTA. In comparison, iron is irreversibly sequestered within the structure of the PAI-DHBA polymer, where siderophores cannot access it, thus leading to iron starvation, which results in growth arrest and death.

It has been shown that iron chelators increase bacterial susceptibility to antibiotics,[5, 12] so we tested the efficacy of two types of antibiotics, the fluoroquinolone Ciprofloxacin and the aminoglycoside Gentamycin, in the presence of 20 mg/mL G25. When both antibiotics and G25 were added together, there was an increase of killing compared to the antibiotic alone or G25 only, as seen in Figures 2-7 and 2-8. When G25 was added at the time of inoculation, the cells were already at a disadvantage by not having access to iron for metabolic needs (Figure 2-7A and 2-8A). This made the *P. aeruginosa* more susceptible to the antibiotics. When G25 was added at the same time as Cipro (Figure 2-7B), the final log CFU/mL was similar to when G25 was added at the beginning. When G25 and Gent were added at the same time (Figure 2-8B), there was an increased killing compared to treatment with only Gent.

During the stationary phase of growth, cell metabolism changes compared to the log phase of growth, so we tested cells in stationary phase for an adjuvant effect with the iron sequestering polymer and ciprofloxacin. In Figure 2-9A, the presence of G25 only, delayed the growth after 12 h, but there was a similar log CFU/mL at 24 h of incubation. The cell count was very low which shows the limited amount of bacteria that could survive in the depleted concentrations of iron. When Cipro was added to the cultures that had been treated with G25 for 12 h, there was approximately an additional 2 logs killing compared to Cipro or G25 only. This shows the stability of G25 and its ability to chelate iron for long periods of time. Interestingly, when G25 was added after 12 h of growth, there was not a significant change in cell count after 24 h; although there was an additional killing when Cipro was added in combination to G25 at 12 h compared to Cipro alone treatment. G25 effects the growth because it is removing an essential element from the bacteria, but by stationary phase the bacteria has been able to take the necessary amount of iron and store it in iron storage proteins. When Cipro was added, it could add more stress to the cells which is then compacted with the addition of G25. This could lead to the increase killing compared to Cipro only.

These results show the PAI-DHBA iron sequestering polymer, G25, provides an adjuvant effect with two types of antibiotics and is capable of irreversibly removing iron from the environment to inhibit cell growth and cause cell death. This kind of treatment is promising to combat multidrug resistance and shows the importance of available iron for bacterial growth.

References

1. Cai, Y., Yu, X.H., Wang, R., An, M.M., Liang, B.B., *Effects of iron depletion on antimicrobial activities against planktonic and biofilm Pseudomonas aeruginosa.* J.Pharm. Pharmacol., 2009. **61**: p. 1257-1262.
2. Stover, C.K., Pham, X.Q., Erwin, A.L., Mizoguch,i S.D., Warrener, P., Hickey, M.J., Brinkman, F.S., Hufnagle, W.O., Kowalik, D.J., Lagrou, M., Garber, R.L., Goltry, L., Tolentino, E., Westbrock-Wadman, S., Yuan, Y., Brody, L.L., Coulter, S.N., Folger, K.R., Kas, A., Larbig, K., Lim, R., Smith, K., Spencer, D., Wong, G.K., Wu, Z., Paulsen, I.T., Reizer, J., Saier, M.H., Hancock, R.E., Lory, S., Olson, M.V., *Complete genome sequence of Pseudomona aeruginosa PA01, an opportunistic pathogen.* Nature, 2000. **406**: p. 959-64.
3. Poole, K., Srikumar, R., *Multidrug efflux in Pseudomonas aeruginosa: components, mechanisms and clinical significance.* Curr.Top Med.Chem., 2001. **1**: p. 59-71.
4. Andrews, S.C., Robinson, A.K., Rodriguez-Quinones, F., *Bacterial iron homeostasis* FEMS Microbiol. Reviews, 2003. **27**: p. 215-237.
5. Reid, D., O'May, C., Kirov, S., Roddam, L., Lamont, I., Sanderson, K., *Iron chelation directed against biofilms as an adjunct to conventional antibiotics.* Am. J. Physiol.: Lung Cell. Mol. Physiol., 2009. **296**: p. L857-L858.
6. Moreau-Marquis, S., O'Toole, G.A., Stanton, B.A., *Tobramycin and FDA-approved iron chelators eliminate Pseudomonas aeruginosa biofilms on cystic fibrosis cells.* Am. J. Respir. Cell Mol. Biol., 2009. **41**: p. 305.
7. Liu, Y., Yang,L.,Molin, S., *Synergistic Activities of an Efflux Pump Inhibitor and Iron Chelators against Pseudomonas aeruginosa Growth and Biofilm Formation.* Antimicrob Agents Chemother, 2010. **54**: p. 3960-3963.
8. Stirretta, K.L.F., J.A; Jayaprakashb, V; Sinhab,B.N; Renc,T; Quadria,L.E., *Small molecules with structural similarities to siderophores as novel antimicrobials against Mycobacterium tuberculosis and Yersinia pestis.* Bioorganic & Medicinal Chemistry Letters, 2008. **18**: p. 2662–2668.
9. El-Gendy, N., Qian, J., Eshelman, K., Rivera, M., Berkland, C., *Antibiotic Activity of Iron-Sequestering Polymers.* 2015. **16**: p. 1480-1488.
10. O'Toole, G.K., H; Kolter, R, *Biofilm Formation as Microbial Development.* Annual Rev.Microbiol., 2000. **54**: p. 49-79.
11. Munoz-Bonilla, A., Fernandez-Garcia, M., *Polymeric materials with antimicrobial activity.* Progress in Polymer Sci., 2012. **37**: p. 281-339.
12. Bergeron, R.J., Brittenham, G.M., Eds. , *The development of iron chelators for clinical use*1993, Boca Raton, FL.: CRC Press.
13. Cody, Y.S., Gross, D.C., *Characterization of pyoverdinpss, the fluorescent siderophore produced by Pseudomonas syringae pv. syringae.* Appl. Environ. Microbiol., 1987. **53**: p. 928-934.
14. Moreau-Marquis, O.T., G.A., Stanton, B.A., *Tobramycin and FDA-approved iron chelators eliminate Pseudomonas aeruginosa biofilms on cystic fibrosis cells.* Am J Respir Cell Mol Biol. , 2009. **3**: p. 305-313.

15. Chalkley, L., Koornhof, H., *Antimicrobial activity of ciprofloxacin against Pseudomonas aeruginosa, Escherichia coli, and Staphylococcus aureus determined by the killing curve method: antibiotic comparisons and synergistic interactions.* Antimicrob. Agents Chemother., 1985. **28**: p. 331-342.

Chapter 3 : Iron Mobilization from BfrB is Essential for Iron Homeostasis in *P. aeruginosa*

Introduction

Iron is an essential metal used as a cofactor or prosthetic group for enzymes that participate in many cellular functions and metabolic pathways, including electron transport, glycolysis, DNA synthesis, the citric acid cycle (TCA), oxygen transport, nitrogen fixation, and defense against toxic reactive oxygen species [1-3]. Although iron is essential, it has poor bioavailability and the free metal ion can catalyze the formation of hydroxyl radicals [4]. At physiological pH the ferric ion (Fe^{3+}) has a solubility of approximately 10^{-18} M [5]. Free ferrous (Fe^{2+}) iron can readily oxidize to ferric iron in the presence of hydrogen peroxide to form hydroxyl radicals, in a reaction known as the Fenton reaction [6]. There is no innate defense for hydroxyl radicals, which are extremely reactive and detrimental to living cells because they damage proteins and DNA [6]. Consequently, the concentration of free intracellular iron in cells is strictly regulated [6].

Bacteria have iron storage proteins known as ferritin-like molecules, which play important roles in iron homeostasis by storing iron and ameliorating iron-induced toxicity, but also by providing a source of iron when bacteria encounter low iron conditions [3]. There are three known ferritin like molecules in bacteria, bacterial ferritin (Ftn), bacterioferrin (Bfr), and DNA protection during starvation (DPS) [7]. Ferritins are found in all domains of life including aerobic and anaerobic organisms [5]. Bacterioferritins are found exclusively in bacteria, and

DPS are present in bacteria and archaea [7]. Bacterial ferritins and bacterioferritins are 24-mer proteins with similar spherical and hollow structures, assembled from a single type of subunit, which can hold approximately 4500 iron ions in their hollow interior cavity [8]. The structure of DPS differs from Ftn and Bfr in that DPS is assembled from only 12 subunits and can accumulate up to 500 iron ions [7]. In *E. coli*, DPS binds to DNA and protects it from iron-induced oxidative degradation [9]. Consequently, among ferritin-like molecules in bacteria, only Ftn and Bfr are thought to function primarily as iron storage proteins.

In *P. aeruginosa*, like other bacteria, it is now known that both Ftn and Bfr are present [10]. When bacterioferritin was first isolated from *P. aeruginosa*, it was proposed that it consisted of two distinct types of subunits, α and β [11]. Further investigation established two genes coding for ferritin-like molecules in *P. aeruginosa*, which were termed *bfrA* and *bfrB* [12], and it was assumed that the products of these genes constitute each of the subunits that constitute *P. aeruginosa* Bfr. This was later questioned based on the different genetic regulation and structural differences of the two genes [13, 14]. By mining published data on the genetic and transcriptional response of *P. aeruginosa* cells at low and high iron conditions, it was revealed there were differences in *bfrA* and *bfrB* transcription. In a study completed by Palma *et al.,* only the *bfrB* gene was reported to respond to high iron concentrations during exponential phase, while there was no change in *bfrA* transcription [14]. It was shown during stationary phase that *bfrA* is slightly up-regulated in response to high iron concentrations [11]. It has also been suggested that *bfrA* may function in defense against oxidative stress, and it has been speculated that *bfrA* may provide iron for heme assembly and incorporation into catalase A [12]. More recently our group cloned the *bfrA* and *bfrB* genes and characterized the corresponding proteins

structurally and biochemically [15] and showed structural differences between the two proteins. Specifically, the product of the *bfrB* gene is a genuine bacterioferritin (BfrB), which binds 12 heme molecules. In contrast, the product of the *bfrA* gene does not bind heme and lacks methionine 52 (or equivalent residue), which coordinates heme molecule in bacterioferritins. Hence the name BfrA is a misnomer, which has been changed to FtnA [13]. These findings demonstrated that in *P. aeruginosa*, like in most bacteria, there are two types of ferritin like molecules, which are now termed FtnA (formerly BfrA) and BfrB. It was also shown there are different requirements for the release of iron from BfrB and from FtnA *in vitro*. For iron to be mobilized from the core of BfrB, Bfd (bacterioferritin associated ferredoxin) is required, whereas mobilization of iron from FtnA does not require a Bfd [1, 13, 16]. In multiple pathogens that contain a bacterioferritin including *P. aeruginosa*, the *bfd* gene is located adjacent to the *bfrB* gene [8]. For iron release from FtnA, only NADPH and a reductase (Fpr) are needed for rapid iron release *in vitro* [7]. It is curious why there would be this redundancy to contain two iron storage proteins, unless one of the proteins participated in other functions.

In our lab, we have extensively studied the bacterioferritin (BfrB) from *P. aeruginosa* and its associated ferredoxin, Bfd. We have shown through *in vitro* studies that mobilization of iron from the BfrB core requires Bfd [8, 17]. We obtained the co-crystal structure of the BfrB:Bfd complex, which confirmed the interaction between the two proteins [8]. The structure also provided a look into the pathway for the electrons to move from the [2Fe-2S] cluster in Bfd to the heme in BfrB, and then into the core to reduce the iron (III) to iron (II), which can be released from the protein (Figure 3-1). The primary residues in BfrB that interact with Bfd during binding have been determined from analysis the co-crystal structure and *in vitro* studies

by mutating residues to alanine (Figure 3-2) [17]. The binding affinity of the BfrB: Bfd complex was determined to be around 3 µM. When the BfrB residues leucine 68 and glutamate 81 were mutated to alanine, the binding affinity became undetectable [17]. The double mutant was also incapable of releasing iron from mineralized BfrB in the *in vitro* iron release assays [17].

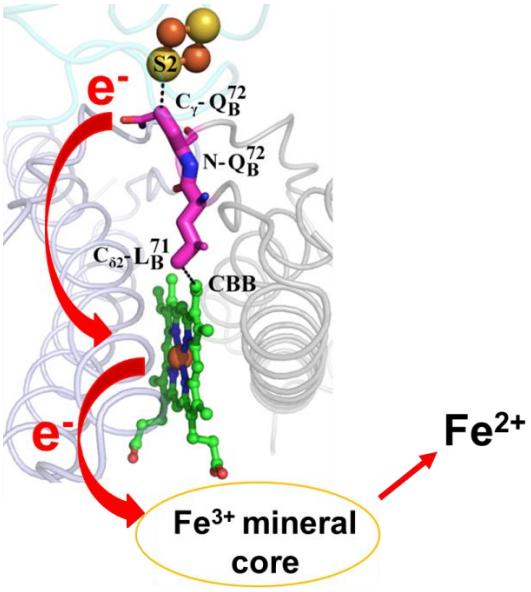

Figure 3-1: Electron path from the [2Fe-2S] cluster in Bfd to reduce Fe^{3+} in the core of BfrB. BfrB is shown in grey and Bfd is the faded cyan. Electrons travel from the [2Fe-2S] cluster of Bfd to the heme and then to the Fe^{3+} mineral core. When Fe^{3+} is reduced, Fe^{2+} is released outside of BfrB [17].

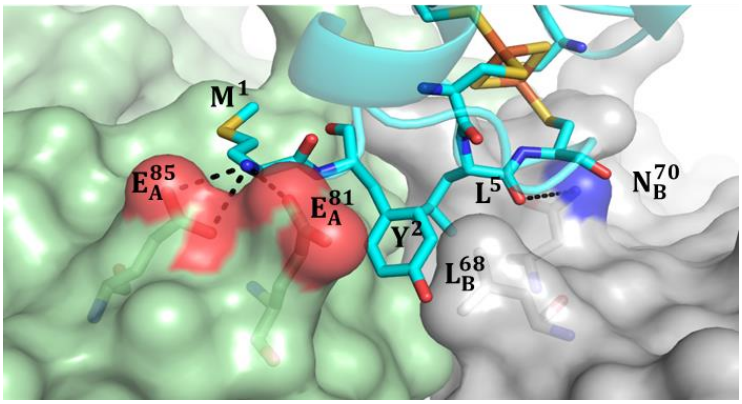

Figure 3-2: BfrB:Bfd interaction site. The BfrB surface is shown in green and grey, Bfd residues are in cyan. Key residues from BfrB that interact with Bfd include E85, E81, L68, and N70. The oxygen atoms in E85 and E81 interact with M1 from Bfd and there is a cleft between E81 and L68 that allows for Y2 from Bfd to anchor at the BfrB surface [17].

In this research, we analyze the disruption of iron homeostasis when we inhibit the BfrB-Bfd interaction in *Pseudomonas aeruginosa*. To this end, gene knockout mutants Δ*bfd* and Δ*bfrB*, and the chromosomal double point mutation on the *bfrB* gene, called *bfrB**, were prepared. The double mutation was introduced into the *bfrB* gene of *P. aeruginosa* on the basis of our *in vitro* results, which showed that the BfrB L68A/E81A double mutant does not interact with Bfd, leading to inhibition of iron mobilization of iron stored in BfrB [17]. We show that iron is stored during late log phase in BfrB and is used in stationary phase when iron concentrations in the environment become depleted. In response to lacking Bfd and disrupting the protein-protein interaction between BfrB and Bfd, the mutants experience iron starvation at a faster rate than WT. We show that by inhibiting the BfrB:Bfd interaction in *P. aeruginosa* cells iron gets "stuck" in the bacterioferritin, so the iron that has been stored is unable to be used by

these mutants. Consequently, there is lower free intracellular iron concentrations in the Δ*bfd* and *bfrB** mutants relative to wt. The ability to mobilize iron stored in BfrB gives wt *P. aeruginosa* cells an advantage when placed in low iron growth conditions compared to the Δ*bfd* or *bfrB** mutants. Under these conditions, we show the function of Bfd binding to BfrB is an essential aspect to regulating free intracellular iron concentrations in *P. aeruginosa*.

Experimental

Bacterial strains, media and growth conditions

All chemicals were obtained from Fisher Scientific unless otherwise stated. The bacterial strain *Pseudomonas aeruginosa* PA01 was purchased by the University of Washington, Manoil Lab. The mutant and complemented strains Δ*bfrB,* Δ*bfd,* Δ*bfrB** were prepared by Jacqueline Stevens in the Chandler Lab at the University of Kansas. Pseudomonas Isolation (PI) media (20 g/L peptone, 1.4 g/L magnesium chloride , 10 g/L potassium sulfate, 25 mg/L Irgasan (Sigma-Aldrich), and 20 mL/L glycerol, pH 7.0) was used for normal growth conditions. An acidic stock solution of 20 mM $FeS0_4$-$7H_2O$ was added to the PI media to give 8 or 10 μM Fe final concentrations. All strains were kept on Pseudomonas Isolation Agar (PIA) (BD Biosciences). Cultures (250 mL PI media in 500 mL Erlenmeyer flasks) were inoculated from a 5 mL overnight culture grown in PI media to an optical density at 600 nm (OD_{600}) of 0.001 and incubated with shaking at 230 rpm and 37 °C. This growth condition was used for all experiments but for growth in low iron. Glassware was rinsed with 1% Trace Select nitric acid (Sigma) and then rinsed 5 times with nanopure water before use.

To culture cells in low iron conditions we used Phosphate media. Phosphate media consists of 24 g/L HEPES, 0.93 g/L Ammonium sulfate, 3.245 g/L succinic acid, 615 mL of 2 mM K_2HPO_4 (Sigma-Aldrich) and 385 mL of 2 mM KH_2PO_4 (Sigma-Aldrich) at pH 7.0. The following trace metals were added to 1 L of phosphate media: 2 mL of 1 M $MgSO_4$, 100 µL of 4 M $CaCl_2$, 10 µL 15 mM Ammonium molybdate, 1 mL 17 mM EDTA, 300 µL 10 mM $CuSO_4$, 100 µL 20 mM $Co(NO_3)_2$, 100 µL 94 mM $Na_2B_4O_7$, and 100 µL 76 mM $ZnSO_4$.

Growth Curves

P. aeruginosa was cultured in 250 mL PI media with 7-8 µM as described in growth conditions. Samples (100 µL) from 250 mL PI cultures were removed every 2 h, serially diluted in phosphate buffer saline (PBS), pH 7.4 and plated on PIA plates. Plates were incubated for 18 h at 37 °C. Colony forming units per mL were determined by counting the number of cells, multiplying by the dilution factor and dividing by the total volume plated.

Imaging Iron Storage in Bacterioferritin

P. aeruginosa strains were cultured in 250 mL PI media with 7-8 µM as described in growth conditions. Samples (15 mL) were collected 6, 8, 10, 12, 24, 36, and 48 h post inoculation and centrifuged in 50 mL conical tubes at 4,000 rpm and 4 °C for 15 min. The supernatant was removed and the cell pellets resuspended in 1 mL of 50 mM Tris-base buffer (pH 8.0) containing 5 mM EDTA and 200 mM NaCl, transferred to a 1.7 mL microcentrifuge tube and centrifuged for 10 min at 13,300 rpm, 4 °C. The supernatant was removed and the cell pellet was frozen at -80 °C overnight. Frozen cell pellets were thawed at room temperature and lysed with 200 µL of 20 µg/mL Lysozyme (Gold Bio) in 50 mM Tris-base buffer (pH 8.0) and

incubated at 37 °C for 45 minutes. 50 µL volume of 10 µg/mL DNase (Gold-Bio) in 50 mM Tris-base buffer (pH 8.0) containing 5 mM $CaCl_2$, 10 mM $MgSO_4$ was added. 5x native loading dye (5.9 mL water, 0.5 mL glycerol, 0.4 mL β-mercaptoethanol, 0.4 mL 1% bromophenol blue, and 0.5 mL 1 M Tris-HCl pH 6.8) was added in a 1:1 ratio to cell supernatant and 80 µL of the resultant solution was loaded onto an 8% native PAGE gel in a Protean II XI electrophoresis cell (Bio-rad). The gel ran for 2 h at constant 25 mA and then 6 h at constant 35 mA. The electrophoresis buffer was kept cold (close to 4 °C) during the separation experiment to prevent over-heating. The native gel was stained for 10 min in the dark by immersion in a solution containing Ferene-dye (0.044 g Ferene, 125 µL thioglycolic acid, 2.4 mL acetic acid and 117.4 mL water).

Growth Curves in Low Iron Media

P. aeruginosa strains were cultured in 250 mL PI media with 7-8 µM as described in growth conditions for 10 hours or 24 hours. 1 mL samples from each time point were removed from 250 mL culture, pelleted and resuspended in Phosphate media. The OD was measured and cells were diluted to an OD_{600}= 0.01 in a total culture volume of 200 µL in a 96 well plate with the lid. The OD was measured for 24 hours in a Spectramax i3x plate reader set at 37 °C. The plate reader was set to orbital shake on high every- other 15 minutes while recording the OD_{600} every 30 minutes.

Pyoverdine Release

The release of pyoverdine was studied in plates and in liquid culture. In the case of plates, single colonies of *P. aeruginosa* (wild type and mutants) were grown overnight (14 h) in 5 mL

Luria-bertani media (25 g/L, pH 7.0). 100 µL of overnight culture was serially diluted in PBS to 10^6 times. Ten 10 µL drops of the 10^6 dilution was plated on PIA plates, dried at room temperature until no drop was visible, and incubated in the dark at 37 °C for 24 h. Complemented strains were grown in 1 mM IPTG (Gold-bio) added 5 mL overnight cultures. 250 µL of a 20 mM IPTG stock solution, dissolved in water, was added to a final volume of 5 mL LB. 5 µL of 1 mM IPTG was spotted on PIA plate and air dried before plating strains. The complemented strains were diluted as done for wt and mutants and spotted on the same location on the PIA plates as the dried IPTG drops. Fluorescence was imaged by UV light.

To measure the release of pyoverdin in 250 mL PI liquid culture, at 12, 24, 36, and 48 hours, 1 mL of culture was removed and centrifuged for 3 minutes at 13,300 rpm, 4 °C. The supernatant was added to 1 mL of chloroform. The water phase was separated and diluted 1000x in 200 mM Tris pH 7.4 with 5 mM EDTA. It was immediately measured using fluorescence by exciting at 400 nm and scanning from 425-600 nm. Emission intensity at 460 nm was compared to CFU/mL to normalize the values between strains.

Total Iron Analysis

At 12 and 24 hours, 15 mL of 250 mL PI culture were removed and centrifuged at 13,300 rpm and 4 °C for 10 min. using a SS-34 Sorvall rotor. Cell pellets were resuspended in 1 mL of PI media containing 0.5 mM diethylenetriaminepentaacetic acid (DTPA) (Sigma-Aldrich). Cell pellets were washed twice with 1 mL PI media with 500 µM DTPA and centrifuged for 10 minutes at 13,300 rpm, 4 °C. The supernatant was removed by a pipette and cell pellets were dried at 60 °C for 1 h. Organic matter was digested with 500 µL of digestion reagent (500 µL

concentrated HCl and 0.225 g of $KMn0_4$ in 10 mL of water). Solution was thoroughly mixed by vortexing then placed in a hot water bath (70 °C) for 4-6 h, or until the solution became mostly colorless. Iron was analyzed by adding 300 μL of the iron detection reagent (6.5 mM ferrozine, 1 M ascorbic acid, and 2.5 M ammonium acetate (Sigma-Aldrich)). After 15 minutes the sample was centrifuged for 5 minutes at 13,300 rpm the absorbance at 564 nm was measured using a Varian-Cary UV-vis spectrophotometer. Iron concentration was determined using the epsilon value of ferrozine, 27.9 $mM^{-1}cm^{-1}$.

Iron Analysis in Spent Media

Iron analysis in spent media was determined by sampling 2 mL into acid washed glass vials in triplicate from 15 mL of culture that had been centrifuged similar to total cell analysis at 6, 12, 24, 36, and 48 h post inoculation. The media was frozen and freeze dried with a Savant Speed Vac SC110 for approximately 4-5 h. Organic matter from media was digested in 500 μL of digestion reagent for 2 hours with vortexing every 30 minutes in a 70 °C water bath. Iron was analyzed by adding 300 μL of the iron detection reagent and vortexed to mix. After 15 minutes the sample was centrifuged for 5 minutes at 13,300 rpm the absorbance at 564 nm was measured using a Varian-Cary UV-vis spectrophotometer. Iron concentration was determined using the epsilon value of ferrozine, 27.9 $mM^{-1}cm^{-1}$. To blank the spectrophotometer, an extra sample at each time point (6, 12, 24, 36, and 48 hours) was taken and digested as the other samples. 300 μL of blank reagent (1 M ascorbic acid, and 2.5 M ammonium acetate) was added. The sample was vortexed to mix, incubated for 15 minutes at room temperature, and centrifuged for 5 minutes at 13,300 rpm. The supernatant from the 6 hour sample was used to blank the

spectrophotometer for the 6 hour samples, the 12 hour sample was used to blank the 12 hour samples, and so forth for each time point.

EPR of Free Intracellular Iron

In the 250 mL PI media cultures, the entire culture was collected at 12 and 24 h of incubation. 100 µL of culture was collected from each strain in triplicates, serially diluted in PBS and plated on PIA to determine cell counts. The cultures were centrifuged for 12 min at 4500 rpm and 4 °C. The cell pellets were resuspended in 6 mL of PI media with the addition of 1 mL of 100 mM DTPA in PI media pH 7.4 and 1 mL of 200 mM deferoxamine (DFO) (Sigma) in PI media pH 7.0 and incubated for 10 min at 37°C, 230 rpm. The cells were centrifuged at 4000 rpm, 4 °C for 10 minutes and washed twice with ice cold PBS. The cells were resuspended with 300 µL of PBS with 10% glycerol, packed into EPR tube, and frozen in dry ice and acetone.

Results

BfrB is the Primary Iron Storage Protein in *P. aeruginosa* PA01

Given that there are two types of iron storage proteins in *P. aeruginosa* [13], FtnA and BfrB, it is important to determine whether iron is stored in both proteins, or if the cell deposits iron reserves primarily in one of them. To determine this, cultures of wt and the Δ*bfrB* mutant were grown in PI media containing about 8 µM of iron. Samples were collected from the cultures at different times, the cells were lysed, the proteins separated on a native PAGE gel, and the gel was stained with the dye Ferene, which specifically stains iron stored in iron storage proteins [18]. The presence of a blue stain signifies stored iron (Figure 3-3A); the darker the blue color, the more iron is present in the protein. We utilized pure samples of recombinant BfrB and FtnA

as standards. Figure 3-3A shows that in the wt strain, iron begins to accumulate to detectable levels during the late log phase of growth (6-8 hours), according to the growth curve in Figure 3-3B. It is noteworthy that iron only accumulates in BfrB. In agreement, in the mutant where the *bfrB* gene has been deleted (Δ*bfrB*) iron is not accumulated at all. In the absence of BfrB, if FtnA would function as an iron storage protein, there would be a stain present, but there is not. This suggests that under the experimental conditions, *P. aeruginosa* PA01 uses BfrB as the primary iron storage protein.

Figure 3-3A also shows that in wt *P. aeruginosa* iron stored in BfrB is utilized during the stationary phase, when iron in the media reaches low concentrations (~ 2 μM Fe): Figure 3-3C, the media started with approximately 10 μM Fe and it shows that iron is taken by the cells relatively rapidly until the concentration of iron in the media reaches approximately 2 μM, at around 24 h; beyond this time, iron is taken significantly more slowly. Inspection of Figure 3-3A shows that beyond 12 h, iron stored in BfrB appears to be mobilized, probably to support cell metabolism.

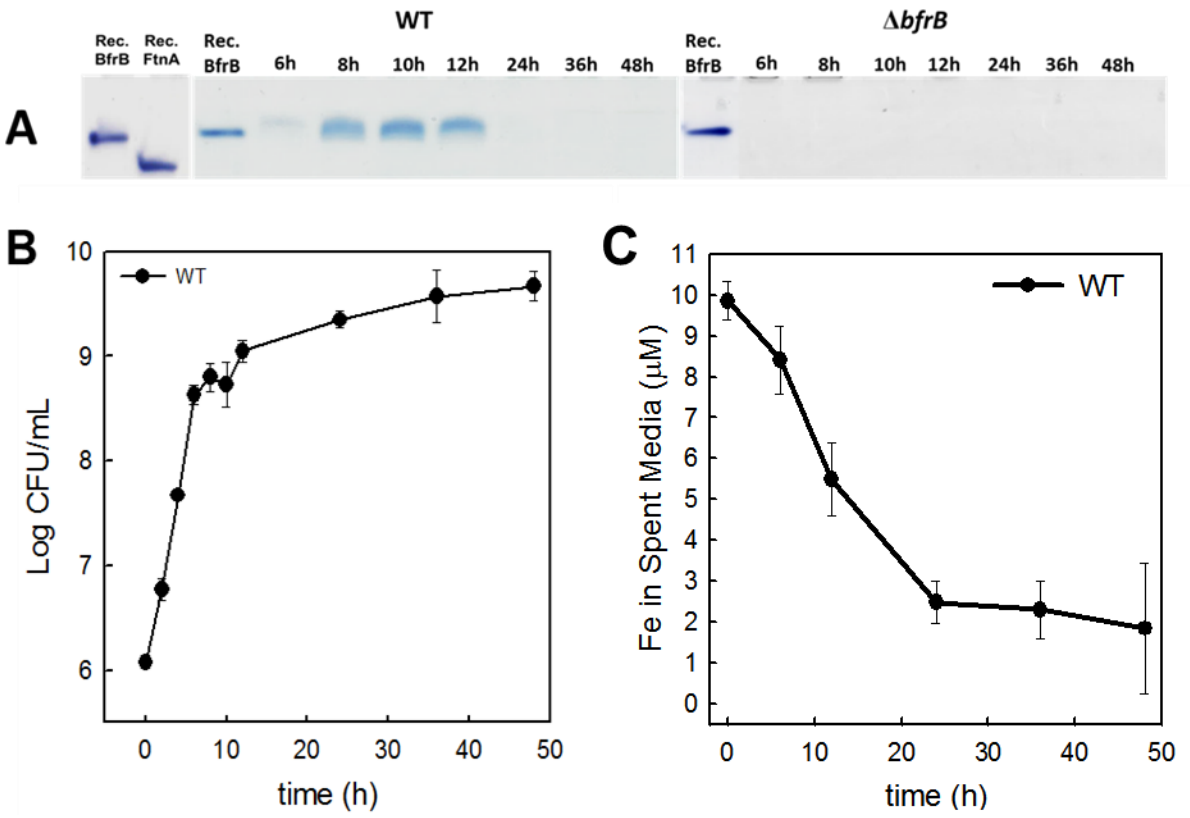

Figure 3-3: Iron storage in BfrB. (**A**) The recombinant (Rec.) mineralized BfrB and FtnA proteins were used as standards in the native PAGE gels and stained with the iron specific, Ferene stain. Note that the native gel can resolve FtnA and BfrB. The bands obtained from separating lysates of wt *P. aeruginosa* cells indicate that iron is accumulated in BfrB during log phase and in early stationary phase. Cell growth is depicted by the growth curve shown in (**B**). Note that lysates of the Δ*bfrB* mutant show that there is no accumulation of iron, which indicates that BfrB is the primary iron storage protein in *P. aeruginosa*. The plot in (**C**) shows the rate at which iron is taken by wt *P. aeruginosa* cells.

Δ*bfd* and *bfrB** Mutants have Iron "stuck" in BfrB

When grown in PI media containing ~ 7-8 μM Fe, all mutant strains grow similarly to wt, as seen in the growth curves shown in Figure 3-4A. As mentioned previously, our *in vitro* studies showed that Bfd is necessary for mobilizing iron from BfrB [8]. Interestingly, we made similar observation in *P. aeruginosa* cells: The native PAGE gels in Figure 3-4B show that in wt *P. aeruginosa* cells the iron stored in BfrB is mobilized, so that it becomes undetectable by the 24^{th} h of culture. In contrast, in Δ*bfd* and *bfrB** mutants, the iron stored in BfrB stays in the protein even at 48 h of culture. These results clearly demonstrate that the insights gained from the *in vitro* studies are actually replicated in the cells. Bfd is necessary for iron release and when it is not present, as in the Δ*bfd* mutant, or is unable to bind BfrB, as in *bfrB** mutant, then iron is not mobilized from the core of BfrB. It should be noted, the standard for *bfrB** on the native gel is the recombinant BfrB with the single mutation E81A. The double point mutation E81A/L68A in *bfrB**, and more specifically the replacement of a charged residue (E81) for a non-charged alanine, changes the size to charge ratio of BfrB, which results in different mobility of the mutant BfrB protein in the native PAGE gels relative to BfrB.

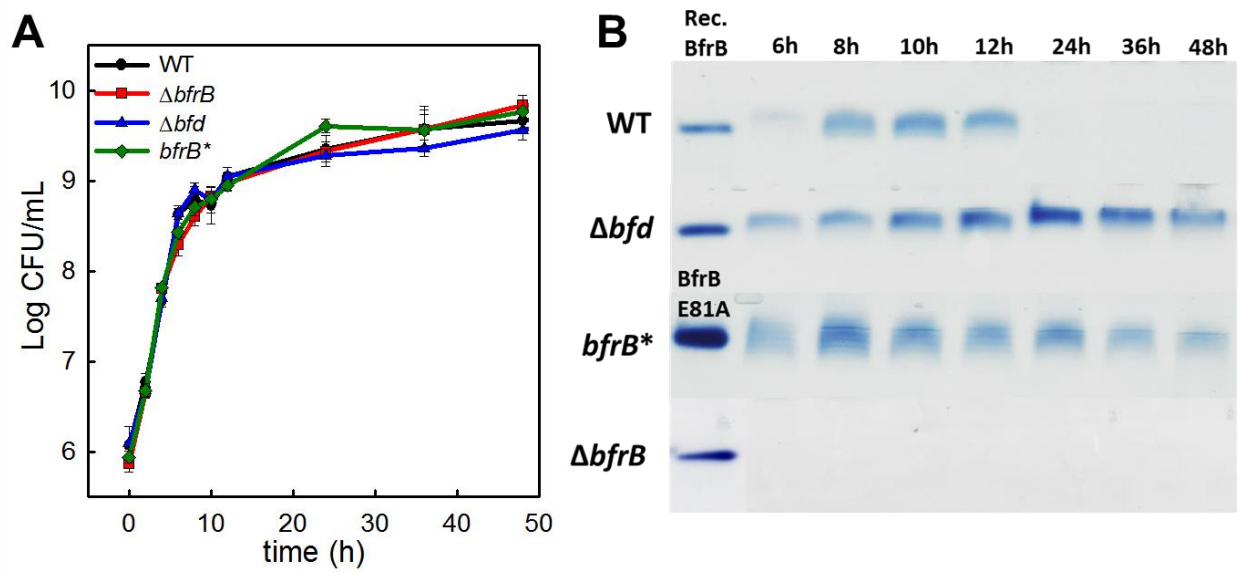

Figure 3-4: Growth curve and iron storage of wt and mutants. (**A**) When the cells are grown in iron sufficient media (> 5 μM), the wt and mutant cells grow at the same rate and to similar cell density. (**B**) Native PAGE gels showing that iron is stored in BfrB in all strains. Although the iron concentration in the media at the start of the experiment is the same for all strains, the wt cells need to mobilize iron stored in BfrB after 24 h of culture, whereas iron stored in BfrB of the Δ*bfd* and *bfrB** mutants appears to be "stuck". These observations indicated that without Bfd, or the ability of Bfd to bind to BfrB (*bfrB**), iron is irreversibly stuck in BfrB. The recombinant protein BfrB E81A is used for the standard for the *bfrB** native gel.

Δ*bfd* and *bfrB** Mutants Release Greater Amounts of Pyoverdine

The consequences of irreversible accumulation of iron in BfrB in the Δ*bfd* and *bfrB** mutants causes a disruption in iron regulation. One manifestation is the increased release of pyoverdine (Pvd) from the two mutants compared to the wt strain. Pvd is a siderophore (high affinity Fe^{3+} chelator) secreted by *P. aeruginosa* when the cells sense iron starvation [19].

Although all the strains are cultured in media with the same concentration of iron, the Δ*bfd* and *bfrB** mutants, which are unable to utilize iron stored in BfrB, we suspect they feel the need to obtain more iron from the environment. Pvd is a fluorescent molecule so its fluorescence can be observed when illuminated by the light of a transilluminator. Figure 3-5A shows the results from overnight cultures of wt, Δ*bfd,* and *bfrB** that were serially diluted, plated on PIA plates, and then incubated in the dark at 37 °C for 24 h. These plates were illuminated with a UV-light and imaged. The images show that the Δ*bfd* and *bfrB** mutants release much more Pvd than the wt strain. To show that large secretion of Pvd by the mutants is due to the absence of the *bfd* gene or the double mutation made in the chromosome in *bfrB**, the *bfd* and *bfrB* mutants were complemented by expression of the *bfd* or *bfrB* genes from a neutral site in the chromosome. As can be seen in Figure 3-5B, the complementation causes a decrease in Pvd release in both mutants. This shows that Pvd release in the mutants is related to iron getting stuck in BfrB and causes the bacteria to feel like it is in low iron conditions. Once the iron is released from BfrB, as seen in the complemented strains, the bacteria no longer feels iron starved and does not need to release high concentrations of Pvd.

The release of Pvd in the liquid cultures was studied as a way to quantitate Pvd release and to correlate the observations of iron uptake, as judged by measuring iron in the media at different times of culture. Figure 3-6A shows that the different strains take iron from the media at different rates. The wt strain exhibits fast intake of iron during the log phase of growth, and once it reaches stationary phase (after 24 h) the rate of iron intake slows down and levels off around 2 μM. Interestingly, Δ*bfrB* has a slower rate of iron uptake, but by 48 h has undetectable levels of iron left in the spent media. It is not clearly understood what is occurring, but because

it does not have the primary iron storage protein, it may take in smaller amounts of iron initially. At 48 h, the cell count is slightly higher compared to wt as seen in Figure 3-4A, so more cells could be utilizing the iron in the spent media which would lead to undetectable levels (less than 1 μM). In the Δ*bfd* and *bfrB** mutants, the rate of iron uptake is faster than that observed with wt, and does not level off; rather, iron in the media becomes nearly completely depleted, as judged by the detection limits of the analytical tool used (~ 1 μM). At 24 h, when iron levels reach below 2 μM in the spent media for Δ*bfd* and *bfrB**, Pvd is released very aggressively, which indicates that the Δ*bfd* and *bfrB** mutants strongly sense iron starvation. In comparison, the wt cells release much less Pvd between 24-36 h, and the iron concentration in spent media remains between 2-3 μM. As the Δ*bfd* and *bfrB** cultures are incubated to 48 h, the fluorescence of Pvd normalized to cell density is more than 4.5 times greater than wt. The synthesis and release of Pvd, as well as the import of iron-chelated Pvd into the cells is energetically costly. This would suggest the mutants sense very low levels of iron compared to wt, which is a strong indication that iron homeostasis is disrupted when the BfrB:Bfd interaction is blocked, either by the absence of Bfd (Δ*bfd*), or by inhibiting the protein/protein interaction in *bfrB**. In the case of the Δ*bfrB* mutant, the free intracellular iron levels appear to be at a concentration that prevents the synthesis and large secretion of Pvd. The reasons for this interesting observation will require additional investigation.

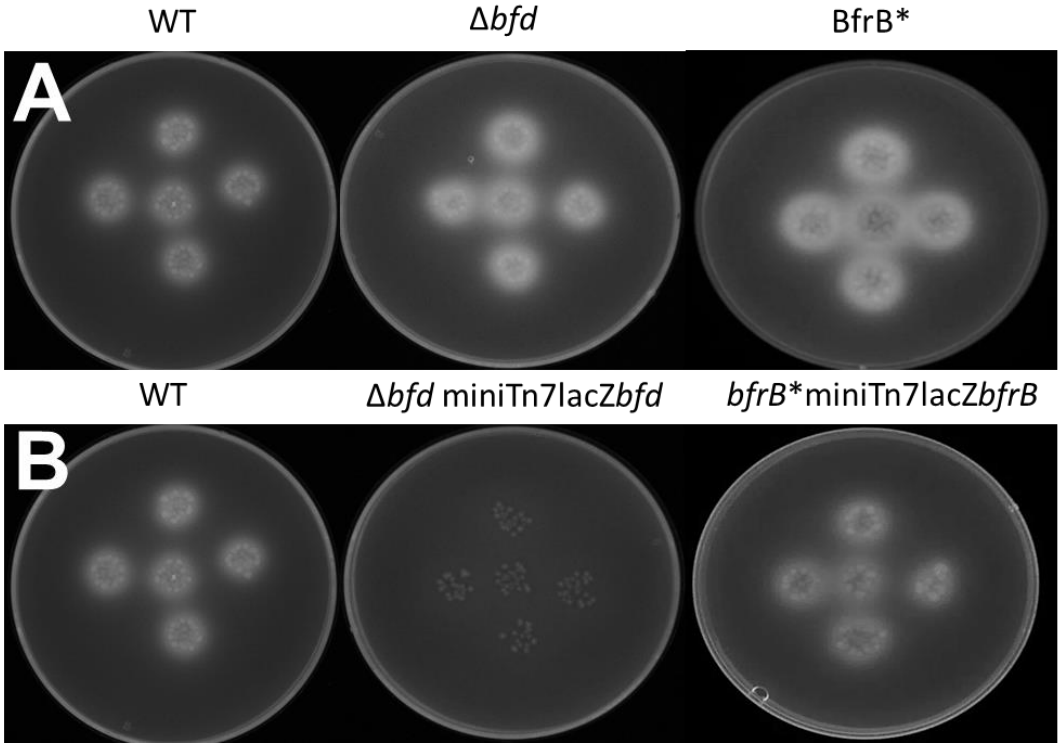

Figure 3-5: The release of Pvd can be seen by shining UV-light on colonies plated on PIA. (**A**) The wt strain releases some Pvd, but the Δ*bfd* and *bfrB** mutants release a much greater amount of Pvd, as seen by the fluorescent intensity surrounding the bacterial colonies. (**B**) The Δ*bfd* and *bfrB** mutants were complemented with the *bfd* and *bfrB* genes, respectively (Δ*bfd*miniTn7lacZ*bfd* and *bfrB**miniTn7lacZ*bfrB*), which causes secretion of Pvd at levels lower or comparable to those seen with the wt strain.

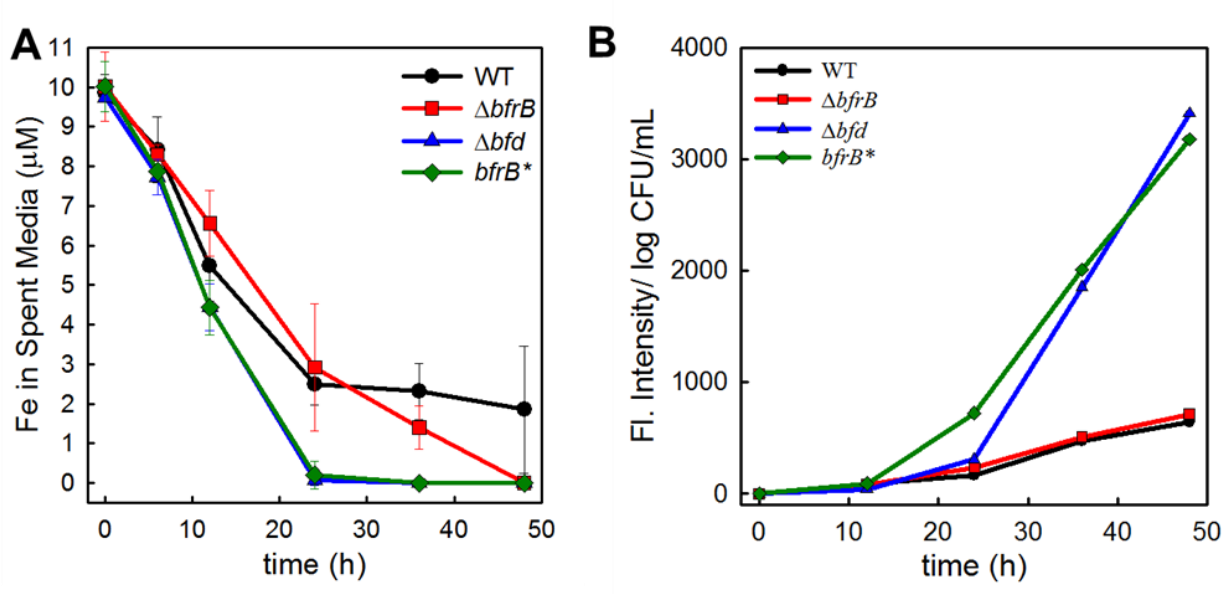

Figure 3-6: Iron left in spent media and the release of Pvd in cultures of wt and mutant *P. aeruginosa* strains. (**A**) The iron left in the spent media was measured overtime for all strains. Δ*bfrB* initially utilizes iron at a slower rate than the other strains, but has undetectable levels of iron at 48 h. The wt strain takes iron at a relatively fast rate through the log phase of growth and at a much slower rate during stationary phase, leaving behind around 2 μM in the media. The Δ*bfd* and *bfrB** strains take iron at a fast rate through log and stationary phases until the levels of iron become undetectable at 24 h. (**B**) The release of Pvd can be measured by its fluorescent intensity. The levels of Pvd were normalized for each strain by the cell count in log CFU/mL. Δ*bfd* and *bfrB** begin to release Pvd earlier and at a fast rate after 24 h, compared to the slow and small amount of Pvd release by wt and Δ*bfrB*. The release of Pvd correlates to the same time iron begins to be undetectable for Δ*bfd* and *bfrB**.

Mutants have Lower Levels of Free Intracellular Iron

Levels of total intracellular iron were measured after culturing the wt or mutant strains for 12 and 24 h in PI media containing 7-8 µM Fe (Figure 3-7A). These time points were chosen because the results summarized in the native PAGE gels of Figure 3-4 indicate that iron storage in BfrB is similar for all strains at 12 h (except Δ*bfrB*), whereas at 24 h iron in BfrB has been mobilized in the wt strain, but it remains "stuck" in BfrB in the Δ*bfd* and *bfrB** strains. There are no significant differences in the total iron levels of wt, Δ*bfd* and *bfrB** since the standard deviations overlap the averages of each strain at 12 h and 24 h. In contrast, the total iron levels in the Δ*bfrB* mutant are approximately 50% of those observed in the wt, Δ*bfd* and *bfrB** strains. Although this information may be interpreted to suggest that the higher levels of intracellular iron in the wt, Δ*bfd* and *bfrB** strains is due to iron stored in BfrB, it is also important to note that the Δ*bfrB* mutant takes in less iron from the media, as shown in Figure 3-6A.. Hence, it appears the Δ*bfrB* mutant takes less iron than wt *P. aeruginosa*, which leads to significantly lower intracellular iron in Δ*bfrB.* Although the analysis of total intracellular iron content is informative, it does not reveal important details about what is occurring in the bacterial cell with respect to iron homeostasis. To gain additional insights into iron regulation and iron homeostasis, we performed EPR experiments to measure the free intracellular iron content. The free intracellular iron content is iron that is unincorporated and may be in transit or bound to the surface of biomolecules [20, 21].

To measure free intracellular iron, cells were sampled at 12 and 24 h, and the samples were prepared for EPR analysis as described in the Experimental Section. The results are summarized in Figure 3-7B. At 12 h of culture the levels of free intracellular iron concentration

in the wt and Δ*bfrB* mutant are similar, while the free iron levels in the Δ*bfd* and *bfrB** mutants are approximately ½ that of wt *P. aeruginosa*. At 24 h the levels of free intracellular iron in all mutant strains are lower than in the wt cells. These results clearly show that in absence of BfrB, or when the BfrB:Bfd interaction is inhibited, there is a disruption in iron regulation.

It is interesting to think in terms of the levels of total and free intracellular iron: In the case of the Δ*bfrB* mutant, the total iron levels at 12 h are approximately ½ those in the wt strain, yet the free iron levels are nearly identical. At 24 h, the total iron levels remain low, and there is a decrease in the levels of free iron, although these values remain higher than in the Δ*bfd* and *bfrB** mutants. The relatively "normal" levels of free iron may explain the "reluctance" of Δ*bfrB* cells to secrete Pvd, despite the fact that the cell becomes iron deficient, as indicated by the total iron levels. In the case of the Δ*bfd* and *bfrB** mutants, the free iron levels are consistently lower that in the wt strain, however, the levels of total iron are very similar to wt at 12 h, and only modestly decreased at 24 h. Considering that iron "stuck" in BfrB contributes to the total iron levels, it is also likely that the Δ*bfd* and *bfrB** also experience iron deficiency, beyond free iron levels.

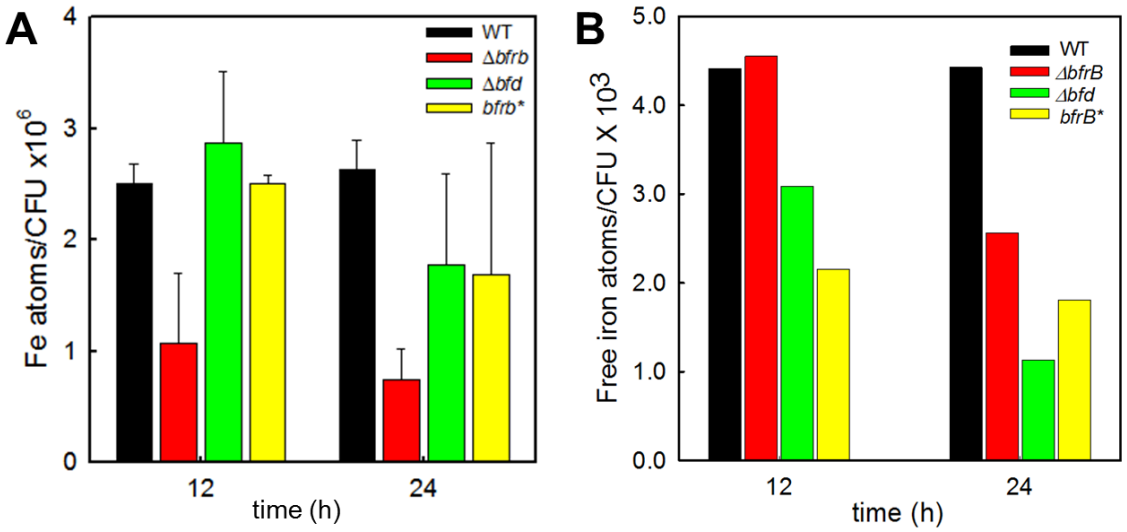

Figure 3-7 Levels of total intracellular iron measurements and free intracellular iron at 12 and 24 h. (**A**) The total iron in the cells at 12 and 24 h is similar for wt, Δ*bfd* and *bfrB**. Δ*bfrB* is lower at both time points. (**B**) Levels of free intracellular iron at 12 and 24 h. The free intracellular iron levels at 12 h are similar in wt and Δ*bfrB* but lower in Δ*bfd* and *bfrB**. At 24 h the levels of free intracellular iron relative to wt are lower in the Δ*bfrB* mutant and even lower in the Δ*bfd* and *bfrB** cells.

Iron Storage and Mobilization from BfrB Gives wt *P. aeruginosa* an Advantage to Overcome Low Iron Conditions

The mobilization of iron stored in BfrB allows *P. aeruginosa* cells to utilize iron reserves when the iron concentration in the environment becomes depleted. In the following experiments we show how wt cells have a growth advantage when iron can be utilized from BfrB: The strains were grown in PI media containing 8 µM Fe for either 10 or 24 h and then transferred to iron-depleted phosphate media. We chose 10 and 24 h because iron stained native gels (see

Figure 3-4) showed iron stored in BfrB at 12 h, but at 24 h most (if not all) the iron stored in BfrB has been mobilized.. Figure 3-8A shows growth curves in iron-depleted media inoculated with cells containing iron in BfrB (10 h inoculum). The curves show that wt cells have a growth advantage over the mutants. In comparison, when iron-depleted media is inoculated with cells that do not have significant iron stored in BfrB (24 h inoculum) the wt cells grow at the same rate as the mutants seen in Figure 3-8B.

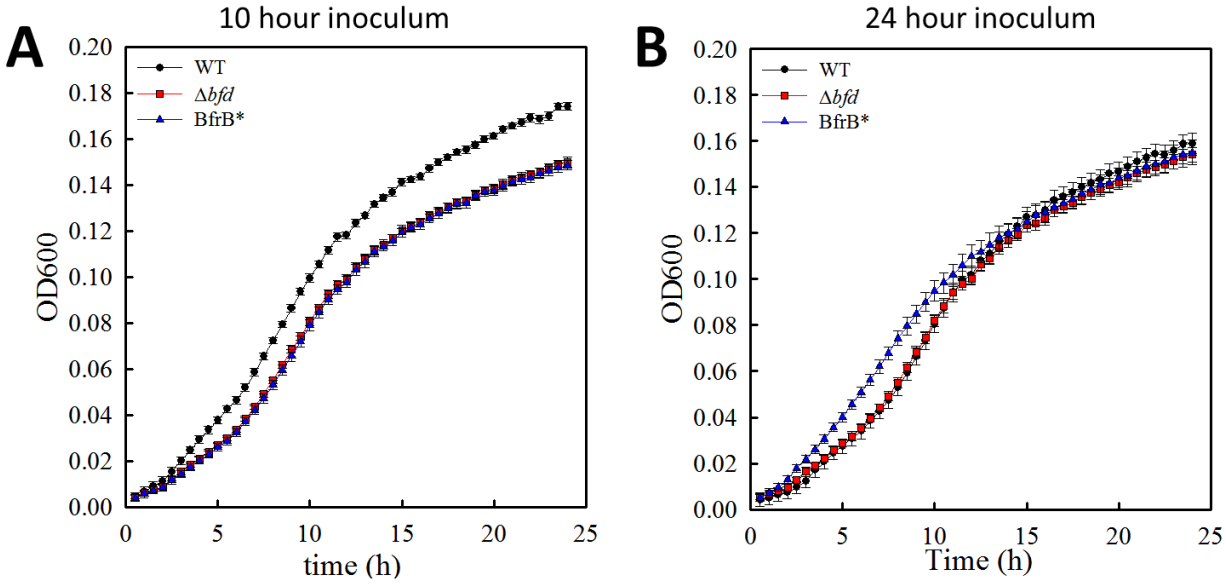

Figure 3-8: The wt strain has a growth advantage when iron stored in BfrB can be utilized. (A) Strains were grown in 8 µM Fe media for 10 h and then transferred to iron-deplete media. The wt cells, which can utilize iron stored in BfrB, grow faster and reach a higher cell density compared to the Δ*bfd* and *bfrB** mutants, which are unable to utilize iron stored in BfrB. (B) Strains were grown in 8 µM Fe media for 24 h, so the wt cells had already mobilized the iron stored in BfrB. Unable to have access to iron reserves, the wt cells grow at a similar rate as the mutants in iron deplete media, which cannot access their iron stored in BfrB.

Discussion

It has been unclear the exact role of the iron storage proteins, FtnA and BfrB in *P. aeruginosa* PA01. The role of FtnA is still being investigated, but through our results we can suggest that the primary role of iron storage belongs to BfrB. As seen in the iron-stained native PAGE gels in Figure 3-4, iron is consistently observed in the bands that align with the bands corresponding to the recombinant BfrB protein. In contrast, native PAGE gels obtained with cell lysates of the Δ*bfrB* mutant there are no iron-stained bands, indicating that iron is not accumulated in iron storage proteins in the mutant cells. These observations lead to the important conclusion that in *P. aeruginosa* cells, FtnA does not accumulate iron, even when BfrB is missing. Consequently, BfrB functions as the iron storage protein in *P. aeruginosa,* whereas the function of FtnA, although yet not understood, is not iron storage.

The function of iron storage proteins has been described as storing iron to prevent oxidative stress from free iron and to also provide a supply of iron when the cell encounters low iron conditions. This latter function of iron storage and subsequent mobilization under iron limiting conditions has been demonstrated in this work for BfrB, as can be seen in the NATIVE PAGE gels in Figure 3-4. When the iron concentration in the media decreased below 3 μM (Figure 3-3A and 3-3C) the wt cells mobilize iron stored in BfrB. Utilization of iron stored in BfrB decreases the need to release high levels of Pvd (Figure 3-6B). In contrast, when we prevent the bacteria's ability to obtain iron stored in BfrB, such as in the *Δbfd* and *bfrB** mutants, we also disrupt iron regulation. Iron that gets stuck in BfrB is no longer accessible to the mutants; therefore, they begin to feel iron starved, despite the fact that the cells continue to aggressively take iron from the media. In fact, these cells release high levels of Pvd, in an

attempt to sequester extracellular iron. Interestingly, we see through EPR results that the free intracellular iron concentration in these mutants is lower than wt. One would think that if high concentrations of Pvd are being released because the cells sense low iron conditions, then iron would go straight to the free intracellular iron pool when iron was brought into the cell. This process does not appear to be happening, but instead, it is probable that iron incorporated from the media is routed by the cell directly into BfrB. From these results, we hypothesize the role of BfrB could also be that of "iron depot and distribution center". Consequently, iron brought into the cell is routed into BfrB. In this context, the BfrB:Bfd interaction, which enable iron mobilization from BfrB also functions to regulate the levels of free iron in the cells, which in turn enable Fur, the master iron regulator to activate or suppress the transcription of genes involved in iron uptake, such as Pvd synthesis. In addition, it is possible that the BfrB:Bfd interaction is also important to mobilize iron for incorporation into iron utilizing proteins, such as heme- and iron sulfur cluster- containing proteins and enzymes.

Recovering stored iron from BfrB gives wt an advantage when growing in low iron media (Figure 3-9A). These types of conditions resemble the low iron environment when pathogens invade a host. The host innate immune system resorts to nutritional immunity which prevents the bacteria from accessing essential nutrients such as iron [22]. Under such conditions, wt cells would be expected to use the iron stored in BfrB whereas the mutants would not be able to survive as well. The mutants also produce large amounts of Pvd which makes the bacteria use a lot of energy to make and bring iron-bound Pvd back into the cell [23]. Also, the low free intracellular iron concentrations in the mutants would suggest that iron-utilizing proteins involved in important physiological processes, such the TCA cycle and DNA synthesis would

not attain their iron cofactors. Ultimately, this would make the bacteria weaker and more susceptible the host immune system. Testing the mutants' virulence in animal models is currently in progress.

The Δ*bfrB* mutant has brought up more questions than answers involving how the bacteria deals with not having a primary iron storage protein. The cell is able to defend itself from bringing in too much iron, but it is still capable of growing and surviving in similar growth conditions as wt. Nevertheless, total iron analysis indicates that the Δ*bfrB* are iron deficient, and consequently may also be less fit to fend against adverse conditions, such as those furnished by the host immune system. Future studies will be completed to understand how iron is processed in this mutant. Studies with the Δ*bfd* and *bfrB** mutants have demonstrated the essential function of iron mobilization from BfrB in iron homeostasis. From these results, we can postulate that BfrB could be an iron distributor in the cell. In conclusion, disrupting iron release from BfrB does disrupt iron homeostasis in *P.aeruginosa*. These findings have provided new and previously unsuspected insights into the regulation of bacterial iron homeostasis.

References

1. Schaible, U.E.K., S.H.E, *Iron and Microbial Infection.* Nature 2004. **2**: p. 946-953.
2. Velayudhan, J., Castor, M., Richardson, A., Main-Hester, K., Fang, F., *The role of ferritins in the physiology of Salmonella enterica sv. Typhimurium: a unique role for ferritin B in iron-sulphur cluster repair and virulence.* Mol. Microbiol., 2007. **63**: p. 1495-1507.
3. Andrews, S.C., Robinson, A.K., Rodriguez-Quinones, F., *Bacterial iron homeostasis* FEMS Microbiol. Reviews, 2003. **27**: p. 215-237.
4. Crow, A., Lawson, T.L., Lewin, A., Moore, G.R., Le Brun, N.E., *Structural Basis for Iron Mineralization by Bacterioferritin.* JACS, 2009. **131**: p. 6808-6813.
5. Carrondo, M.A., *Ferritins, iron uptake and storage from the bacterioferritin viewpoint.* EMBO J., 2003. **9**: p. 1959-1968.
6. Touti, D., *Iron and oxidative stress in bacteria.* Arch. Biochem. Biophys., 2000. **373**: p. 1-6.
7. Velayudhan, J.C., M; Richardson, A; Main-Hester, K; Fang, F. , *The role of ferritins in the physiology of Salmonella enterica sv. Typhimurium: a unique role for ferritin B in iron-sulphur cluster repair and virulence.* . Mol. Microbiol., 2007. **63**: p. 1495-1507.
8. Yao, H., Wang, Y., Lovell, S., Kumar, R., Ruvinsky, A.M., Battaile, K.P., Vakser, I.A., Rivera, M., *The structure of the BfrB-Bfd complex reveals protein-protein interactions enabling iron release from bacterioferritin.* J. Am. Chem. Soc., 2012. **134**: p. 13470-13481.
9. Karas, V.O., Westerlaken, I., Meyer, A.S., *The DNA-Binding Protein from Starved Cells (Dps) Utilizes Dual Functions To Defend Cells against Multiple Stresses.* J. Bacteriol., 2015. **19**: p. 3206-3215.
10. Andrews, S.C., Robinson, A.K., Rodriguez-Quinones, F., *Bacterial iron homeostasis.* FEMS microbiology review 2003. **27**: p. 215-237.
11. Moore, G.R., Kadir, Fahmi H.A., Al-Massad, Fareeda, K., Le Brun, Nick, E., Thomson, Andrew, J., Greenwood, Colin, Keen, Jeffrey, N., Findlay, John, B.C., *Structural heterogeneity of Pseudomonas aeruginosa bacterioferritin.* 1994. **304**: p. 493-497.
12. Ma, J.F., Ochsner, U. A., Klotz, M.G., Nanayakkara, V. K., Howell, M.L., Johnson, Z., Posey, J.E., Vasil, M.L., Monaco, J.J., Hassett, D.J., *Bacterioferritin A modulates catalase A (KatA) activity and resistance to hydrogen peroxide in Pseudomonas aeruginosa.* J. Bacteriol., 1999. **181**: p. 3730-3742.
13. Yao, H., Jepkorir, G., Lovell, S., Nama, P.V., Weeratunga, S., Battaile, K.P., Rivera, M., *Two distinct ferritin-like molecules in Pseudomonas aeruginosa: the product of the bfrA gene is a bacterial ferritin (FtnA) and not a bacterioferritin (Bfr).* Biochem., 2011. **50**: p. 5236-5248.
14. Palma, M., Worgall, S., Quadri, L.E.N., *Transcriptome analysis of the Pseudomonas aeruginosa response to iron.* Arch. Microbiol., 2003. **180**: p. 374-379.
15. Weeratunga, S., Lovell,S., Yao,H., Battaile,K., Fischer,C., Gee,C., Rivera,M, *Structural Studies of Bacterioferritin B from Pseudomonas aeruginosa Suggest a Gating Mechanism for Iron Uptake via the Ferroxidase Center.* Biochemistry, 2010. **49**: p. 1160-1175.

16. Andrews, S.C., *Iron storage in bacteria.* Adv Microb Physiol, 1998. **40**: p. 281-351.
17. Wang, Y., Yao, H., Cheng, Y., Lovell, S., Battaile, K.P., Midaugh, C.R., Rivera, M., *Characterization of the Bacterioferritin/Bacterioferritin Associated Ferredoxin Protein-Protein Interaction in Solution and Determination of Binding Energy Hot Spots.* Biochem., 2015. **54**: p. 6162-6175.
18. Chung, M.C., *A specific iron stain for iron-binding proteins in polyacrylamide gels: application to transferrin and lactoferrin.* Anal. Biochem., 1985. **148**: p. 498-502.
19. Cornelis, P., *Iron Uptake and metabolism in pseudomonads.* Applied microbiology and biotechnology, 2010. **86**: p. 1637-1645.
20. Imlay, J.A., *Cellular defenses against superoxide and hydrogen peroxide*, in *Annu Rev Biochem.*2011. p. 755-776.
21. Jean-François Jacques, J.F., Jang, S., Prevost, K., Desnoyers, G., Desmarais, M., Imlay, J., Masse, E., *RyhB small RNA modulates the free intracellular iron pool and is essential for normal growth during iron limitation in Escherichia coli.* 2006. **62**: p. 1181–1190.
22. Hood, M.I., Skaar, E.P., *Nutritional immunity: transition metals at the pathogen-host interface.* Nat.Rev.Microbiol., 2012. **10**: p. 525-537.
23. Imperi, F., Tiburzi,F., Visca, P., *Molecular basis of pyoverdine siderophore recycling in Pseudomonas aeruginosa.* PNAS, 2009. **48**: p. 20440-20445.

Chapter 4 : Dynamic motions in bacterioferritin are necessary for ferroxidase activity

Introduction

Iron is an essential element for multiple functions in bacteria, but needs to be tightly managed in the cell. Due to the ability of free Fe^{2+} to cause oxidative stress in the cell and Fe^{3+} to rust out in aerobic conditions, the cell has developed iron storage proteins to store iron. Bacterioferritins (Bfr) are 24-mer, heme containing iron storage proteins that belong to the ferritin superfamily, but are specific to only bacteria (Figure 4-1A and 4-1B) [1]. The structure and function of the bacterioferritin (BfrB) in *P. aeruginosa* has been extensively studied in our laboratory. It has been shown that the iron ions are stored in the cavity of Bfr as a ferric hydroxyphosphate molecule [2]. For iron to be stored in the cavity of BfrB, free ferrous iron first needs to be oxidized at the ferroxidase centers. Ferroxidase centers in bacterioferritins are located in the middle of each subunit. In BfrB the histidine 130 at the ferroxidase center provides a gating motion to channel the oxidized iron into the core of the protein (Figure 4-1C) [3]. In an iron free ferroxidase center, the crystal shows the histidine 130 is rotated away. When iron is present, the H130 has two conformations. It is either coordinated with iron or it is rotated in the away position [3]. This suggests ferrous iron from the exterior of the protein is capable of moving through the ferroxidase channel where a di-Fe^{2+} moiety are coordinated by the ferroxidase ligands including H130. As the di-Fe^{2+} moiety is oxidized to di-Fe^{3+} the H130 moves to its gate open state, allowing for Fe^{3+} to enter the interior cavity of the protein [3].

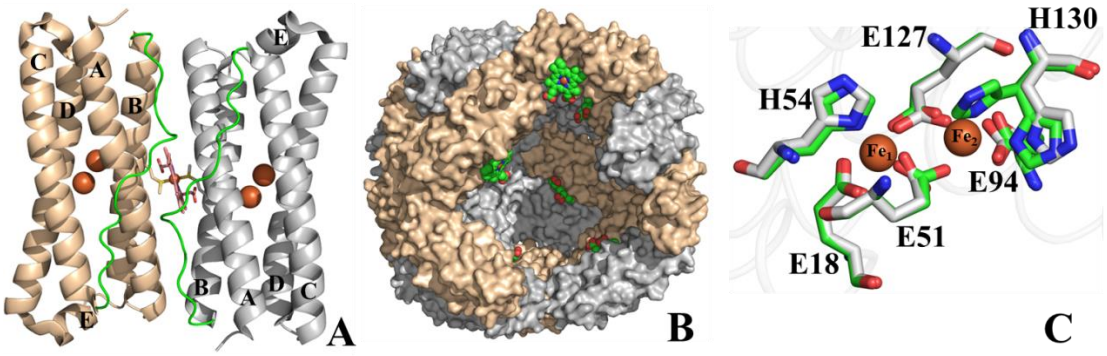

Figure 4-1: Structure of BfrB: (**A**) Subunit dimer and associated heme. Each subunit is made up of a 4-helix bundle (helices **A**-**D**), a perpendicular short helix (**E**), and a loop connecting the B and C helices (green). (**B**) Cross sectional view of the full 24-mer structure of BfrB that shows the inside cavity where mineral Fe^{3+} is stored; the heme is highlighted in green. (**C**) The residues that make up the ferroxidase center are shown in grey when no iron is present and in green when iron is located in the center. H130 is adopts two conformations, iron bound and iron free, when iron is present.

The structure of BfrB suggests there may be communication between the interior of the protein and the outside pores. The structures of bacterioferritins have eight 3-fold pores, six 4-fold pores, and twenty-four B-pores. The intersection of three subunits forms the 3- fold pores. The 3-fold pores consist of layers that alternate negative and positive charge (Figure 4-2A). The intersection of four subunits makes up the 4-fold pores (Figure 4-2B). The pore is lined by the corresponding E-helices. The narrowest portion is composed of two layers made by the side chains of four N148 and four Q151 (Figure 4-3A). The B pores are formed at the intersection of three subunits not aligned with an axis of symmetry. There are four B pores surrounding each 4–

fold pore, so there is a total of twenty-four B-pores in the structure of a 24-mer bacterioferritin (Figure 4-2B). The narrowest section of the B-pores consists of residues D132 and T136 from one subunit and D34 from a different subunit (Figure 4-3B). They are lined with hydrophilic and negatively charged residues. It has been suggested the B-pores could allow for Fe^{2+} to traffic across the Bfr shell [4]. Molecular dynamic simulations have shown that K^+ ions move in and out of the BfrB shell via B- and ferroxidase pores in wt BfrB, but traffic of ions was not observed to occur along the 3-fold or 4-fold pores [5]. The MD simulations also suggested that the traffic of K^+ ions through the B-pores is possible due to the conformational movements in helix D. In the MD simulations the C-terminal half of helices D exhibited recurring kinking/straightening and folding/unfolding transitions that are coupled to the lateral oscillations of the short E-helices that make up the 4-fold pores. This results in a continual expanding and contracting of the B-pores [5]. These results suggested there are cooperative dynamics in the 24-mer structure, which may be crucial for iron traffic across the bacterioferritin shell and iron handling inside the ferritin cavity.

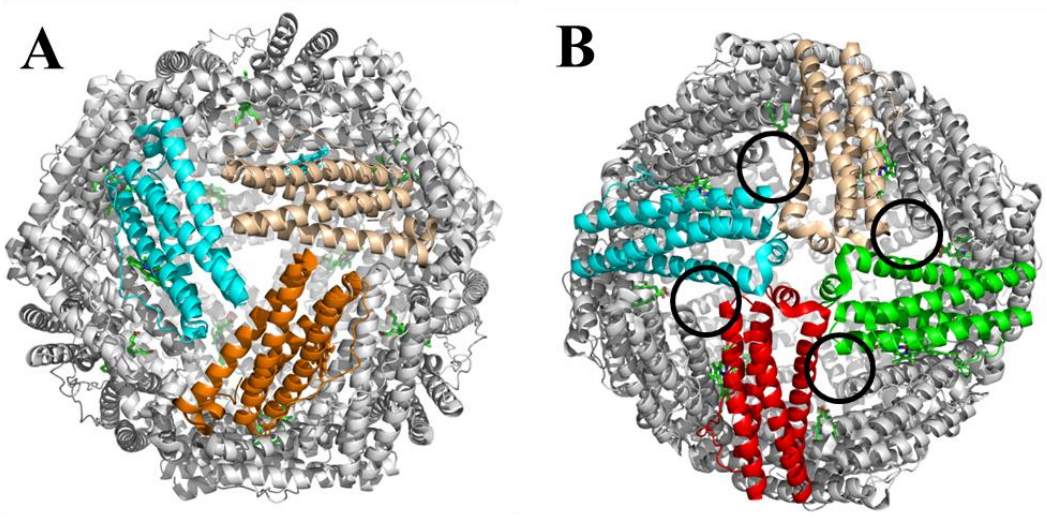

Figure 4-2: (**A**) The 3 colored helices are highlighted to show one of the eight 3-fold pores. (**B**) The colored helices make up one of the 4-fold pores. Four B-pores (circled) surround each of the 4-fold pores [6].

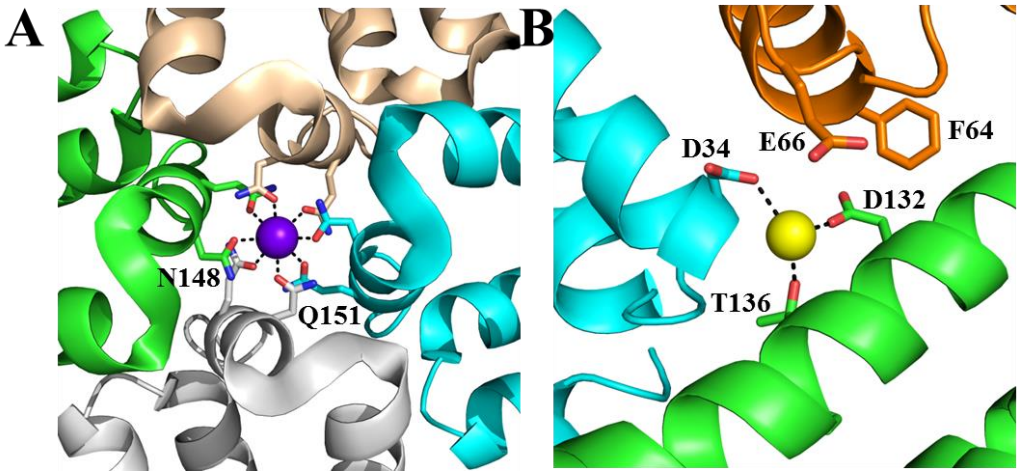

Figure 4-3: (**A**) Zoomed-in view of a 4-fold pore and a potassium ion (purple sphere) coordinated by the residues N148 and Q151. (**B**) Zoomed view of a B-pore with a sodium ion (yellow sphere) coordinated by the residues D34, D132, and T136 [6].

The function of Bfr has been intensely studied, but it is still unknown how ions traffic in and out of the protein shell and how the movement of individual subunits in the 24-mer structure affects its function. To further investigate the notion that Fe^{2+} could traffic through the B-pores, a single mutation was introduced in BfrB to replace residue D34 with the hydrophobic phenylalanine at the B-pore (D34F BfrB). This mutation was analyzed and compared to wt BfrB through molecular dynamic simulations, x-ray crystallography, and *in vitro* iron uptake assays. In the B-pore, D34 is a negatively charged residue, which is located at the narrowest section and coordinates a Na^{+} (Figure 4-3-B). The site-directed mutation not only affected the nearby

residues, but it changed the flexibility and reactivity of the ferroxidase centers, which are located at considerable distance from the mutation site. The MD simulations and the crystal structures helped explain the experimental observations by showing cooperative motions of the subunits, extending from 4-fold pores, via the B-pores, into the ferroxidase centers. The ferroxidase centers are essential for efficient oxidation and mineralization of iron by the 24-mer bacterioferritin assembly. The structural studies of BfrB mutants soaked in iron provided experimental support for iron traffic through B-pores, and an accumulation of iron binding sites in the interior surface of the mutant gives insight into the paths followed by iron and phosphate, from entry ports in the Bfr shell toward possible mineralization sites in the interior cavity.

Experimental Procedures

Site-directed Mutagenesis and Protein Expression

The pET11a vector containing the *bfrB* gene [7] was mutated to D34F using the QuikChange II Site-Directed Mutagenesis kit (Stratagene, La Jolla, CA) using the manufacturer instructions. The following primer pair sequences were used:

Forward: 5'GCATAGCCGCATGTGGAATTTTTGGGGCCTGAAACGTCTGG3'

Reverse: 5'CCAGACGTTTCAGGCCCCAAAAATTCCACATGCGGCTATGC3'

PCR products were digested using Dpn I and transformed into XL1-Blue competent cells (Agilent Technologies) for DNA amplification. Plasmid DNA was isolated using the QIAprep Spin Miniprep Kit (QIAGEN), and the sequences verified by ACGT Inc. (Wheeling, IL). Recombinant DNA plasmids with the correct sequence were transformed into *Escherichia coli* ArcticExpress (DE3)RIL competent cells (Agilent Technologies) for subsequent protein

expression. The protocols for protein expression, purification, and reconstitution with heme were carried out as previously described [3, 7].

Iron Mineralization Assay

As-isolated BfrB (wt and mutants) contain only a very small amount of iron in their core.[7] Reconstitution with an iron core was carried out as previously reported:[7] A 10 mM solution of ferrous ammonium sulfate was prepared inside an anaerobic chamber (Coy Laboratories, Grass Lake, MI), placed in a container with a rubber septum, and removed from the chamber. Concentrated HCl was added to the ferrous ammonium sulfate solution (50 μL/100 mL) through the septum with the aid of a Hamilton micro- syringe (final pH ≈ 2.0), and the resultant solution was titrated into a stirred solution of 2 μM BfrB and 1.0 mM TCEP in 100 mM phosphate buffer, pH 7.6, in aliquots delivering 50 Fe^{2+} ions/BfrB. Fifteen minutes were allowed after the addition of each aliquot; upon the addition of the total iron load (500 Fe atoms/BfrB), the solutions were stirred overnight at 4 °C and then passed through a Sephadex G25M size exclusion column (GE Healthcare). The iron content of the samples, prior and after reconstitution with iron, was analyzed using a colorimetric ferrozine-based assay[8] as reported previously:[7] 50 μL concentrated HCl was added to 50 μL of mineralized BfrB and the mixture was incubated for 15 min at room temperature prior to the addition of 50 μL of ascorbic acid (25 mg/mL) and 250 μL of saturated sodium acetate. The concentration of iron was determined using the absorbance at 562 nm (ε_{562} nm = 27.9 mM^{-1} cm^{-1}) 15 min after the addition of ferrozine (5 mg/mL).

Crystallization and Data Collection

All crystallization experiments were conducted in Compact 300 or CombiClover 500 (Rigaku Reagents) sitting drop vapor diffusion plates at 20 °C. Equal volumes of BfrB (10 mg/mL in 100 mM potassium phosphate buffer, pH 7.6 and 1 mM TCEP) and crystallization solutions were equilibrated against 75 μL reservoir volume. Within 1 day, red prismatic crystals were obtained from Wizard 2 (Rigaku Reagents) condition E2 (35% (v/v) 2-methyl-2,4-pentanediol, and 100 mM MES pH 6.5, 200 mM Li_2SO_4). Crystals were transferred to a fresh drop of crystallization solution, which served as the cryoprotectant, and stored in liquid nitrogen for data collection. Fe-soaked crystals were prepared by soaking native crystals for 10 min in 50 mM $FeCl_2$ freshly dissolved in crystallization solution and then frozen in liquid nitrogen. X-ray diffraction data were collected at the Advanced Photon Source beamline 17-ID (IMCA-CAT) using a Dectris Pilatus 6 M pixel array detector.

Structure Solution and Refinement

Intensities were integrated using XDS [9] via the XDSAPP [10] interface or the Autoproc [11] software package and the Laue class analysis, and data scaling were performed with Aimless [12]. All crystals were isomorphous ($P2_12_12_1$, 24 molecules/asu) with the previously determined BfrB structure (PDB: 3IS7) [3]. Structure solution was conducted by molecular replacement using a single subunit from PDB: 3IS7 as the search model with Phaser [13]. All space groups with 622 point symmetry were tested in the molecular replacement searches. The top solution was found in the space group $P6_322$ with four molecules in the asymmetric unit. Structure refinement and manual model building were conducted with Phenix [14] and Coot [15] respectively. Disordered side chains were truncated to the point where electron density could be

observed. Structure validation was conducted with Molprobity [16]. Coordinates and structure factors were deposited to the Worldwide Protein Data Bank, and the accession codes are provided in Table 1.

Table 1: Crystallographic Data for BfrB D34F

	as-isolated (D34F)	Fe-soaked (D34F)
Data Collection		
unit cell parameters (Å, °)	a = 125.68	a = 125.49
	b = 203.54	b = 203.40
	c = 206.97	c = 207.25
space group	$P2_12_12_1$	$P2_12_12_1$
resolution (Å)[a]	49.41–2.05	49.39–2.20
	(2.09–2.05)	(2.24–2.20)
wavelength (Å)	1.00000	1.73769
temperature (K)	100	100
observed reflections	2,240,862	1,490,791
unique reflections	328,340	257,692
$<I/\sigma(I)>$[a]	13.1 (2.2)	18.1 (3.4)
completeness (%)[a]	99.5 (98.9)	96.3 (71.8)
multiplicity[a]	6.8 (6.6)	5.8 (2.4)
R_{merge} (%)[a,b]	11.7 (95.1)	6.2 (25.9)
R_{meas} (%)[a,d]	12.6 (103.1)	7.4 (35.6)
R_{pim} (%)[a,d]	4.8 (39.7)	2.4 (21.4)
$CC_{1/2}$[a,e]	0.998	0.998
	(0.710)	(0.885)
Refinement		
resolution (Å)	41.06–2.05	48.39–2.20
reflections (working/test)[f]	311,642/ 16,559	485,422/ 24,416
R_{factor}/R_{free} (%)[c]	15.3/19.2	14.9/18.7
no. of atoms (protein/Heme/K^+/iron/sulfate/water)	30,434/516/6/0/2,0660/2,066	30,262/516/6/144/40/ 2,278
Model Quality		
r.m.s deviations		
bond lengths (Å)	0.016	0.010
bond angles (°)	1.265	0.985
average B-factor (Å^2)		
all atoms	28.6	24.8
protein	28.2	24.1
heme	25.6	24.4
K^+	21.5	39.9
iron		45.1
sulfate		53.4
water	35.7	31.2
coordinate error (maximum likelihood) (Å)	0.20	0.20
Ramachandran Plot		
most favored (%)	99.5	99.8
additionally allowed (%)	0.5	0.2
PDB code	4TOD	4TOE

[a]Values in parenthesis are for the highest resolution shell.

[b]Rmerge = ΣhklΣi |Ii(hkl) – <I(hkl)>|/ΣhklΣi Ii(hkl), where Ii(hkl) is the intensity measured for the ith reflection and <I(hkl)> is the average intensity of all reflections with indices hkl.

[c]Rfactor = Σhkl ||Fobs (hkl) | – |Fcalc (hkl) ||/Σhkl |Fobs(hkl)|; Rfree is calculated in an identical manner using 5% of randomly selected reflections that were not included in the refinement.

[d]Rmeas = redundancy-independent (multiplicity-weighted) Rmerge [12, 17]. Rpim = precision-indicating (multiplicity-weighted) Rmerge [18-20].

[e]CC1/2 is the correlation coefficient of the mean intensities between two random half-sets of data [20, 21].

[f] For the data sets obtained from iron soaked crystals or native data sets collected at the iron peak wavelength, the number of reflections used during refinement is greater than the number unique reflections reported for data scaling. This is because Friedel pairs were kept separate during refinement and the anomalous scattering factors for the Fe^{2+} atoms were refined.

Molecular Dynamic Simulations

(MD simulations were carried out by Dr. Huan Rui and Prof. Wonpil Im from the Molecular Biosciences Department and Center for Bioinformatics, University of Kansas)

BfrB D34F was first immersed in a pre-equilibrated cubic water box of 160 Å in all three dimensions. This box is the same size as that used in the Grand Canonical Monte Carlo/Brownian Dynamics simulations of wt BfrB described previously [5, 22]. Both the box

and the BfrB molecule were centered at the origin. The initial ion configurations were the same as those in the E2, E10, and E40 systems described previously; 29 the free K+ ion numbers are 2840 (E2), 1042 (E10), and 714 (E40) and the numbers of HPO_4^{2-} ions are 1231 (E2), 332 (E10), and 168 (E40). In each of the D34F mutant systems, 24 K+ ions were added in the bulk solution to make the total charge of the systems neutral, and they were distributed with 2000 Monte Carlo moves, which were either accepted or rejected based on Metropolis criteria. Water molecules within 2.4 Å from the ions and the BfrB heavy atoms were removed. The systems were then subjected to a 900-ps equilibration cycle with decreasing positional harmonic restraints on heavy atoms not including water oxygen. In the BfrB interior, the removed water molecules that were close to BfrB before the equilibration cycle were quickly replaced by water from the interior cavity of BfrB, creating small vacuum pockets. To overcome this problem, an additional sphere of pre-equilibrated water with 40 Å radius was added to the system on top of the other water molecules (also see ref [5]). Any of these newly added water molecules that were within 2.4 Å of either the BfrB heavy atoms or the other water molecules in the system was deleted. Each of the resultant systems was again equilibrated with diminishing positional harmonic-restraint potentials on the heavy atoms for another 900 ps and then subjected to a 40-ns production. All the simulations were carried out in NPT (constant particle number, pressure, and temperature) ensembles using the NAMD2.941 simulation package. The simulation inputs were obtained from the Quick MD Simulator module in CHARMM-GUI.42 The simulations were performed with CHARMM all-atom parameter set PARAM2243 including the dihedral cross-term corrections (CMAP)44 and a modified TIP3P water model [23]. The van der Waals interactions were smoothly switched off at 10−12 Å by a force switching function, [24] and the

electrostatic interactions were calculated using the particle-mesh Ewald method [25] with a mesh size of ~1 Å for fast Fourier transformation, $\kappa = 0.34$ Å^{-1}, and a sixth-order B-spline interpolation. The temperature (300 K) and pressure (1 atm) were kept constant during all the simulations by Langevin dynamics and the hybrid Nosé-Hoover Langevin piston method, respectively. The Langevin damping coefficient was set to 1 ps^{-1}; the decay period and damping time scale were 50 fs, respectively.

Results

D34F X-ray Crystal Structure

The structure of the mutant D34F was determined by growing crystals of the purified recombinant protein (as-isolated) or by soaking the protein in Fe^{2+} solution (Fe-soaked). The mutant was prepared to replace the negatively charged aspartate (which was observed to bind a Na^{+} ion in B-pores of BfrB) with the hydrophobic phenylalanine. The major changes seen in the structure of the D34F mutant are in the B-pores and in the ferroxidase center. The D34F mutant did not cause any change to the 4-fold pore compared to wt (Figure 4-4). In the 3-fold pore, the structure is almost identical, despite the presence of sulfate and iron ions (Figure 4-5). The differences seen in the crystal structure of D34F compared to wt BfrB strongly suggested a decrease in the flexibility of the ferroxidase center ligands and changes in residue movement when crystals are soaked iron solution. Prior to soaking crystals in iron solution, the D34F mutant did not have iron coordinated at the ferroxidase center, similar to wt. Soaking in iron solution caused iron to bind to the ferroxidase centers, but as will be discussed below, the details

of iron binding are different between wt and D34F BfrB. In addition, there was iron bound to locations at the different pores not seen in wt, and iron atoms were seen in the B-pores.

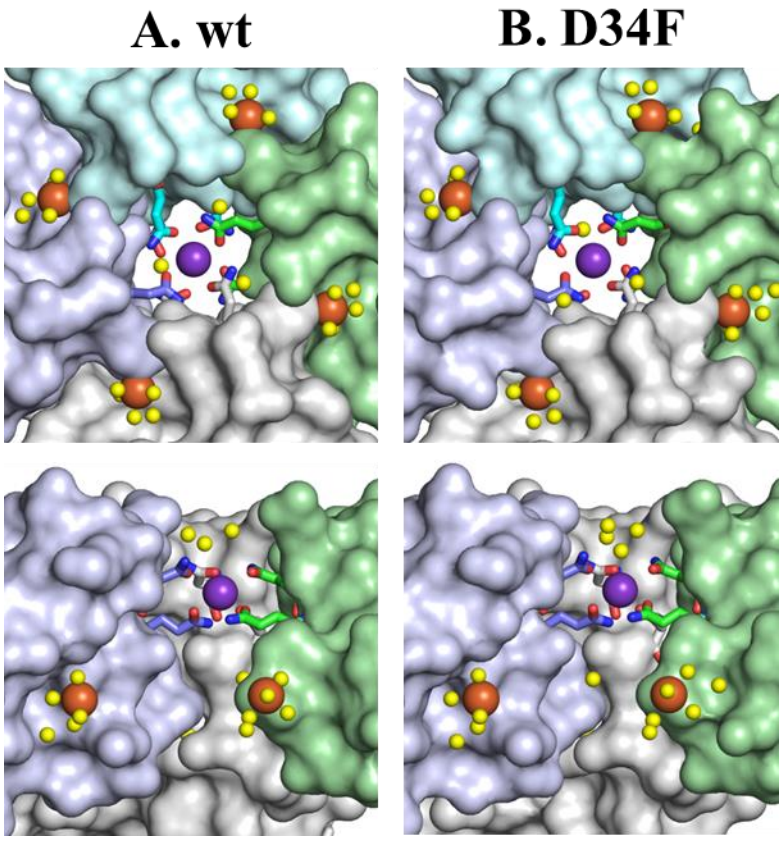

Figure 4-4: Zoomed-in view of 4-fold pore in (**A**) wt and (**B**) D34F BfrB. Top: view of a 4-fold pore from the interior cavity. Bottom: cross-sectional view. Iron atoms are orange spheres, water molecules are yellow spheres, sodium ion is a purple sphere, nitrogen atoms are shown in blue, and oxygen atoms in red [6].

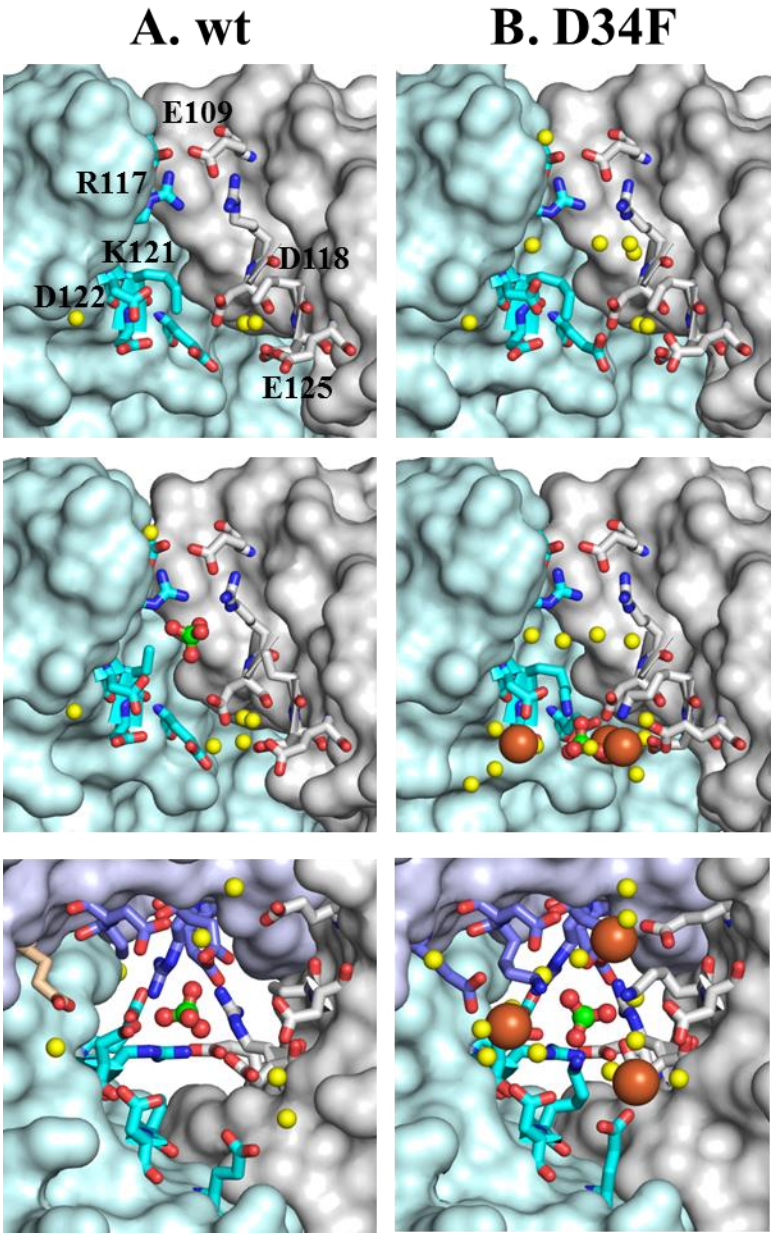

Figure 4-5: View of the 3-fold pore in wt and D34F BfrB. The top row is a cross-sectional view of a 3-fold pore in the as-isolated structures. The middle row is the same view as the top view but in Fe-soaked crystals. The bottom row shows a 3-fold pore viewed from the interior cavity

in Fe-soaked crystals. Fe atoms are the orange spheres, water molecules are yellow spheres, sulfur atom are green, oxygen atoms are red and nitrogen atoms are blue [6].

Changes to B-Pores

Side chains lining the B-pores are E66, D34, T136, and D132 in wt BfrB. They form a corkscrew from the outer E66 to the inner D132 (Figure 4-6A). The bulky hydrophobic mutation (D34F) caused the E66 residue to rotate away from the pore as seen in the top image of Figure 4-6B. The relatively bulky phenylalanine (Phe) side chain not only blocks the pore but also disrupts the hydrophilicity of the corkscrew. Not only is there an increase in water molecules seen at the pore, there is also the presence of an iron atom coordinated by D132 in the Fe-soaked structure. In the crystal structure of another mutant prepared by our lab, with mutations made at the surface of the protein, C89S/K96C, we observed the presence of two Fe atoms. One Fe atom was coordinated by D132 and the surface of the protein. This location is where the Phe residue in the D34F mutant is also located. The second Fe atom was coordinated by the residues D34 and E66 which is similar to the iron atom found in the D34F mutant as is seen in the bottom picture of Figure 4-6B. The crystallographic data shows that iron molecules are seen in the B-pores. In the case of D34F, the hydrophobic ring could possibly block iron from going through the pore which is why we see an iron atom on the inside of the pore. The crystal structure data supports the previous published MD simulations that suggested the B-pore could be used to traffic iron [5].

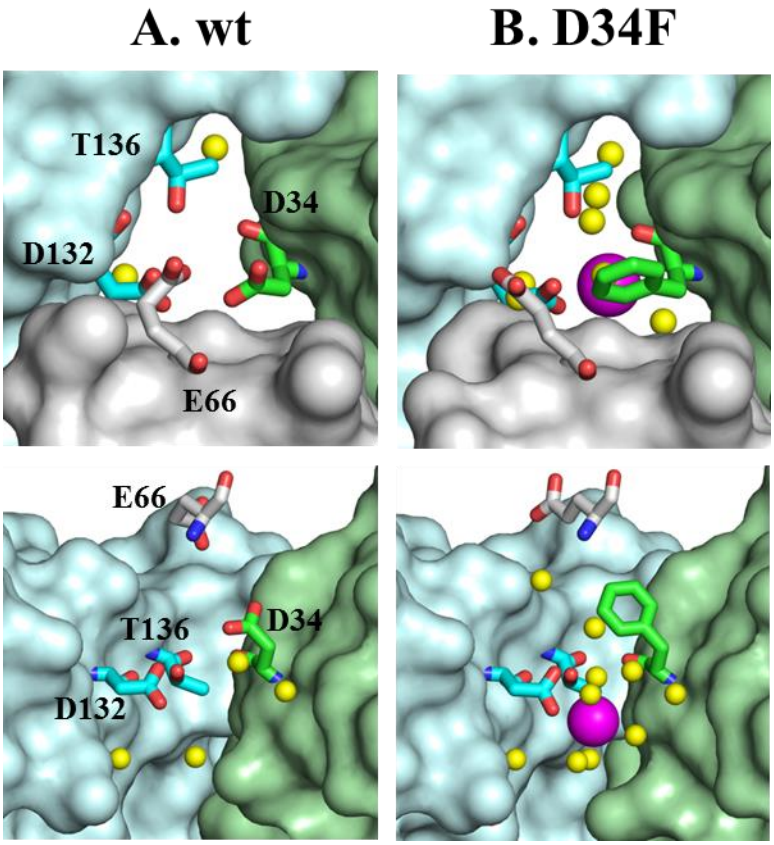

Figure 4-6: Zoomed-in view of the B-fold pore in wt and D34F BfrB. The top row shows a view from the exterior of the protein. The bottom row is a cross sectional view with the grey subunit seen in the top row removed. The water molecules are yellow spheres, the iron ion is shown as a magenta sphere, oxygen atoms are red, and nitrogen atoms are blue [6].

Ferroxidase Activity

In the as-isolated proteins, both, wt and the D34F mutant do not have iron present in the ferroxidase center. Crystals of as-isolated protein soaked in an iron solution causes iron to be incorporated at the ferroxidase centers. In the structures of Fe-soaked wt BfrB, two iron atoms are present in each ferroxidase center, with the average distance between the two iron atoms of

approximately 4.1 Å, suggesting it is a di-Fe^{2+} site. In the wt protein, the H130 side chain undergoes a conformational change from "gate open" to "gate closed" to allow entry of the oxidized iron into the core of the protein (Figure 4-7A). The D34F mutant has iron bound at the ferroxidase center, but the H130 does not go through the similar conformational changes as wt. The H130 side chain stays in the "gate open" position and does not coordinate iron, and the E81 side chain does not rotate, so the iron atoms are not bridged and coordinated by these residues (Figure 4-7B). These observations made *in crystallo* suggest that the mutation made at the B-pore disrupts the flexibility and dynamics of the iron ligands in the ferroxidase center.

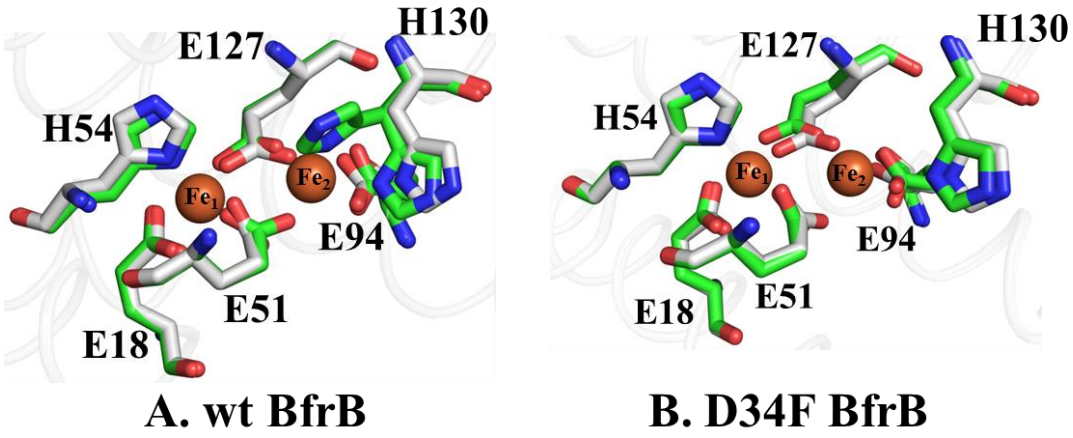

Figure 4-7: View of the ferroxidase center, as-isolated (grey) and Fe-soaked (green). (**A**) In the WT structure of as-isolated protein the side chain of H130 is rotated away, but when the crystals are soaked in iron (Fe-soaked) the H130 side chain is observed in the gate open and gate closed conformations, which allow for the oxidized iron to be taken into the interior of the BfrB cavity. (**B**) The structure of the D34F mutant shows that even after soaking in iron the H130 side chain does not coordinate iron and remains in the gate open conformation [6].

Iron Oxidation and Uptake

Mineralization experiments were carried out with the purified proteins to investigate whether iron could be loaded into the core. As stated in the experimental section, 500 Fe atoms were attempted to be loaded into the core of the proteins by adding 50 Fe atoms/ BfrB at the time. In this experiment, there are two competing reactions, (*i*) the oxidation of Fe^{2+} at the ferroxidase center of BfrB and storage into the cavity, and (*ii*) the autoxidation of Fe^{2+} in solution to Fe^{3+}, which forms an insoluble ferric colloid. The wt BfrB was capable of mineralizing (storing) 430 ± 22 Fe atoms; while in contrast, the D34F mutant was only able to store 110 ± 30 Fe atoms. The oxidation rates were unable to be measured because the formation of the Fe^{3+}-O spectroscopic signal is around 300 nm which can be found both outside and inside BfrB. The inability of iron to be mineralized in the D34F mutant is likely a consequence of the effects caused by the mutation on the ferroxidase center flexibility, as suggested by the above-described analysis of the X-ray crystal structures: If the conformational flexibility of the ferroxidase center ligands is impaired, then the ferroxidase center is unable to coordinate the di-Fe^{2+} center, which is required to oxidize iron to a di-Fe^{3+}, before conformational changes in the H130 side chain allow the Fe^{3+} to be translocated into the BfrB core, so instead, Fe2+ is oxidized outside of the protein.

Molecular Simulations

The molecular dynamics (MD) simulations performed on the D34F mutant showed that the mutant is less flexible than the wt protein. The MD simulations show that the D34F mutant exhibits fluctuations in the long loops connect helices B and C and the N- and C- termini. The wt protein exhibits fluctuation in the same regions, but in addition it shows conformational

flexibility in C- terminal half of helices D, and in the N-terminal half of helix C. In Figure 4-8 it can be seen that the fluctuations seen in the wt protein are significantly greater than in the D34F mutant at all sites except the long loop connecting helices B and C. The D34F mutation blocks the B-pore and packs against the L63 side chain, which disrupts the folding/unfolding transitions in the C-termini of helix D and the breathing motion of the B-pore. The dampened motion from the hydrophobic packing limits the conformational freedom of F34 and F63 side chains to one rotamer. The permeability of the B-pore becomes limited.

The MD simulations also show how the ferroxidase activity was affected by the D34F mutation. In the wt protein, the flexibility in the C-terminal half of helix D functions to couple breathing motions in the 4-fold and B-pores with the ferroxidase center ligands. These motions help the movement of H130 to enable its gating motion, thus facilitating and translocation of the Fe^{3+} into the cavity. In the D34F mutant, the flexibility of helix D is much lower and prevents the gating motion of the H130 side chain. Hence, the results of the MD simulations confirm the insights from the crystal structure that the H130 side chain is "trapped" in the gate open confirmation (Figure 4-9). The MD simulations show 3 rotamer states of H130 in Figure 4-9A for wt, but only one rotamer state for D34F mutant in Figure 4-9B. The changes in the rotameric states (x_1, x_2) for the D34 and F64 side chains in wt BfrB are seen in Figure 4-9C contribute to the breathing motion of the B-pore. In comparison, the distribution of the rotameric states seen in the D34F mutant in Figure 4-9D is significantly reduced.

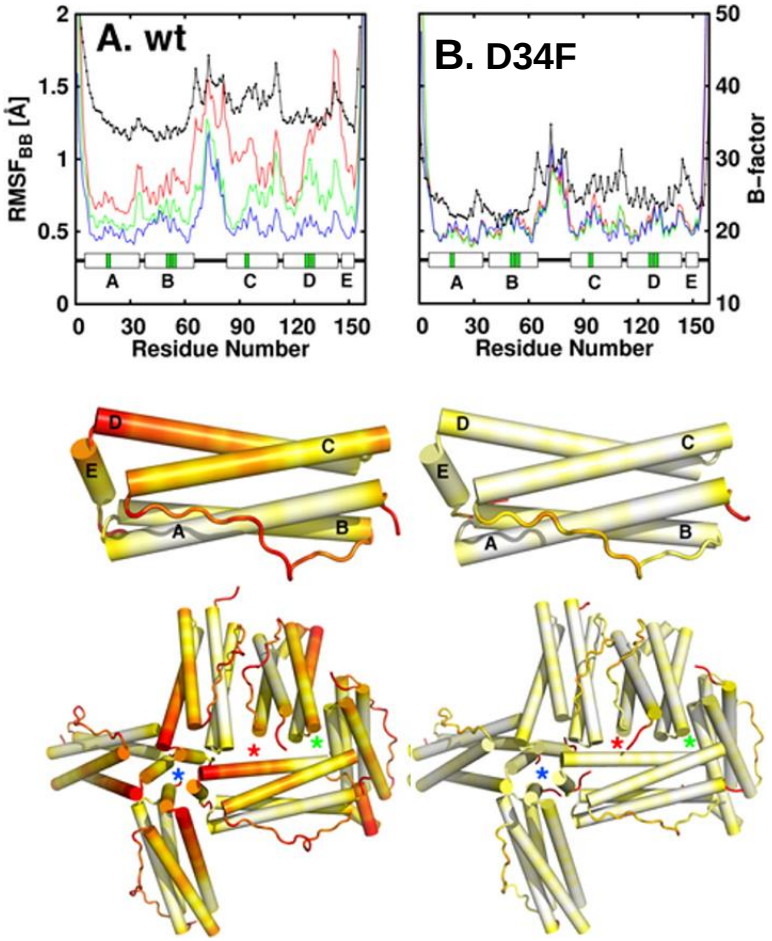

Figure 4-8: Molecular dynamics simulation of the fluctuations in wt and D34F BfrB. The top row shows plots of per-residue backbone RMSF in system E2 (red), E10 (green), E40 (blue), and per-residue crystallographic B-factors (black); helices A-E are indicated as boxes, and ferroxidase center residues are highlighted in green. The middle row depicts the per-residue backbone RMSF (systems E2) mapped onto a BfrB subunit, and the bottom row shows per-residue backbone RMSF mapped on six subunits of the 24-mer assembly to illustrate relative flexibility at the 4-fold (blue stars), 3-fold (green stars), and B-pores (red stars). Flexibility increases in the color scale from white to red [6].

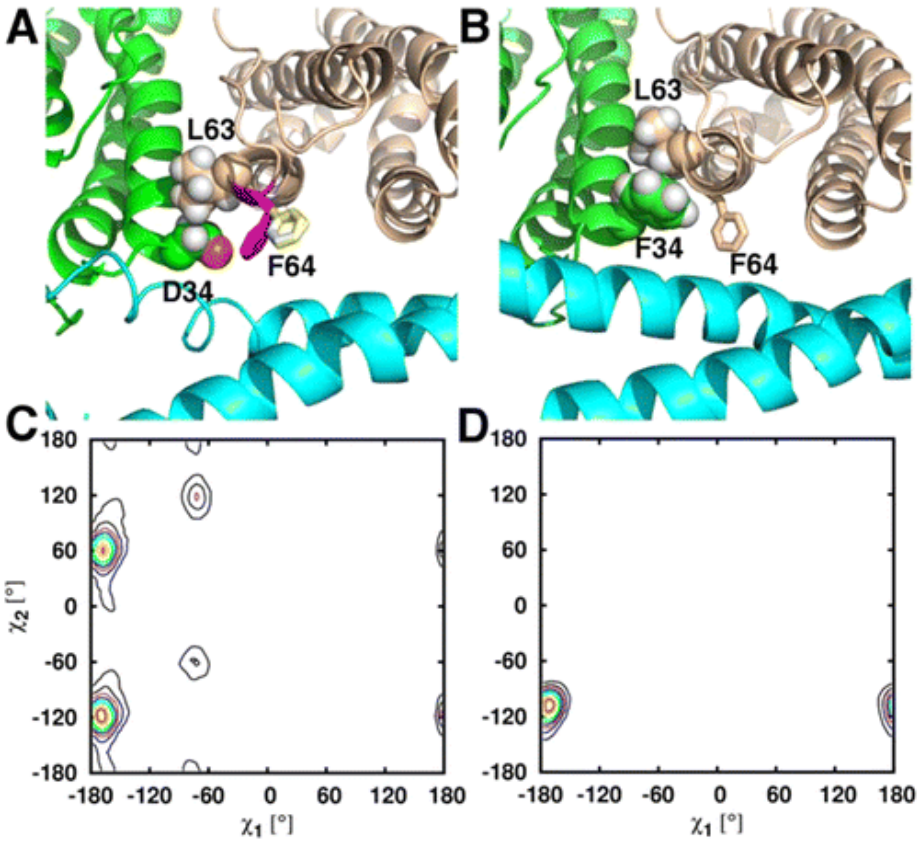

Figure 4-9: Close up view of a B-pore taken during the MD simulations of (**A**) wt and (**B**) D34F BfrB. The three rotameric states of the F64 side chain in wt BfrB are depicted in white, yellow, and magenta sticks in (**A**), and the three rotameric states of D34 are indicated in the plot shown in (**C**). The rotameric exchange of D34 and F64 contributes to the breathing motions of the B-pores as well as ion traffic across B-pores in wt BfrB. In the D34F structure packing of F34 against L63 (spheres) likely contributes to the lower flexibility of B-pores in the mutant, due to only one conformational rotamer of the F34 side chain (**D**) and only one conformation of the F64 side chain, wheat sticks in (**B**) [6].

Discussion

The molecular dynamics simulations that suggested the B pores were the location of iron release[5] led to the D34F mutant being prepared as a way to study disruption of iron release from BfrB. Although we could not study the effect on iron release because the mutant is not capable of storing iron, we used the D34F mutant to show that dynamic fluctuations of connecting the B-pores with the ferroxidase center are necessary to provide the gating motion of H130 at the ferroxidase, which is crucial for iron oxidation and uptake by BfrB. Using X-ray crystal structure and molecular dynamics simulations we were able to complement the results seen in the laboratory with the iron uptake experiments where D34F was able to only uptake about 24% of the Fe atoms compared to 85% seen in wt.

The crystal structure showed that mutating the negatively charged D34 to the hydrophobic phenylalanine blocks the B-pores and decreases the hydrophilicity of the B-channels, which allowed us to obtain a snapshot of Fe ions in the B-pores, where they are coordinated by D132 (Figure 4-6). The flexibility of the ferroxidase center was affected and caused by the mutation and caused the H130 residue to remain in the gate open conformation (Figure 4-7). The molecular dynamic simulations showed that F34 inhibited the fluctuations of the side chains that were necessary to make the conformational change at the ferroxidase center. F34 caused a decrease in the breathing motions of the B-pore because it packs against the L63 side chain. This packing also affected the folding and unfolding transitions of the C-terminal portion of helix D which lowered its flexibility and the ability of H130 to undergo the conformational change (Figure 4-9). Hence, these results show that concerted motions involving the B-pores and the ferroxidase centers are necessary for ferroxidase activity. In fact, disrupting

the flexibility by introduction of the D34 F mutation impairs ferroxidase activity and iron mineralization in the BfrB core. The results also provide further insight into iron traffic through the B-pores in BfrB.

References

1. Bradley, J.M., Le Brun, N.E., Moore, G.R., *Ferritins: furnishing proteins with iron.* J. Biol. Inorg. Chem, 2016.
2. Crow, A., Lawson, T.L., Lewin, A., Moore, G.R., Le Brun, N.E., *Structural Basis for Iron Mineralization by Bacterioferritin.* JACS, 2009. **131**: p. 6808-6813.
3. Weeratunga, S., Lovell,S., Yao,H., Battaile,K., Fischer,C., Gee,C., Rivera,M, *Structural Studies of Bacterioferritin B from Pseudomonas aeruginosa Suggest a Gating Mechanism for Iron Uptake via the Ferroxidase Center.* Biochemistry, 2010. **49**: p. 1160-1175.
4. Macedo, S., Romao, C.V., Mitchell, E., Matias, P.M., Liu, M.Y., Xavier, A.V., LeGall, J., Teixeira, M., Lindley, P., and Carrondo, M.A., *The Nature of the Di-Iron Site in the Bacterioferritin from Desulfovibrio desulfuricans.* Nat. Struct. Biol., 2003. **10**: p. 285-290.
5. Rui, H., Rivera, M., Im, W., *Protein Dynamics and Ion Traffic in Bacterioferritin.* Biochem., 2012. **51**(49): p. 9900-9910.
6. Yao, H., Rui, H., Kumar, R., Eshelman, K., Lovell, S., Battaile, K.P., Im, W., Rivera, M., *Concerted Motions Networking Pores and Distant Ferroxidase Centers Enable Bacterioferritin Function and Iron Traffic.* Biochem., 2015. **54**: p. 1611-1627.
7. Weeratunga, S.K., Gee, C.E., Lovell, S., Zeng, Y., Woodin, C.L., Rivera, M., *Binding of Pseudomonas aeruginosa Apobacterioferritin-Associated Ferredoxin to Bacterioferritin B Promotes Heme Mediation of Electron Delivery and Mobilization of Core Mineral Iron.* Biochem., 2009. **48**: p. 7420-7421.
8. Ringleing, P.L., Davy, S.L., Monkara, F.A., Hunt, C., Dickson, D.P.E., McEwan, A.G., and Moore, G.R. , *Iron Metabolism in Rhodobacter Capsulatus. Characterization of Bacterioferritin and Formation of Non-Haem Iron Particles in Intact Cells.* Eur.J. Biochem., 1994. **233**: p. 847-855.
9. Kabsch, W., *Automatic indexing of rotation diffraction patterns.* J. Appl. Crystallogr., 1988. **21**: p. 67-72.
10. Krug, M., Weiss, M.S., Heinemann, U., and Mueller, U., *XDSAPP: a graphical user interface for the convenient processing of diffraction data using XDS.* J. Appl. Crystallogr., 2012. **45**: p. 568-572.
11. Vonrhein, C., Flensburg, C., Keller, P., Sharff, A., Smart, O., Paciotek, W., Womack, T., and Bricogne, G. , *Data processing and analysis with the autoPROC toolbox.* Acta Crystallogr., Sect.D. Biol. Crystallogr., 2011. **67**: p. 293-302.
12. Evans, P.R., *An introduction to data reduction: space-group determination, scaling, and intensity statistics.* Acta Crystallogr., Sect.D. Biol. Crystallogr., 2011. **67**: p. 282-292.

13. McCoy, A.J., Grosse-Kuntstleve, R. W., Adams, P.D., Winn, M.D., Storoni, L. C., and Read, R.J., *Phaser crystallographic software.* J. Appl. Crystallogr., 2007. **40**: p. 658-674.
14. Adams, P.D., Afonine, P.V., Bunkoczi, G., Chen, V.B., Davis, I.W., Echols, N., Headd, J.J., Hung, L.W., Kapral, G.J., Grosse-Kunstleve, R.W., McCoy, A.J., Moriarty, N.W., Oeffner, R., Read, R.J., Richardson, D.C., Richardson, J.S., Terwilliger, T.C., Zwart, P.H., *PHENIX: a comprehensive Python-based system for macromolecular structure solution.* Acta Crystallogr D Biol Crystallogr., 2010. **66**: p. 213–221.
15. Emsley, P., Lohkamp, B., Scott, W.G., Cowtan, K. , *Features and development of Coot.* Acta Crystallogr D Biol Crystallogr, 2010. **66**: p. 486–501.
16. Chen, V.B., Arendall, W.B., 3rd, Headd, J.J., Keedy, D.A., Immormino, R.M., Kapral, G.J., Murray, L.W., Richardson, J.S., Richardson, D.C., *MolProbity: all-atom structure validation for macromolecular crystallography.* Acta Crystallogr D Biol Crystallogr., 2010. **66**: p. 12–21.
17. Evans, P., *Scaling and assessment of data quality.* Acta.Crystallogr. Sect. D, Biol. Crystallogr., 2006. **62**: p. 72-82.
18. Weiss, M.S., *Global indicators of X-ray data quality.* . J. Appl. Crystallogr., 2001. **34**: p. 130-135.
19. Diederichs, K.a.K., P. A., *Improved R-factors for diffraction data analysis in macromolecular crystallography.* Nat. Struct. Biol., 1997. **4**: p. 269-275.
20. Karplus, P.A., Diedrichs, K., *Linking crystallographic model and data quality.* Science, 2012. **336**: p. 1030-1033.
21. Evans, P., *Biochemistry. Resolving some old problems in protein crystallography.* Science, 2012. **336**: p. 896-987.
22. Lee, K.I., Jo, S., Rui, H., Egwolf, B., Roux, B., Pastor, R.W., Im, W., *Web interface for Brownian dynamics simulation of ion transport and its applications to beta-barrel pores.* Journal of computational chemistry, 2012. **33**: p. 331–339.
23. Durell, S.R., Brooks, B., Arieh, B.N., *Solvent-Induced Forces Between Two Hydrophilic Groups.* . J Phys Chem., 1994. **98**: p. 2198–2202.
24. Steinbach, P.J., Brooks, B., *New Spherical-Cutoff Methods for Long-Range Forces in Macromolecular Simulation.* . J Comput Chem., 1994. **15**: p. 667–683.
25. Essmann, U., Perera, L., Berkowitz, M.L., Darden, T., Lee, H., Pedersen, L.G., *A Smooth Particle Mesh Ewald Method.* . J Chem Phys., 1995. **103**: p. 8577–8593.

Chapter 5 : Inhibitors of the BfrB-Bfd Interaction Increase Susceptibility to Antibiotics

Introduction

Antibiotic resistance is becoming an increasing problem due to excessive amounts of antibiotics used for human therapy as well as animal farming [1]. The increasing exposure of antibiotics allows for more opportunities for bacteria to develop resistance. Bacteria are capable of becoming resistant by coding genes that are resistant to a single drug, increasing expression of efflux pumps, which exports a wide range of drugs, and developing mutations to specific protein targets that would decrease the susceptibility to man-made compounds [1]. The development of resistance has become so extreme, in 2013 the CDC reported that approximately 23,000 deaths were caused by antibiotic resistant pathogens [2] and they developed a national strategy to combat antibiotic-resistant bacteria [3]. In this strategy they outlined 5 goals aimed at stopping and controlling the spread of antibiotic resistant pathogens. One of these goals is the development of new antibiotics [3]. In the past twenty years there have not been new classes of antibiotic developed, and the new antibiotics that have been released to the market target the same cellular processes as the old antibiotics [4]. This has led to the need to develop antibiotics that have different targets. Research has been started to search for new targets, such as virulence factors, quorum sensing, fatty acid biosynthesis, and cell division [5-8], as well as targeting cellular mechanisms like efflux pumps to restore the efficacy of current antibiotics [9]. The

work being completed in our lab has been focusing on another new target, which is disrupting iron homeostasis by inhibiting the protein-protein interaction of the iron storage protein bacterioferritin B (BfrB) and the bacterioferritin-associated ferredoxin (Bfd) in *Pseudomonas aeruginosa*. To develop compounds that can specifically bind BfrB at the Bfd-binding site, our lab has been utilizing concepts in fragment-based drug design (FBDD) and structure-based design.

A library of 200 fragments, which are defined as molecules with molecular weights less than 300 Da, was screened by NMR to discover hits that bind to BfrB at the Bfd-binding site. Fragment hits were then used in co-crystallization trials with BfrB, and computational approaches were used to predict hits at the binding site. A crystal structure of a fragment that bound to the Bfd binding spot on BfrB was obtained, which allowed us, in collaboration with Dr. Richard Bunce (Oklahoma State University), to grow and modify the compounds to increase binding affinity. Knowing the structure of the BfrB-Bfd interaction site, we were capable of modifying the fragments to interact with the key residues at the binding site. To determine if the modified compounds were increasing affinity and specificity, several assays were performed: (*i*) The binding affinity of compounds for BfrB was measured using SPR or fluorescence polarization methods, (*ii*) the efficacy of compounds to inhibit iron release from recombinant BfrB was measured using an *in vitro* iron release assay developed in our laboratory, (*iii*) I investigated potential adjuvant effects of our compounds to enhance the bactericidal activity of existing antibiotics against *Pseudomonas aeruginosa*. This assay is important to determine if the compounds would be able to cross the bacterial membrane and become biologically active. To

test the efficacy of the compounds on *P. aeruginosa*, killing assays and growth curves were performed in the presence of the compound and/or antibiotics.

P. aeruginosa is a gram-negative opportunistic pathogen that causes infections in immune compromised patients such as burn victims and cystic fibrosis patients [10]. It is also the most common multi-drug resistant gram-negative pathogen to cause pneumonia in hospitalized patients [11]. Many of the clinical isolates are resistant to antibiotics such as aminoglycosides and ciprofloxacin[11]; therefore the synergistic effect of our compounds with the antibiotics ciprofloxacin and the aminoglycoside tobramycin was tested. I showed that compounds demonstrated by our laboratory to (*i*) engage the Bfd-binding site of BfrB, (ii) inhibit *in vitro* iron release from BfrB, potentiate the antibiotic activity of antibiotics. For example, one compound was able to increase the killing of *P.aeruginosa* by 2 logs. The compounds have also shown to cause a slight delay in growth when added immediately after inoculation. As the compounds are continued to be modified to increase binding affinity, the experiments to determine adjuvant effects with antibiotics will continue. The results presented below provide promising progress towards the development of possible new antibiotics or adjuvants to current antibiotics, as well as probes that can be used to further investigate bacteria's response to the disruption of iron homeostasis.

Experimental

Bacterial Strains and Media

The *Pseudomonas aeruginosa* strain PA01, purchased from the University of Washington, Manoil Lab and the strain PA14, obtained from the Chandler lab at the University of Kansas, were used. The media used in killing curves was either M63 or Luria-bertani (LB). M63 was modified from O'Toole and Kolter [12]. M63 media is prepared by dissolving 2 g/L KH_2PO_4 (Sigma), 13.6 g $(NH_4)2SO_4$ (Sigma), 3 µM $FeSO_4$-$7H_2O$ (Fisher) and 1 mM $MgSO_4$ (Fisher) per 1L water, and autoclaving. Then 2 g glucose (Fisher), 5 g casamino acids (Fisher), 0.25 g tryptophan (Sigma), 4 g citric acid (Sigma), are added, and the pH is adjusted to 7.0 with the addition of KOH and the solution is filter sterilized. LB was prepared by weighing 25 g/L of dry, pre-made LB (Fisher), dissolving in 1 L of water and adjusting the pH to 7.0.

Killing Assays

Single colonies were grown in 5 mL of M63 media at 230 rpm and 37 °C overnight. The overnight inoculum was adjusted to 0.01 using a 1 cm cuvette. 191 µL of the diluted overnight culture was added to multiple wells in a 96 well plate. The plate was wrapped with parafilm and placed in a shaker incubator for incubation at 200-210 rpm and 37 °C for 5 h (Final OD = 0.2-0.3) to reach the beginning of the exponential growth phase. Then 5 µL of antibiotic stock solution and/ or compound were added to the wells to the desired concentrations. DMSO was used as a control in Cipro treated only cultures. Before treatment of compound and Cipro as well as after incubating for a designated amount of time, the entire culture in a well would be

removed by a pipette, serially diluted in PBS, and ten 10 µL drops would be plated on Pseudomonas Isolation Agar (PIA). The PIA plates would be incubated overnight at 37 °C for 15- 18 h. Single colonies would be counted and the colony forming unit/ mL (CFU/mL) would be determined. All compounds were kept in stock solutions dissolved in 100% DMSO. Care was taken to ensure that the volume of compound added kept the concentration of DMSO below 3% to a final volume of 200 µL cultures.

Antibiotic and Compound Stock Solutions

Ciprofloxacin-HCl (MP Biomedicals) and Tobramycin (Fisher) were dissolved in autoclaved nanopure water, filter-sterilized with 0.2 µm filter syringe, and stored at -20 °C in sterile microcentrifuge tubes. Ciprofloxacin stock solutions were prepared in a volumetric flask at 10 mg/mL and serially diluted to 20 or 40 µg/mL to be stored at -20 °C. Tobramycin was prepared at 10 mg/mL and diluted to 2 or 5 mg/mL stock solutions that were stored at -20 °C. Storage of antibiotic stock solutions at -20 °C was for a maximum of 3 months before being discarded. Fresh frozen stock solutions were thawed and used only once for each assay.

Growth Curves with Compound Only

Single colonies were grown in 5 mL of LB media at 230 rpm and 37 °C overnight. The overnight inoculum was diluted in LB media to an optical density of 0.5, which was measured using 1 cm cuvettes (OD_{600} = 0.2 for 250 µL culture in Spectramax i3x plate reader). 245 µL of diluted overnight culture and 5 µL of stock compound solution in DMSO for a final volume of 250 µL culture per well in a 96 well plate. The 96 well- plate was placed in Spectramax i3x

shaking plate reader, set to 37 °C, high orbital shaking every 15 minutes for 15-24 hours, and reading OD 600 nm every 30 minutes.

Growth Curves with Cipro and Compound

Single colonies were grown in 5 mL of LB media at 230 rpm and 37 °C overnight. The overnight inoculum was diluted in LB media to an optical density of 0.05 using a 1 cm cuvette. 235 µL of diluted overnight culture, 5 µL of stock compound solution in DMSO, and 10 µL of stock Cipro solution were added for a final volume of 250 µL culture per well in a 96 well plate. The 96- well plate was placed in the Spectramax i3x shaking plate reader set to 37 °C, high orbital shaking every 15 minutes for 15 hours, and reading OD 600 nm every 30 minutes. After 15 h of incubation, the entire content of the wells was suspended in 1 mL of sterile phosphate buffer saline (PBS) pH 7.4, and serially diluted in 10-fold increments. Ten 10 µL drops from each of the dilutions were plated on PIA. Drops were allowed to dry for 30-60 minutes, and then incubated at 37 °C for about 15-18 h. Single colonies were counted and the CFU/mL was determined by multiplying the dilution factor by the number of colonies and divided by the volume plated.

Results

Compound FC996

After screening a library of fragments the most promising hits were tested by laboratory members (Dr. Huili Yao and Dr. Yan Wang) in order to determine the efficacy of compounds at inhibiting iron release from BfrB, as well as testing the effect they had on *P. aeruginosa* growth

and susceptibility. To construct the killing curves, bacteria were grown in M63 media to the start of the exponential growth phase and then treated with antibiotics and/or compound. Prior to treatment, an entire well was removed from the 96 well- plate, serially diluted in PBS, and plated on PIA. The cell count obtained from this well served as the control before treatment. After treatment, the cell culture was incubated for an additional 3 or 4 h and then the cell count was determined by serial dilutions and plating on PIA. One of the fragments tested, labelled compound FC996, was shown by lab members to bind BfrB at the Bfd-binding site. As can be seen in Figure 5-1, treatment of *P. aeruginosa* cells with a combination of compound **1** (1, 2, or 3 mM) and ciprofloxacin (0.8 µg/mL), increased the killing of *P. aeruginosa.* The increase in killing efficacy with compound **FC996** is not yet substantial. The most likely reason is that the binding affinity of compound **FC996** for BfrB is approximately 1.2 mM. This low binding affinity is typical of fragments. At this stage, the important observation is that the compound binds the target (BfrB) and elicits increases the killing efficacy of ciprofloxacin. As will be shown below, as we improve the binding affinity of compounds by synthetic elaboration of compound **FC996**, the new compounds significantly increase the killing efficacy of ciprofloxacin.

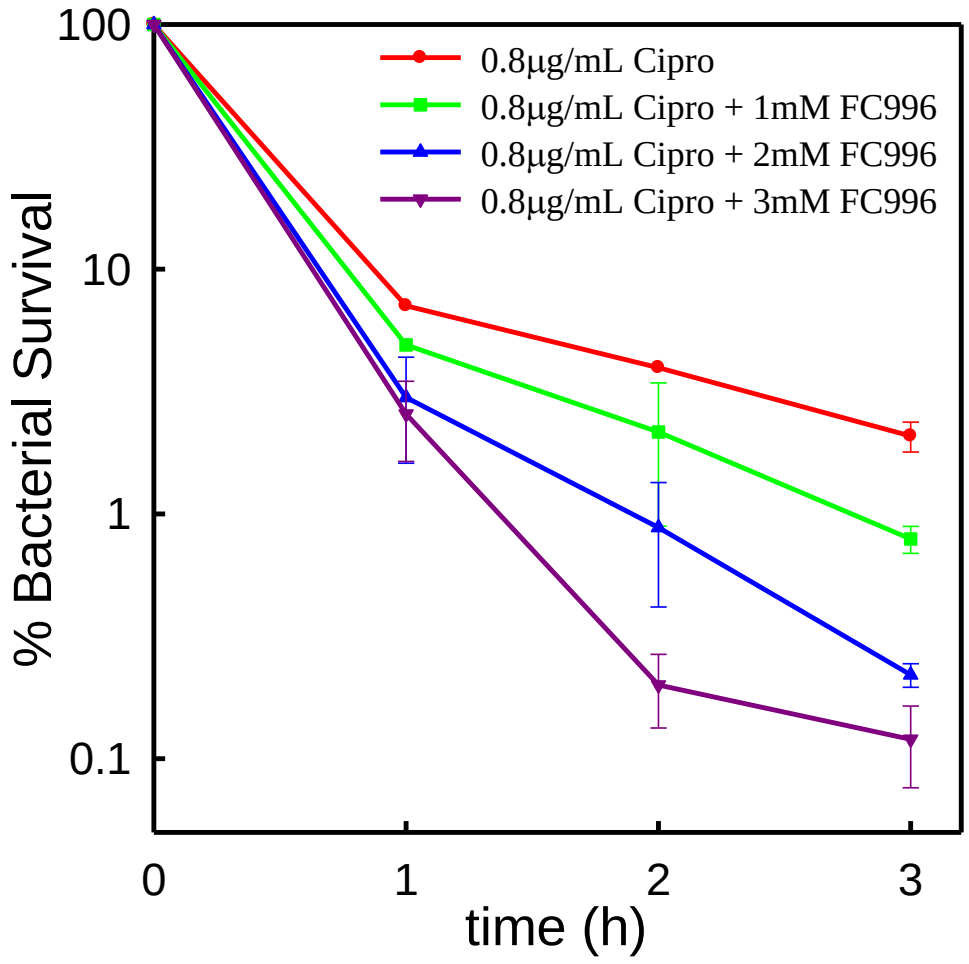

Figure 5-1: Bacterial survival 3 h after treatment with compound **FC996**. 1, 2, and 3 mM compound was tested with 0.8 µg/mL of ciprofloxacin. After 3 hours of treatment, the bacterial survival treated with Cipro only (red) was 5%, with 1 mM compound plus cipro (green) 1%, 2 mM compound + Cipro (blue) 0.5%, and 3 mM compound plus Cipro (purple) 0.1%.

Compound BN-XVI-069

As the compounds were elaborated synthetically, the binding affinity increased, as well as their adjuvant effect on Cipro. Compound BN-XVI-069 (**69**) showed very promising results.

It was shown by X-ray crystallography that **69** binds BfrB at the Bfd-binding spot. When this compound was used together with ciprofloxacin, the killing efficiency of the antibiotic was increased by 2 logs compared to treatment with Cipro only (Figure 5-2A). An isomer of **69**, compound BN-XVI-010 (**10**) did not show strong binding to BfrB and did not increase the killing efficacy of Cipro against *P. aeruginosa* cells (Figure 5-2B). These observations indicate that binding of compounds to the Bfd-binding site on BfrB is important to increase the killing activity of ciprofloxacin.

To determine if compound **69** was going to help other families of antibiotics, it was tested with the aminoglycoside, Tobramycin. *P. aeruginosa* cultures were grown to log phase and then treated with 50 µg/mL of Tobramycin and 200 or 400 µM compound **69** for 4 hours. The addition of compound **69** caused an increase in killing compared to Tobramycin alone. Compound **69** also showed to be dose dependent by having a larger effect of killing with 400 µM compared to treatment with only 200 µM as seen in Figure 5-3. Treating with Tobramycin does not kill the bacteria as fast as Cipro which is why the treatment was longer. Also, the killing difference was not as large compared to Cipro, but there was still an effect. This may suggest that the compounds will be more effective when used with fluoroquinolones compared to aminoglycosides, or it will take a compound that has higher binding affinity and is more stable to increase the killing to make it similar as the Cipro treated cultures. Compound **69** was also shown to begin breaking down over time. This gave an explanation why after 3-4 hours it would reach a plateau of killing. This led to modifying the structure again to increase the stability and binding affinity.

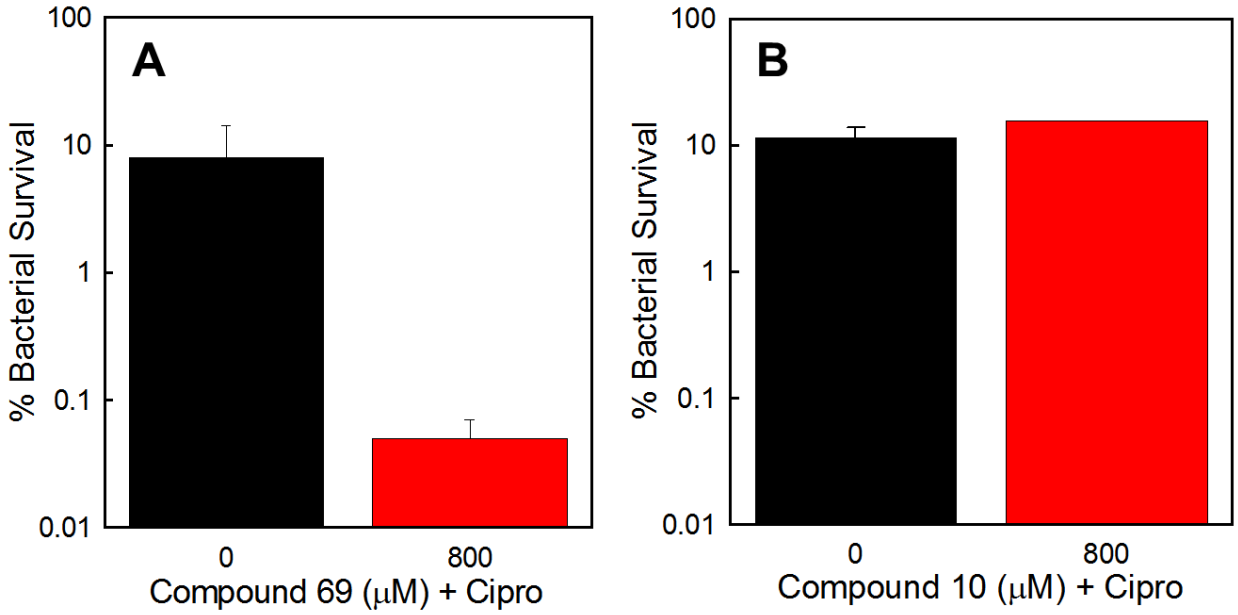

Figure 5-2: Comparison of the adjuvant properties of isomeric compounds. (**A**) Cultures were grown in M63 media to mid-log phase and treated with 800 μM compound **69** plus Cipro or 1 μg/mL Cipro only. After 3 h of treatment with compound **69**, which binds BfrB at the Bfd binding site, potentiates the killing activity of Cipro by 2 logs; treatment with **69** + Cipro (red bar), treatment with Cipro alone (black bar). (**B**) Compound **10** is an isomer of **69** but does not bind BfrB and therefore does not potentiate the killing activity of Cipro.

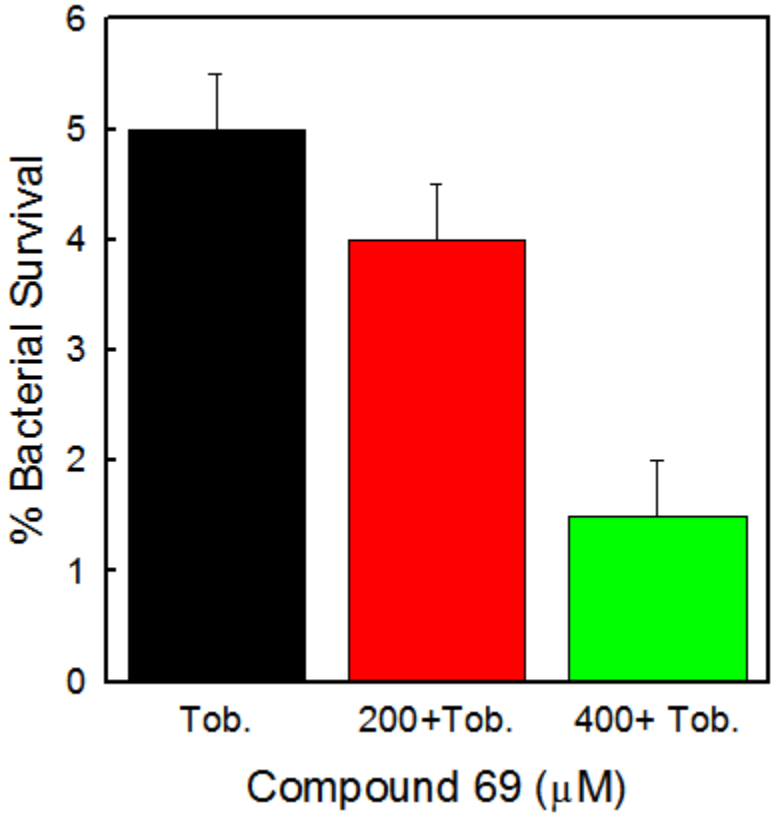

Figure 5-3: Bacterial survival 4 h after treatment with 50 µg/mL Tobramycin and Compound **69.** The effect caused by the compound is dose dependent and increases killing in combination with Tobramycin. The treatment with Tobramycin only (black bar) resulted in 5% survival, Tobramycin + 200 µM **69** (red bar) 4% survival, and Tobramycin + 400 µM **69** (green bar) 1.5% survival.

Compound GKK-008-057

Compound GKK-008-057 (**57**) is another compound showing promising results regarding the potentiation of ciprofloxacin. As seen in Figure 5-4, treatment with compound alone causes a small effect when added to cultures in mid-exponential growth. The figure also shows that 3 h

after the treatment of *P. aeruginosa* cells with 1 μg/mL ciprofloxacin alone results in about 10% survival. In comparison, when cells are treated with Cipro (1 μg/mL) and compound, there is a clear dose dependent response, from 200 to 600 μM compound, which is the limit of solubility of the compound in aqueous solutions. At concentrations near 600 μM the compound tends to precipitate, which may explain the increase in the standard deviations at this concentration.

The effect of compound **57** on cell growth was studied by adding it at the beginning of a culture in LB media. LB media was used instead of M63 because M63 has been reported to induce the formation of microcolonies [12] which we suspected would disrupt an accurate reading of the OD_{600}. Figure 5-5 shows results obtained from incubating *P. aeruginosa* cells in the presence of compound **57.** The presence of compound causes a slight delay in initial growth but the cell density, as judged by OD_{600}, is lower in the treated cultures. The higher the concentration of **57** added, the lower the cell density.

P. aeruginosa growth was also tested in the presence of Cipro concentrations below and close to the minimum inhibitory concentration (MIC) of the antibiotic. Cipro and compound **57** were both added immediately after inoculation in LB media. The cells were grown for 15 hours at 37 °C, and cell growth was monitored by measuring the OD_{600} at 30 min intervals in a shaking plate reader (Figure 5-6C). At 15 h the cultures were serially diluted and plated to enumerate the viable cells, log CFU/mL (Figure 5-6A, 5-6B). Note that by keeping the concentration of Cipro constant (0.2 μg/mL), treatment with a combination of Cipro and increasing concentrations of **57** results in a decrease of viable bacterial cells. There is about a 2 log difference in cell viability between cultures treated with 0.2 μg/mL Cipro only and cultures treated with a combination of

0.2 μg/mL Cipro and 400 μM **57**. Hence, the treatment of *P. aeruginosa* cultures with the compound affects the growth of the cells as well as enhances the efficacy of Cipro.

The compounds were also tested in the presence of the *P. aeruginosa* strain PA14. PA14 has the *bfrB* and *bfd* genes, so it was of interest to determine if the compounds would have a similar effect. Figure 5-7 shows that the final cell density (OD_{600}) is lower as the concentration of **57** increases, observations that are similar to those described above with *P. aeruginosa* PAO1. This suggest that **57** exerts a dose dependent growth delay of the bacteria indicating that the compounds being developed in the lab could be used not only against *P. aeruginosa* PA01, but also other *P. aeruginosa* strains, and perhaps other pathogens where the *bfr* and *bfd* genes show high conservation of amino acids used by each protein to interact with the other [13].

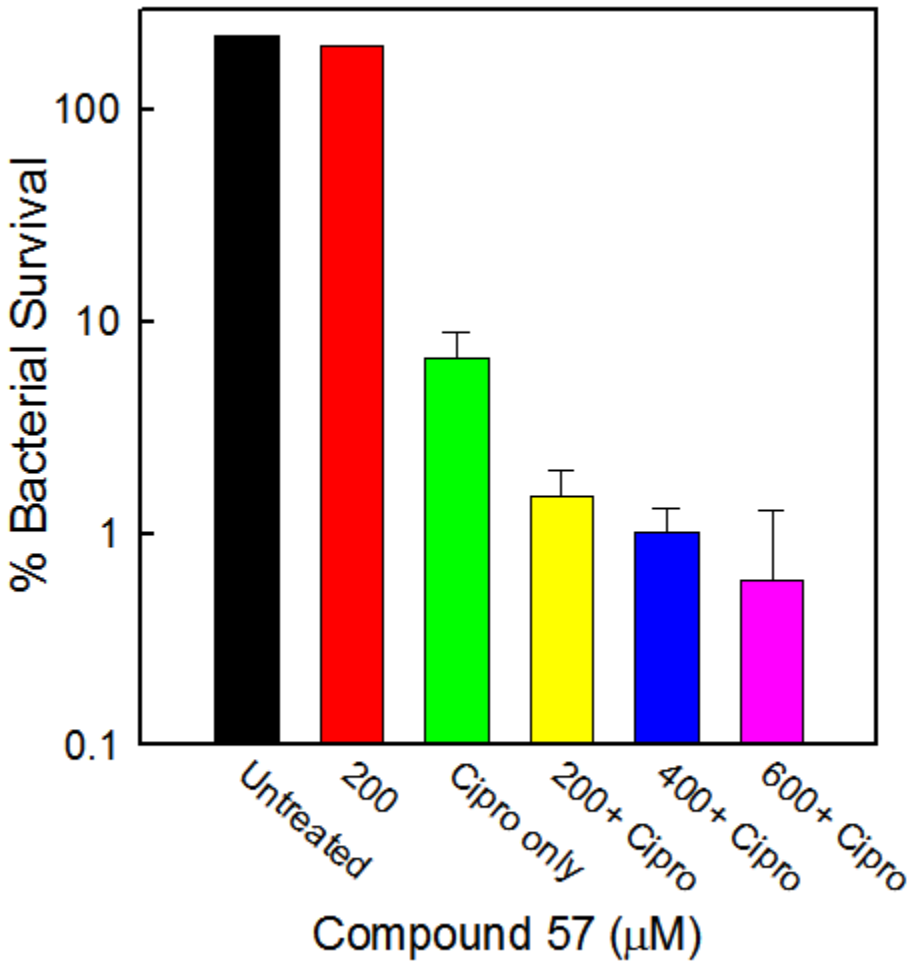

Figure 5-4: Bacterial survival 3 h after treatment with compound **57** and 1 μg/mL Cipro. Treating mid-log phase cultures with only **57** at 200 μM (red bar) shows minimal differences compared to untreated (2% DMSO) cultures (black bar). Treatment of mid-log phase cultures with 1 μg/mL Cipro only results in approximately 10% survival. Treatment of mid-log phase cultures with a combination of Cipro (1 μg/mL) and compound **57** shows that cell survival is lowered by more than one order of magnitude.

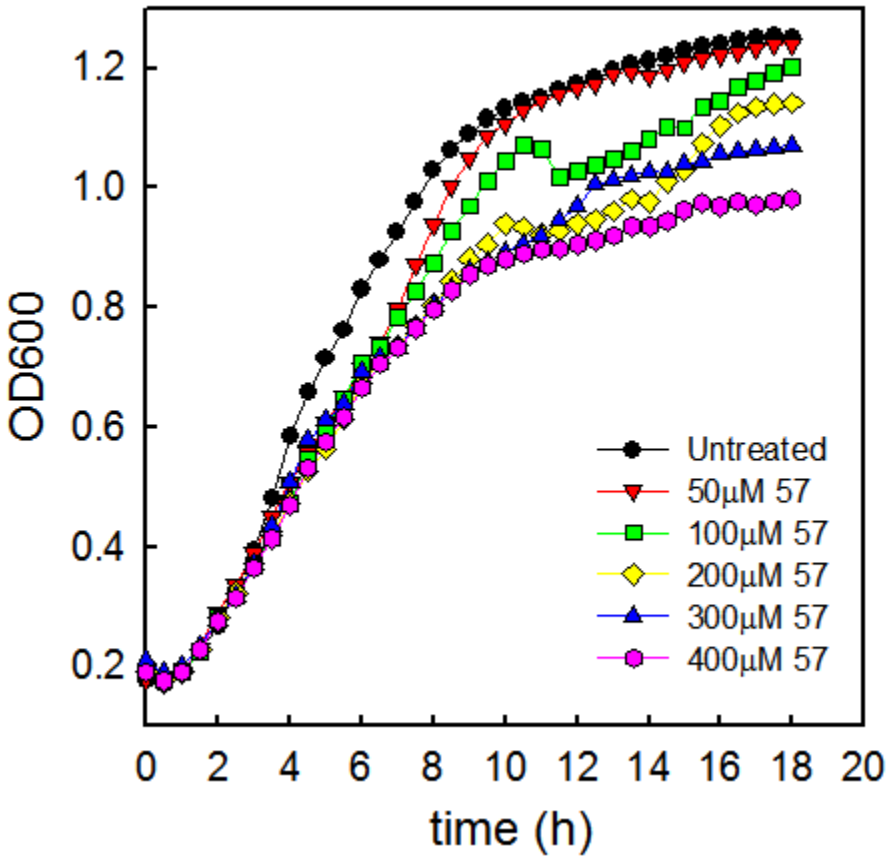

Figure 5-5: *P. aeruginosa* PAO1 growth curves in the presence of 50, 100, 200, 300, and 400 µM **57** or untreated (2% DMSO). The final cell density is lower as the concentration of **57** is increased. The presence of **57** at all concentrations slows the log phase growth compared to untreated cultures.

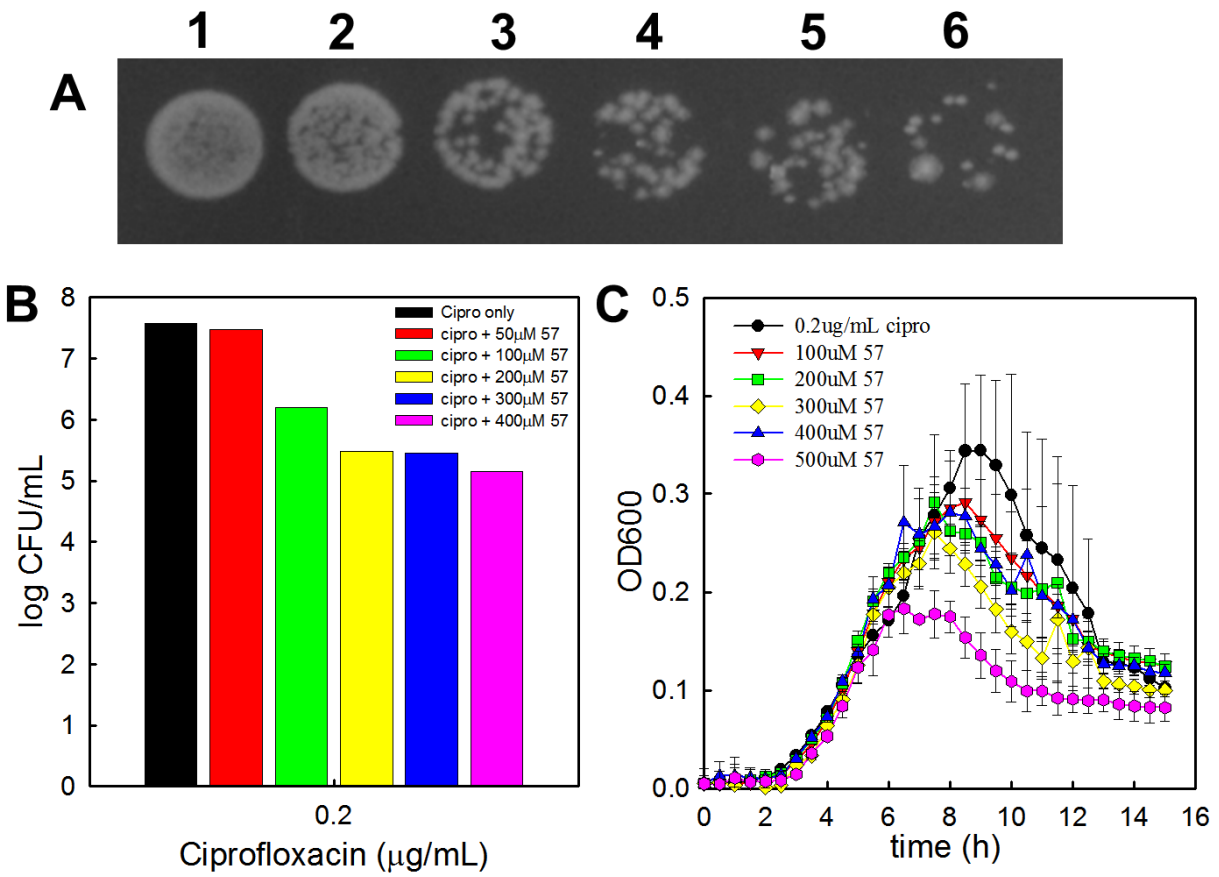

Figure 5-6: Growth in the presence of 0.2 μg/mL Cipro and compound **57**. (**A**) After incubating for 15 h, cultures were diluted in PBS and plated on PIA. Plating at the same dilution factor shows that the number of viable cells decreases with increasing concentration of compound: (1) 0.2 μg/mL Cipro only, (2) 0.2 μg/mL Cipro + 50 μM **57**, (3) 0.2 μg/mL Cipro + 100 μM **57**, (4) 0.2 μg/mL Cipro + 200 μM **57**, (5) 0.2 μg/mL Cipro + 300 μM **57**, (5) 0.2 μg/mL Cipro + 400 μM **57**. (**B**) Log CFU/mL counts of cell viability from 15 h cultures corroborate the effects of treatment with 0.2 μg/mL and increasing concentrations of **57**. (**C**) Growth curve of *P. aeruginosa* in the presence of 0.2 μg/mL Cipro with 2% DMSO and 0.2 μg/mL Cipro in addition to compound **57** at different concentrations.

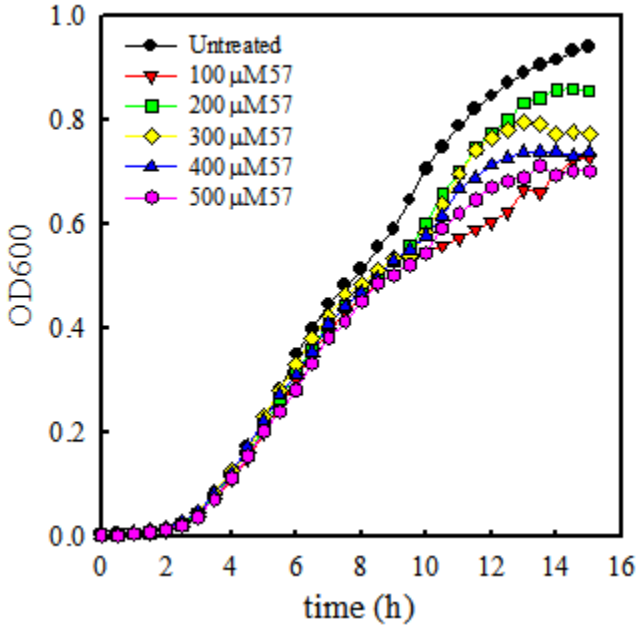

Figure 5-7: Growth curves of PA14 in the presence of compound **57** only. As the concentration of the compound increases, there is a slight delay in the log phase and the final OD_{600}. This suggests that the compounds could be promising for other strains of bacteria that have the BfrB and Bfd proteins.

Discussion

The synthetic evolution of the fragment hits has allowed improvement of compound binding affinity (K_d from 1,200 µM to 10 µM). The increases in binding affinity have been accompanied with concomitant increases in ciprofloxacin adjuvant activity against *P. aeruginosa* PAO1. In this context, fragments, which showed the lowest binding affinity, also showed modest adjuvant activity, increasing the killing activity of Cipro by less than a log at 5 mM. In contrast, compounds that bind BfrB with approximately 10 µM K_d exhibit enhanced killing activity of Cipro by 2 logs at their maximum solubility in aqueous solutions (600 µM). The compounds

have a larger killing effect when added with ciprofloxacin, but they also increase the cell's susceptibility to tobramycin also. Increasing the susceptibility to commonly used antibiotics could be a possible solution to rescue antibiotics for which bacteria have already developed resistance. To test this idea, future work will test the effect of the compounds we are developing against clinical isolates of *P. aeruginosa* with demonstrated ciprofloxacin resistance.

When compounds that hit BfrB on the Bfd binding site are added alone during mid-log phase it does not decrease the cell count significantly, but it does slow down the growth when it is added immediately after inoculation as seen in Figure 5-5. In addition when compound **57** and Cipro are added at the beginning of growth, it has shown up to 2 logs lower cell count with 400 μM of **57**. The effect of the compounds on the cell is not completely understood, but the Rivera group is working to test a hypothesis that sudden inhibition of iron mobilization from BfrB, caused by blocking the BfrB:Bfd interaction with the compound, causes a sudden disruption of iron homeostasis. We suspect this would prevent efficient incorporation of Fe into iron utilizing enzymes, such as those in the TCA cycle, thus rendering the bacterial cell less fit to combat the deleterious effects caused by antibiotic treatment.

Compound **57** has also shown to lower the final cell count in the presence of *P.aeruginosa* PA14 which suggests the compounds could be used to treat several strains of *P. aeruginosa* and perhaps other pathogens that have the same residues at the BfrB-Bfd interaction site.

The use of the compounds will not only be significant in their adjuvant effects to antibiotics, but they will also act as excellent probes to study bacterial iron homeostasis. Mutant cells lacking *bfrB* or *bfd* genes likely adapt during growth. In contrast, treating bacteria with

compounds that inhibit the BfrB:Bfd interaction can cause immediate disruption of iron homeostasis (see Chapter 3), to which bacteria can't adapt immediately. Hence, studying the effects caused by compound treatment will likely provide new insights into our understanding of bacterial iron homeostasis. Future analysis of the transcriptomics and phenotypes of the cells treated with compound could provide insight to the many unanswered questions of iron homeostasis. In this context, it is important to underscore that antibiotics have not only been used to treat infections, but they have also been used to further understand how bacteria function [14, 15]. Hopefully, the inhibitors of the BfrB-Bfd interaction can do the same for iron homeostasis in multiple pathogens.

At the time of this publication work is still ongoing to increase the binding affinity of the compounds and their effect on iron release *in vitro* and their adjuvant effect with antibiotics in *P. aeruginosa* strains PA01 and PA14.

References

1. Nikaido, H., *Multidrug Resistance in Bacteria.* Annu. Rev. Biochem, 2009. **78**: p. 119-146.
2. CDC., *Antibiotic Resistance Threats in the United States,* U.S.D.o.H.a.H. Services, 2013.
3. CDC., *National Strategy for Combating Antibiotic-Resistant Bacteria,* 2014.
4. Aminov, R.I., *A Brief History of the Antibiotic Era: Lessons Learned and Challenges for the Future.* Front. Microbiol., 2010. **134**: p. 1-7.
5. Su, Z., Honek, J.K., *Emerging bacterial enzyme targets.* Curr. Opin. Investig. Drugs, 2007. **2**: p. 140-149.
6. Njoroge, J., Sperandio, V., *Jamming bacterial communication: new approaches for the treatment of infectious diseases.* EMBO Mol Med, 2009. **4**: p. 201-210.
7. Lock, R.L., Harry, E.J., *Cell-division inhibitors: new insights for future antibiotics.* Nat. Rev. Drug Discov., 2008. **4**: p. 324-338.
8. Clatworthy, A.E., Pierson, E., Hung, D.T., *Targeting virulence: a new paradigm for antimicrobial therapy.* Nat. Chem. Biol., 2007. **9**: p. 541-548.
9. Lomovskaya, O., Bostian, K.A., *Practical applications and feasibility of efflux pump inhibitors in the clinic--a vision for applied use.* Biochem Pharmacol., 2006. **7**: p. 910-918.
10. Borriello, G.W., E; Roe, F; Kim, A; Ehrlich, G; Stewart, P, *Oxygen Limitation Contributes to Antibiotic Tolerance of Pseudomonas aeruginosa in Biofilms.* Antimicrob. Agents Chemother., 2004. **48**: p. 2659-2664.
11. El Solh, A.A., Alhajhusain, A., *Update on the treatment of Pseudomonas aeruginosa pneumonia.* J. Antimicrob. Chemother, 2009. **64**: p. 229-238.
12. O'Toole, G.K., H; Kolter, R, *Biofilm Formation as Microbial Development.* Annual Rev.Microbiol., 2000. **54**: p. 49-79.
13. Wang, Y., Yao, H., Cheng, Y., Lovell, S., Battaile, K.P., Midaugh, C.R., Rivera, M., *Characterization of the Bacterioferritin/Bacterioferritin Associated Ferredoxin Protein-Protein Interaction in Solution and Determination of Binding Energy Hot Spots.* Biochem., 2015. **54**: p. 6162-6175.
14. Spratt, B.G., *Distinct penicillin binding proteins involved in the division, elongation, and shape of Escherichia coli K12.* PNAS 1975. **72**: p. 2999-3003.
15. Shannon B Falconer, T.L.C., Eric D Brown, *Antibiotics as probes of biological complexity.* Nature Chemical Biology, 2011. **7**: p. 415-423.